Detecting and Correcting Bends in Medical-Grade Endoscopes using Computer Vision and Cold-Rolling Processes

A Major Qualifying Project (MQP) submitted to the faculty of Worcester Polytechnic Institute in partial fulfillment of the requirements of the degree of Bachelor of Science

Submitted By:

Abigail Clemence (ME)

Nikita Igoshin (ME)

Chenhao Li (ME)

Praniva Pradhan (ME)

Jessica M Rhodes (RBE)

George Malcolm Shelton (ECE)

Advised By:

Professor Pradeep Radhakrishnan (MME/RBE)

Sponsor:

Henke Sass Wolf of America

(Austin Scott, George Ardamerinos)

Abstract

This project developed a semi-automated machine for precisely measuring and straightening medical-grade endoscopes of various diameters. The current method involves manual straightening, resulting in low accuracy. The project required identifying the location and measurement of bends, straightening of bent endoscopes, and verification and validation of the integrated system. Endoscope contours are captured using computer vision, and endoscope parameters such as diameter and length are determined to calculate maximum runout. This information is used by the straightening subsystem, which involves a cold rolling process to remove these bends. Two systems were integrated into a single machine, and various tests were conducted to verify the performance. The tested prototype, set to incorporate into Henke Sass Wolf of America (HSWoA) operations, aims to ensure endoscopes are within swift and reliable specifications.

Acknowledgments

The team would like to thank our advisor, Professor Pradeep Radhakrishnan (Mechanical Engineering), for all his guidance, support, and dedication to our team throughout this project. The team would also like to thank our sponsor, Henke Sass Wolf of America, especially Austin Scott and George Ardamerinos for all their support, knowledge, and time over the course of the year. Additionally, the team would like to thank Ms. Barbara Furhman, Administrative Assistant (Mechanical Engineering), for helping our team purchase all the materials. The team also thanks the D Term 2023 and B Term 2023 ME4320 teams for their contributions.

Authorship

SECTION	AUTHOR(S)	PRIMARY EDITOR(S)
Abstract	All	All
Acknowledgments	A. Clemence	C. Li
1 Introduction	P. Pradhan	A. Clemence
1.1 Problem Statement and Objectives	P. Pradhan	A. Clemence
1.2 Report Overview	A. Clemence	P. Pradhan
2 Background	A. Clemence	C. Li, J. Rhodes
2.1 Endoscope Inventory	A. Clemence, P. Pradhan	C. Li
2.2 Materials	P. Pradhan	A. Clemence
2.3 HSWoA Current Straightening Rig	J. Rhodes, A. Clemence	A. Clemence, C. Li
2.4 Current Endoscope Repair	P. Pradhan	A. Clemence
2.5 Runout	P. Pradhan	A. Clemence
2.6 Cold Rolling Process	P. Pradhan	A. Clemence
3 ME4320 Course Contributions	P. Pradhan, G. Shelton	A. Clemence
3.1 D-Term 2023	P. Pradhan, G. Shelton	A. Clemence, J. Rhodes
3.2 B-Term 2023	G. Shelton	A. Clemence, J. Rhodes,
4 General Methodology	A. Clemence	C. Li
4.1 Mission Statement	P. Pradhan	C. Li
4.2 Objectives	P. Pradhan	C. Li
4.3 Requirements	P. Pradhan	C. Li
4.4 Accomplishments Completed by Term	A. Clemence	C. Li, P. Pradhan
5 Measurement of Endoscopes	N. Igoshin	J. Rhodes
5.1 LiDAR Consideration	G. Shelton	P. Pradhan
5.2 Introduction to Endoscope Measurement Processes	N. Igoshin	J. Rhodes
5.3 Calibration Process Steps	N. Igoshin	P. Pradhan
5.4 Program Results and Parameters	N. Igoshin	P. Pradhan
5.5 Light Conditions	N. Igoshin	P. Pradhan
5.6 Endoscope Detection Methods Testing	C. Li	J. Rhodes, G. Shelton
5.7 Runout Calculator	C. Li	J. Rhodes
5.8 Runout Calculator Code Testing Method – Diameter Calculator	C. Li	J. Rhodes, G. Shelton
5.9 Final Measurement Code	C. Li, J. Rhodes	A. Clemence, G. Shelton
5.10 Camera Selection	G. Shelton	C. Li
6 Station Overview	N. Igoshin, P. Pradhan	N. Igoshin
6.1 Station Requirements	P. Pradhan, G. Shelton	N. Igoshin
6.2 Endoscope Mount Selection	P. Pradhan	N. Igoshin
6.3 Measurement Station Parts Specification	N. Igoshin, P. Pradhan	N. Igoshin
7 Straightening Device	N. Igoshin	P. Pradhan
7.1 Straightening Device Overview	N. Igoshin	P. Pradhan

7.2 Required Straightening Force	N. Igoshin	P. Pradhan
7.3 FEA Minimum Force Verification	N. Igoshin	P. Pradhan
7.4 Vertical Stepper Motor/Lead Screw	N. Igoshin	P. Pradhan
7.5 Straightening Device Components Specification	N. Igoshin	P. Pradhan
7.6 Roller Adapter	N. Igoshin	P. Pradhan
7.7 Horizontal Stepper Motor/Lead Screw	N. Igoshin	P. Pradhan
7.8 Summary of Straightening Device Changes	N. Igoshin	P. Pradhan
8 Electrical System Configuration	G. Shelton	A. Clemence
8.1 Microcontroller Selection	G. Shelton	A. Clemence
8.2 Measurement Substation Electrical System	G. Shelton	A. Clemence
8.3 Straightening Substation Electrical System	G. Shelton	A. Clemence
9 Testing and Results	All	All
9.1 Measurement Station	N. Igoshin	C. Li
9.2 Measurement Code	C. Li	A. Clemence
9.3 Electrical Systems	J. Rhodes, G. Shelton	A. Clemence
9.4 Straightening Code	J. Rhodes	A. Clemence
9.5 Straightening Device	J. Rhodes	A. Clemence
9.6 Combined Code System	J. Rhodes	P. Pradhan
10 Discussion	J. Rhodes	P. Pradhan
10.1 Requirements	N. Igoshin	P. Pradhan, J. Rhodes
10.2 Broader Impacts	P. Pradhan	A. Clemence
11 Conclusions and Recommendations	All	All
11.1 Measurement Station	N. Igoshin, G. Shelton	J. Rhodes
11.2 Straightening Device	N. Igoshin, G. Shelton	P. Pradhan, J. Rhodes
11.3 Electrical Systems	J. Rhodes, G. Shelton	P. Pradhan
11.4 Combined System	J. Rhodes	P. Pradhan
11.5 Future Work	All	All
11.6 Reflections	All	All
12 References	All	All
13 Appendix	All	All

Table of Contents

Table of Figures

Table of Tables

1 Introduction

Henke Sass Wolf, headquartered in Tuttlingen, Germany, boasts a rich history dating back to its founding by Georg Andreas Henke in 1921. Initially renowned for manufacturing optical instruments, the company has evolved into the foremost OEM manufacturer specializing in medical endoscopy devices, veterinary products, and dental syringes [1]. In the realm of surgery, where precision is paramount, it is common for medical equipment to incur bends or damage during procedures. For Henke Sass Wolf of America [1], located in Dudley, Massachusetts, the process of repairing endoscope products has followed a consistent approach over the years, relying on manual correction performed by skilled technicians (a process which is further explained in Background chapter 2.4). The endoscopes HSWoA strive to straighten are medical devices used by people all around the world [1].

An endoscope is a rigid or flexible tubular medical device allowing for a direct view into the body. These devices are used for endoscopies, which are medical procedures to visualize the human body's internal organs or natural cavities [2]. Figure 1 below depicts a typical endoscope straightened and repaired by HSWoA. This instrument is a hollow metal rod with an image sensor, optical lens, and an attached light source. The endoscopes often range in length from 50 mm up to 600 mm and can have diameters ranging from 2.3mm to 10mm. This instrument is introduced through natural openings, such as the mouth (bronchoscopy) or the rectum (sigmoidoscopy). The medical procedure involving any endoscope is commonly called an endoscopy used to detect and identify diseases affecting the esophagus, stomach, colon, ears, nose, throat, urinary tract, and abdomen [3].

Figure 1: Typical Endoscope Repaired by HSWoA [1]

Consistent usage of endoscopes results in the gradual formation of bends in the shaft. An example of a bent endoscope that HSWoA might receive that requires straightening is shown in Figure 2 below. These bends give rise to challenges across various aspects of endoscopic procedures. They obstruct the field of view, posing difficulty for medical professionals in visualizing and examining targeted areas within the body. The images or video feed that is captured can be distorted, leading to inaccuracies in observations and compromised diagnostics [4]. Such issues can significantly affect the quality of medical assessments and decisions based on endoscopic findings. Furthermore, bends complicate the procedural process, impeding the smooth navigation of the endoscope through the body's cavities [5]. Figure 3 below depicts a visual comparison of the clarity of the view through a repaired endoscope versus a damaged endoscope.

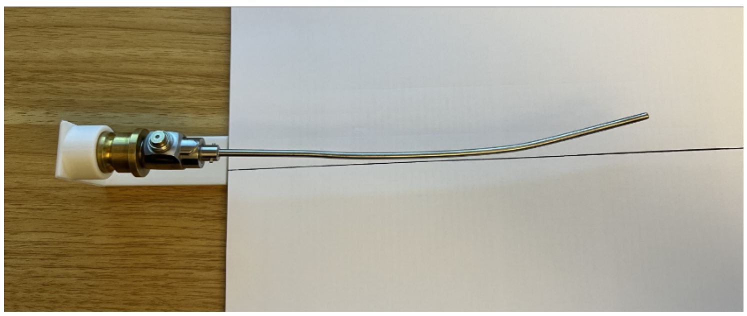

Figure 2: Bent Endoscope Provided by HSWoA for Straightening (Pradhan, P. 2024)

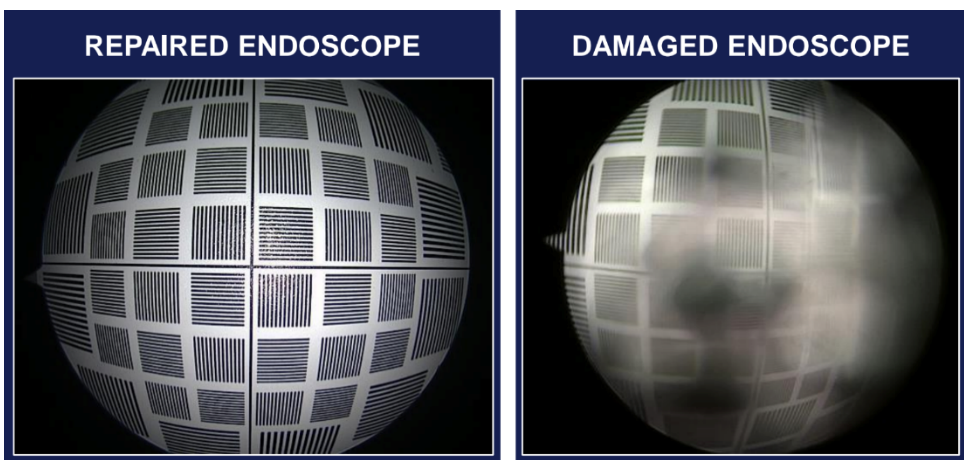

Figure 3: Representative image showing a properly repaired visual of an endoscope on the left compared to a damaged endoscope on the right reproduced as is from D-Term team [1]

Assessing bends in endoscopes involves the measurement of runout, cylindricity, and straightness. Runout measurement entails quantifying the deviation of a rotating component from its ideal axis of rotation [6]. Factors contributing to runout include misalignment, bearing wear, or manufacturing imperfections.

The existing technique for straightening endoscopes relies on visual measurements. Technicians compare the endoscope to a diagram featuring three straight lines, a central line with a 2.5 mm offset on each side. Figure 4 below displays the straightening rig and reference board with three straight lines that HSWoA uses as a backdrop to determine if endoscopes are considered straight or bent. An endoscope is placed in line with the center of the three lines and is considered straight if it remains between the outer two lines along its entire length. If the endoscope bends beyond the parameters of the outer two lines, it is classified as bent. An example of a bent endoscope commonly received and straightened by HSWoA is shown in Figure 5. Straightening endoscopes is performed manually as shown in Figure 6 below. The technician employs personal estimations to gauge the extent of bend in the endoscope. Ensuring the precision of this method poses challenges because it is subjective and dependent on individual judgments. This method's estimations do not consider factors such as the actual flexibility of the endoscope or variations in anatomical structures, leading to potential inaccuracies in the straightening process.

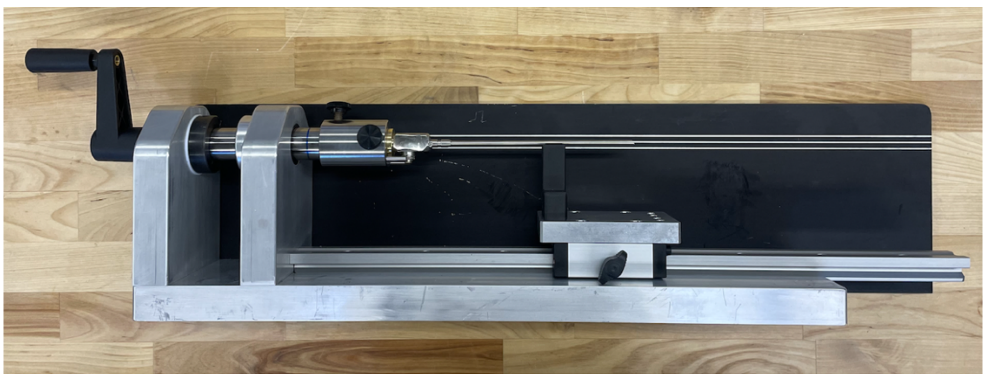

Figure 4: Straightening Rig with Loaded Endoscope and Reference Board Currently Used by HSWoA (Steriti, S. 2023).

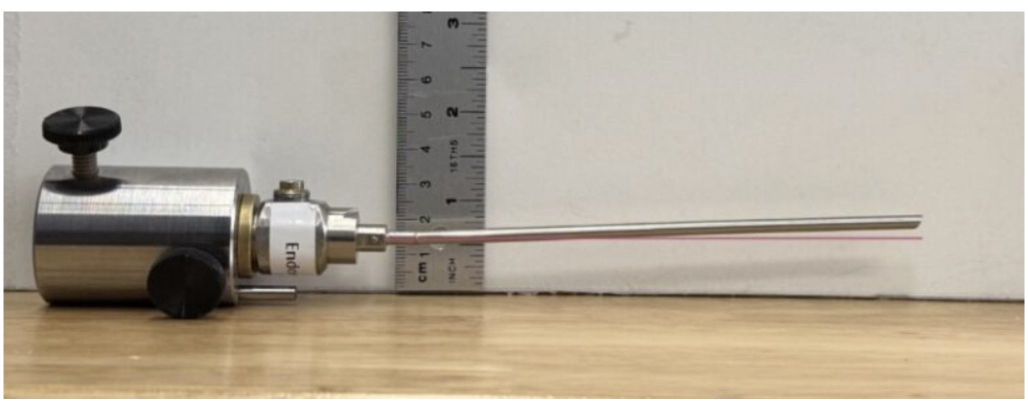

Figure 5: Bent Endoscope that Requires Straightening (Pradhan, P. 2024)

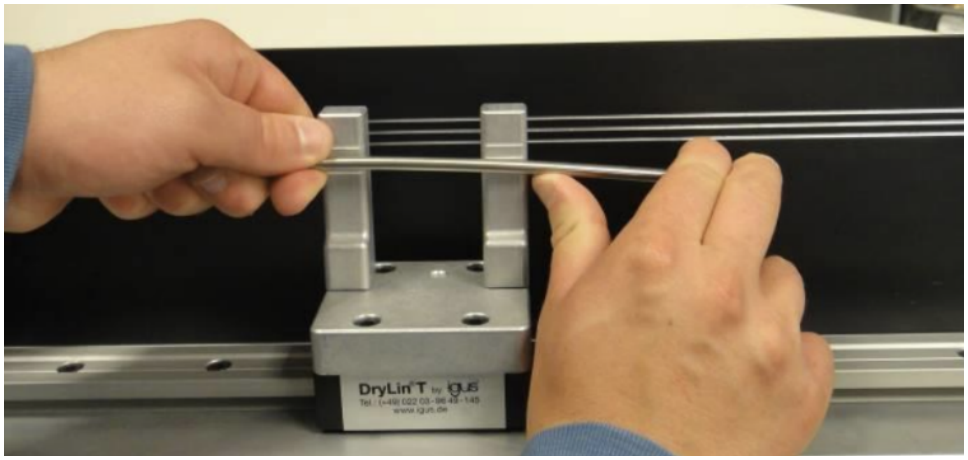

Figure 6: Current Endoscope Repair Method Used by HSWoA.

The team worked to tackle the issue of the current manual runout correction procedure for endoscopes, which relies on subjective visual measurement and manual adjustments, leading to inconsistency and time consumption. The team's objective was to create and validate designs for an advanced runout correction system for HSWoA that reduces human intervention to a minimum while delivering faster and more precise results compared to existing methods. Employing a mathematical approach that integrates an autonomous straightening system with computer vision data will enhance the accuracy of the endoscope straightening process. This involves capturing an image of the initial bend in the endoscope, applying a calculated force through rollers to straighten the endoscope, and validating the results by capturing another image of the successfully straightened endoscope.

1.1 Problem Statement and Objectives

The primary goals of this project to create a system to accurately measure and straighten endoscopes were to:

- Develop an autonomous measurement system with the capability to precisely identify the positions and angles of deflection in bends within rigid endoscopes of varying sizes.
- Design and implement a straightening device to effectively correct bends, restoring the original straight configuration of rigid endoscopes.
- Implement a rigorous verification process to guarantee the precision of the straightening procedure for each endoscope.

1.2 Report Overview

The report is organized as follows:

- Chapter 2 presents background information, initial research, and context for understanding the entirety of this report, such as the team's inventory of endoscopes, HSWoA's current straightening processes, and research on terminology including runout and cold rolling processes.
- Chapter 3 presents the contributions of students on the ME4320 course teams who started this project in Spring 2023 and includes essential analysis and concepts used as this team's foundation for this project. This chapter highlights the contributions of both the D-term 2023 and B-term 2023 ME4320 course teams.
- Chapter 4 presents the general methodology performed by the team by overviewing the mission statement, objectives, and requirements of this project, as well as accomplishments made by term.
- Chapter 5 presents the steps performed to define and test the team's measurement system, including calibration processes, endoscope detection, runout calculations, and code testing, final measurement code, camera selection information, etc.
- Chapter 6 presents an overview of the station, the station requirements, endoscope mount selection information, and measurement station parts specification for a background mount.
- Chapter 7 presents details of the straightening device, including the forces required, finite element analysis for verifying minimum required forces, and additional component specifications and details.
- Chapter 8 presents the team's electrical system configuration and overviews the microcontroller selection process, as well as both the respective measurement and straightening electrical systems.
- Chapter 9 presents the team's testing procedures and results in areas including the measurement station and code, electrical systems, straightening code and device, and the combined system code.
- Chapter 10 presents a discussion of the achieved requirements and the broader impacts of this project.
- Chapter 11 presents the conclusions drawn from this project, the team's recommendations for future improvements of the overall system, and individual reflections written by each team member.
- Chapter 12 presents all sources referenced throughout the completion of this project.
- Chapter 13 presents appendices with additional information to fill any remaining gaps in readers' understanding of this project.

2 Background

This chapter presents the research gathered and steps taken at the beginning of the 2023-24 academic year to provide the necessary foundation for this project. The chapter outlines details of the endoscopes provided to the team by HSWoA, the current procedures for straightening endoscopes at the HSWoA facility in Massachusetts, an explanation of runout, and cold rolling process research performed by the team.

2.1 Endoscope Inventory

HSWoA provided the team with several endoscopes of various lengths and diameters to begin testing. The inventory log that the team created to track all the endoscopes and create labels for each one can be found in Appendix A. This log records aspects such as each endoscope's diameter (in mm), total length (in cm), stem length (in cm), number of bends (measured visually), current location, and additional notes. The following image, Figure 7, shows the various endoscopes the team was given, which were labeled 1-17.

Figure 7: Endoscopes Provided by HSWoA for Completion of this Project (Pradhan, P. 2024) [1]

2.2 Materials

The construction of endoscope tubes and bodies predominantly uses 1.4301 Stainless Steel, a variant of 304 Stainless Steel (SS). This material exhibits exceptional resistance to corrosion at elevated temperatures, possesses weldability, malleability, high toughness, and ductility. The utilization of 304 SS is favorable due to its corrosion resistance, a paramount quality given the need for hygiene in medical applications. However, the material's high ductility makes endoscopes susceptible to developing runout during usage. 304 SS has a yield strength of 226.3 MPa and a tensile strength of 579.5 MPa at a temperature of 20°C. The ultimate stress point for 304 SS is 579.5 MPa. Beyond this point, the material experiences permanent and irreversible deformation, leading to fracture or rupture. During use of the endoscopes, there will typically be forces between 226.3 and 579.5 MPa acting on each one used, which causes slight plastic deformation in the shaft. The following graph, shown in Figure 8, displays a strain (in mm/mm) versus stress (in MPa) curve of several types of stainless steel, which the team performed initial research on [7].

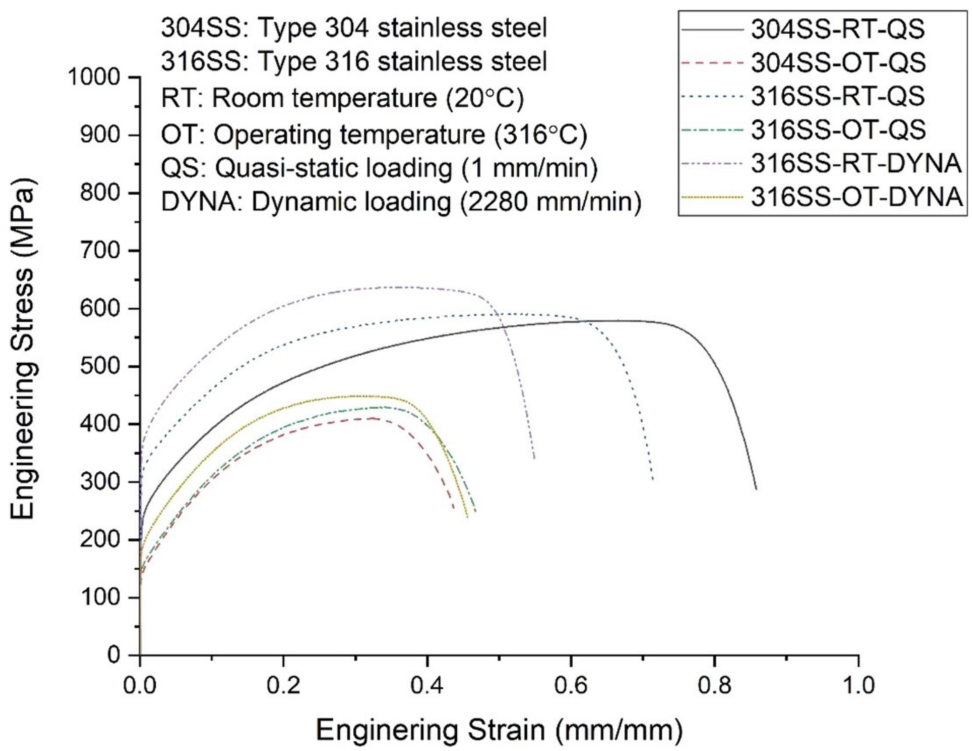

Figure 8: Strain vs. Stress Curve of Several Types of Stainless Steel (Reproduced as is from [7])

The straightening mechanism employed in endoscopes introduces cyclical loading to the stainless-steel material, creating a potential long-term issue related to material fatigue. Material fatigue, a consequence of prolonged cyclical loading, gradually diminishes the steel's yield strength, ultimately leading to fracture, even when subjected to forces below the original yield strength. The continuous bending and fixing involved in the straightening process contributes to the development of fractures, even when forces applied are well below the stainless steel's yield strength. The straightening process ensures that stresses remain within manageable limits, and the cyclical loading, though present, is of a minor magnitude.

2.3 HSWoA Current Straightening Rig

HSWoA currently uses a simple design consisting of an endoscope held between two metal walls by shaft collars and roller bearings. A manual hand crank is attached to the end to rotate the endoscope. Attached to the side of the device is a metal plate engraved with three lines that represent the boundaries of what is considered straight or not by the HSWoA. The top and bottom lines are spaced 4.5 mm apart, with the middle line perfectly centered. Figure 4 (shown in the introduction) shows the straightening rig with a loaded endoscope and reference board currently used by HSWoA. This setup is currently used by an operator who looks at the endoscope at eye level and rotates the endoscope using the crank. The operator looks for occasions where the endoscope bends past the top or bottom line. The operator then uses their hands to manually bend the endoscope back into place.

2.4 Current Endoscope Repair

HSWoA's current process for endoscope repair relies heavily on manual human intervention. The procedure involves placing the endoscope within a fixture that aligns it within three reference lines. To straighten the endoscope, first the brass adapter is attached to the proximal end, ensuring it fits securely. Then, fix the appropriate hub onto the needle run-out fixture spindle using the knob set screw. Different hubs accommodate various endoscope sizes to ensure concentric rotation. Insert the brass adapter (with the endoscope attached) into the hub and secure it with the knob set screw, ensuring correct orientation. The operator identifies runout by observing the deflection on the scales. To locate bends, slide the scale towards the distal end until the needle deviates from the center line. Rotate the outer tube to align the needle with the run-out scale and gently bend it towards the center line. This process is repeated until all bends are corrected, and the needle aligns with the center line. Figures 5 and 6 (displayed in the introduction) show a bent endoscope in the straightening rig that requires straightening, and the current endoscope repair method used by HSWoA. This approach to straightening endoscopes is inherently imprecise and lacks standardization.

2.5 Runout

Runout is defined as "the shaft is spinning on an axis of rotation that is offset from the geometric center of the shaft at the point of seal lip contact" [6]. This measurement provides control ratio for circular objects. Figure 9 below demonstrates shaft runout. Shaft runout is how much a shaft deviates from its circular rotation. Every shaft has a center of rotation called its centerline, and any variance from this centerline is considered shaft runout. In medical devices, runout may cause inaccurate placement or alignment, leading to issues like tissue injury or implant failure. To ensure medical devices are safe and effective, it is crucial to accurately measure and control runout.

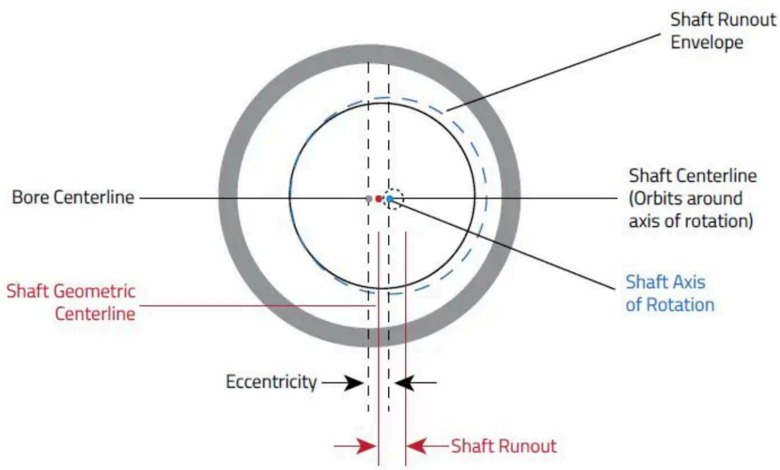

Figure 9: Shaft Runout (Reproduced as is from [8])

2.6 Cold Rolling Process

Cold rolling is a manufacturing process used to straighten metal sheets or strips. In this process, the metal is passed through a pair of rollers at room temperature, exerting pressure to straighten bent sheets. The rollers can be cylindrical or shaped to impart specific profiles or textures onto the metal surface. As the metal passes through the rollers, it undergoes plastic deformation, causing the grains within the material to elongate and orient themselves parallel to the direction of rolling. Cold rolling can be performed as a single-pass or multi-pass process [8].

This chapter discusses details of the endoscopes the team used for testing the prototype developed throughout this project, current procedures for straightening and repairing endoscopes at HSWoA, research on runout and its definition and research on cold rolling processes. The next chapter will discuss the contributions of the ME4320 course teams including the D-term 2023 teams, concept generation and runout measurement, that established the initial concepts for the MQP team as well as the B-term 2023 straightening system team.

3 ME4320 Course Contributions

This chapter details the contributions made to this MQP by the runout measurement, concept generation, and straightening system ME4320 course teams. The D-term teams developed initial prototypes that the MQP team used as a foundation for this project. The B-term team developed the straightening device that would eventually be integrated into the station.

3.1 D-Term 2023

The project began in the spring of 2023 with thirteen students under Professor Pradeep Radhakrishnan. These students are divided into two different sub-teams: runout measurement and concept generation. An additional team assisted on this project in the fall of 2023 with six students under Professor Pradeep Radhakrishnan. These students developed a prototype of the straightening device and a prototype system for the measurement system. The D-term teams were about to successfully narrow down multiple methods of achieving the project requirements through research, rapid prototyping, and initial testing. Due to their efforts, the MQP team had a baseline example for the concepts that when realized would result in success for the project.

The D-term teams made significant progress but failed on a few fronts. The straightening team was able to create a prototype of the roller system in which the rollers simulated the way they would engage with the endoscope in a finalized design. This prototype worked well, but its main failures were the uses of human actuation for the rotational and axial movement of the endoscope within the rollers. During this prototype's testing, some trials showed more control over the speed and number of rotational and axial movements within the system than others. Recreating a system that could accomplish the same movements and parameters used by the team proved to be extremely difficult. The second failure was similar. In this prototype, a Mecmesin MultiTest 2.5 dV Test System was used to all force to the upper roller, depressing it to engage with the endoscope. This worked well for the prototype because it was a modular system, but based on their testing it would be difficult to create a machine that can apply a measured force of the same magnitude in the same way if the design were used as it was. This method was ultimately deemed unsuccessful as it caused permanent deformation to endoscopes due to the force produced being too high [9].

The runout measurement team was able to develop a system that could create a point cloud of an endoscope using a webcam. The main failure of this design was the lack of information this point cloud provided; it provided just a visualization of the endoscope. There was no method to process and evaluate the point cloud to determine the numeric runout measurement of the endoscope and it relied on visual confirmation of looking straight at it, which is not something that could easily be taken and expanded on [10].

Based on the D Term teams success and failures, some primary takeaways are the use of the cold roller process opposed to 3-point bending or some third option when selecting a method for physically straightening the endoscope. Due to the amount of testing as well as research the D-term team was able to execute, it was clear which method efforts should be focused on and to further design going forward. This allowed the team to work primarily on conceptualizing the system design that would best house and execute the cold rolling process, as opposed to losing time evaluating the reliability of the process to extensive testing. Similarly, based on the runout measurement team's prototype and results, it was determined that computer vision would be one of the methods pursued. Based on the recommendations and results, it was decided that Python would be used for processing and capturing images opposed to MATLAB. It was also determined that other methods of detecting bends in endoscopes would be researched aside from computer vision [9,10].

3.1.1 Runout Measurement Team

The runout measurement team focused on developing a camera-based measurement system. Their objective was to create a device capable of measuring the locations and degrees of bends in a medical endoscope tube. The collected data should be compatible with the methods devised by the concept generation team to correct the measured bends. This team determined accurate camera-based measurement relies on proper configuration of lighting, camera position, and resolution. Options for lighting include using a reflector or diffusor, while ensuring the camera angle is straight on with the piece and either perpendicular or parallel to the rig. The motor was affixed to the rig and linked to the endoscope holder using pulley gears and a belt. Additionally, the camera mount was designed with steel rods for elevation and secured in place using 3D printed brackets. Steel rods were also utilized to create bushings for holding the reference rods during accuracy testing. The ME4320's design rig, shown in Figure 10 below, integrates MATLAB, an Arduino, a stepper motor, LED strips, acrylic with a light diffuser, and a camera. MATLAB runs the program to determine the angle, location, and degree of bends in the endoscope, which is then transmitted to the straightening team. The camera operates through MATLAB, while the Arduino rotates the stepper motor. LED strips provide backlighting for the endoscope, and a sheet of diffused acrylic is placed underneath. Prior to measurement, the software calibrates the camera using a checkerboarded panel to establish real-world values. It detects the edges of the checkerboard squares and references them when identifying the location of endoscope bends. The collected data is presented as a 3D model of the endoscope for interpretation and use by the straightening team [10].

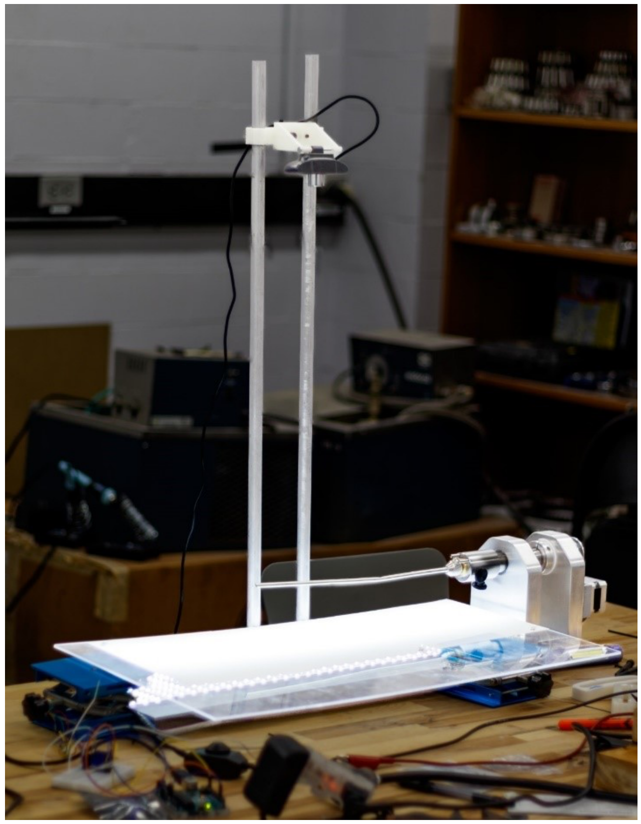

Figure 10: Assembled Endoscope Runout Measurement Rig Used by the D Term 2023 ME4320 Course Teams [Piccione, T. et al. 2023]

Conducting multiple tests is essential to determine optimal conditions by comparing measurements obtained with an image-based device to a known measurement. Computer vision is used for calibration numbers for distorting images and detecting and analyzing endoscope nozzles. In their completed device designed for measuring runout in bent endoscopes, shown in Figure 10, key components include a microcontroller, a camera, and a motor. The camera and lenses play a pivotal role in capturing precise measurements, and the stepper motor provides precise control over speed and positioning. To obtain initial measurements, the ME4320 team utilized Tracker Pro software. They tracked the endoscope's edge location precisely as it rotated, simulating the process using MATLAB image processing. Additionally, experimentation was done with various lighting conditions to determine optimal image outcomes, including diffusers, reflectors, and both frontal and backlighting. It was discovered that backlighting with a diffuser yielded the best results. Several tests were conducted to ensure the device's accuracy. Standardized steel rods with known bends were created to compare measurements obtained from the software. To verify the stepper motor's speed alignment with the programmed code, the team timed its rotation five times and calculated the angular speed. Different camera heights and resolutions were tested to identify the most accurate combination. Calibration of the camera was achieved using a checkerboard with real-world unit measurements printed on a 1cm-by-1cm sheet. The camera detected the length of the boxes and utilized this data to collect information from the endoscopes. While the camera calibration was a useful method, this team had a mean error per 20 taken images for camera calibration of 1.18 pixels [10].

In the current setup, the team utilized various components from the ME4320 team, including camera vision, checkerboard calibration, LED lighting, similar motors and motor controllers, and adjusted the general camera position for conducting measurements. However, aiming to enhance accuracy, the team made significant improvements. They transitioned to OpenCV and upgraded to a 4K resolution camera. Moreover, they implemented a black box to control lighting, ensuring LED panels are the sole light source in the station. The ME4320 team recommended using an LED panel to backlight the endoscope in the rig. They believed that a pre-manufactured LED panel would be more durable and provide easier maintenance. Through testing, the team found that side light produces more accurate results. While a premade LED panel did provide appropriate light conditions, its large and inflexible nature was unable to be incorporated into the station. Due to this, the team made custom LED panels with LED strips attached on acrylic siding. The ME4320 team also recommended utilizing Python software for program execution and stepper motor control. Several issues arose with MATLAB usage, which, although fixable, consumed significant time and effort. These challenges could have been mitigated by employing Python, which offers an open-source software library called OpenCV. The team found success in implementing this recommendation. OpenCV and Python were used to develop endoscope detection software and produced readings with accuracy of 0.5 mm [10].

3.1.2 Concept Generation Team

The concept generation team focused their research on two methods: the 3-point bending method and the oblique rollers. Their objective was to devise validated designs for a new runout correction system for HSWoA that minimizes human involvement and delivers faster and more precise outcomes compared to existing approaches. The collected data should be compatible with the methods devised by the Runout Measurement team to correct the measured bends. They determined accurate straightening relies on proper configuration of force, endoscope rotation, and sweeps [9].

The 3-point bending method utilized the Mecmesin MultiTest 2.5 dV Test System. The ME4320 team believed that this method would seamlessly integrate with the runout team's measurement tool, automating the correction process, and ensuring precise adjustments. Its universal application for all endoscope sizes is facilitated by pushing forces. of pushing forces. The machine can receive input directly from the measurement team, consisting of coordinates of maximum deformation and orientation, enabling real-time correction without any downtime. The expectation is for the machining process to take no longer than 1 minute, ensuring efficiency. The machine’s accuracy is ensured by its ability to reverse bends based on known deflection data. Basic components required include actuators, DC and stepper motors, and horizontal rails [9].

The team implemented a method where a perpendicular force was applied to a stationary endoscope, as depicted in Figure 11 below. Using a manual runout device, they identified areas with significant bending by rotating the endoscope and aligning those points with the force application. Then, they input the displacement variable, causing the machine to exert force until the desired distance was achieved. This approach successfully corrected bends and straightened the runout. Subsequent testing showed significant improvement, reducing maximum deflection from 15.428 mm to 2.833 mm, an impressive 81.64% change. However, this method caused permanent deformation of the endoscope, leading to concerns about potential damage. Therefore, the team recommended discontinuing its use and instead suggested employing the oblique roller method for straightening devices [9].

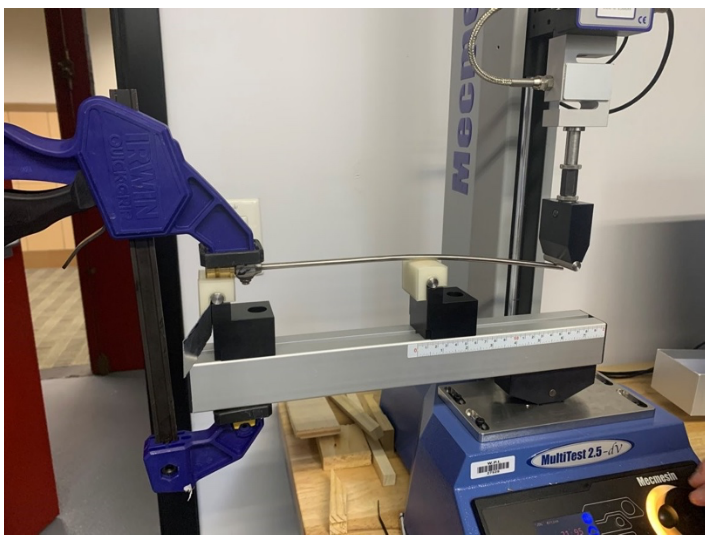

Figure 11: Cantilever 3-point Bending Testing Performed by the D Term 2023 ME4320 Course Teams [Boisvert, M. et al. 2023]

The oblique roller design incorporated an enlarged acrylic housing, providing a stable base for the endoscope and ensuring even force distribution, as shown in Figure 12 below. The team determined a key benefit of oblique rollers that it ideally requires only one pass through the rollers to correct any runout, making the process fast and efficient. Additionally, runout data isn’t necessary which simplifies the process. It can accommodate all endoscope sizes by adjusting the roller height, but manual setup, including adjusting roller height and fixing the rod, may be challenging to automate. By replacing PLA pins with threaded steel rods, the team not only increased strength, preventing crushing, but also enabled the use of nuts for roller security. Subsequent testing revealed promising results, with the straightening method reducing the maximum deflection from 8.155 mm to 3.040 mm, reflecting a significant 62.72% improvement. The team found the roller design to be most effective for straightening. However, it was found that at least 10 sweeps were required to straighten endoscopes instead of the suggested one. The team used stepper motors and a lead screw to apply force through the rollers, incorporating the force application from the three-point bending method [9].

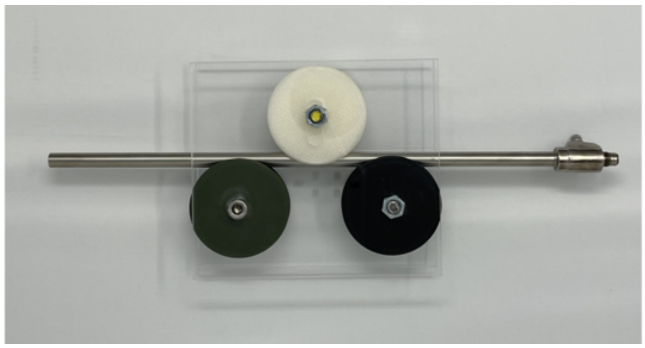

Figure 12: Oblique Rollers Created by the D Term 2023 ME4320 Course Teams [Boisvert, M. et al. 2023]

This team determined the optimal approach is a hybrid design. This design combines an enhanced linear roller system with the integration of three-point bending, enabling comprehensive repair of both proximal and distal ends of the endoscope. The decision is based on the feasibility of applying and automating the roller concept, which is straightforward. While the linear roller method has limitations near the welded fixture or at the far end, incorporating elements from the three-point bending method mitigates these shortcomings, allowing effective repair at any location along the endoscope. The hybrid design sacrifices the simplicity of the linear roller method, requiring precise measurements and calculations to move the machine both along and perpendicular to the rollers for accurate correction at either. The team also conducted numerical quantification of the spring back, as recommended by the ME4320 team. Spring back refers to the tendency of a material to return to its original shape or form after being subjected to deformation. Accounting for spring back and compensating for it during the straightening process is essential to ensure the desired outcome of a fully straightened endoscope. The team applied an additional downward distance of 8 mm from the center of the endoscope to account for spring back [9].

3.2 B-Term 2023

The previous team focused on refining and automating the linear roller design for a straightening device, initially developed by the D term ME 4320 team. Their primary goal was to enhance the functionality of the roller system for straightening endoscopes, ensuring it met several critical design requirements. These included keeping the endoscope stationary while the rollers moved linearly onto it using motors, accommodating a range of endoscope sizes from 1.9 mm to 10 mm in diameter, and ensuring the entire straightening process did not exceed two minutes.

In the design phase, the team created a CAD model which satisfied the straightening device requirements. They later divided the design into two main categories for more focused development: the roller system and the base plate. Initially, the roller assembly featured a dual baseplate system with small rollers positioned between them, connected to a C-Beam linear actuator for movement. However, they realized that the smaller rollers were insufficient for larger-sized endoscopes. Consequently, they replaced them with larger rollers and switched from cylinder actuators to stepper motors with lead screws for more precise control of roller positioning.

The previous team had several issues with the straightening device that impacted its performance and reliability, primarily due to mistakes in the design and lack of proper parts. One significant issue was the lack of rigidity in the assembly. The assembly's inability to maintain structural integrity under operational stress often led to uneven pressure application during endoscope engagement, which is critical for effective straightening. This fluctuating engagement with the endoscope could potentially damage the endoscope instead of straightening it. Another problem arose from the rollers not being able to rotate freely, a flaw that was traced back to a mistake in the CAD design. This likely originated from incorrect specifications or tolerances in the roller mounts or the mechanisms intended to control their movement. Consequently, the rollers did not maintain their intended positions during operation, reducing the effectiveness of the straightening process and complicating the adjustment to different sizes of endoscopes. Addressing these problems would involve revisiting the CAD design to rectify the free rotation of the rollers and enhancing the rigidity of the assembly to ensure stable and consistent engagement with the endoscope.

3.2.1 Motor Control

There are a variety of motor drivers and modules that can be used to control stepper motors, chosen based on current requirements and restrictions. The B-term ME 4320 team used 2 1.2A NEMA 17 stepper for the up and down actuation of the rollers. And NEMA 23 stepper motor connected to the lead screw for horizontal movement. For this, the TMC2208 motor driver controlled via with an Arduino Uno, later changed to an Arduino Mega when more digital ports needed to be unitized. Initially prototyping made the use of a breadboard for connecting between the pins of the Arduino mega and the TMC2008 motor driver, later iterations found that TMC2208 modules were soldered to prototyping boarding to allow for higher from the power supply to power the motors.

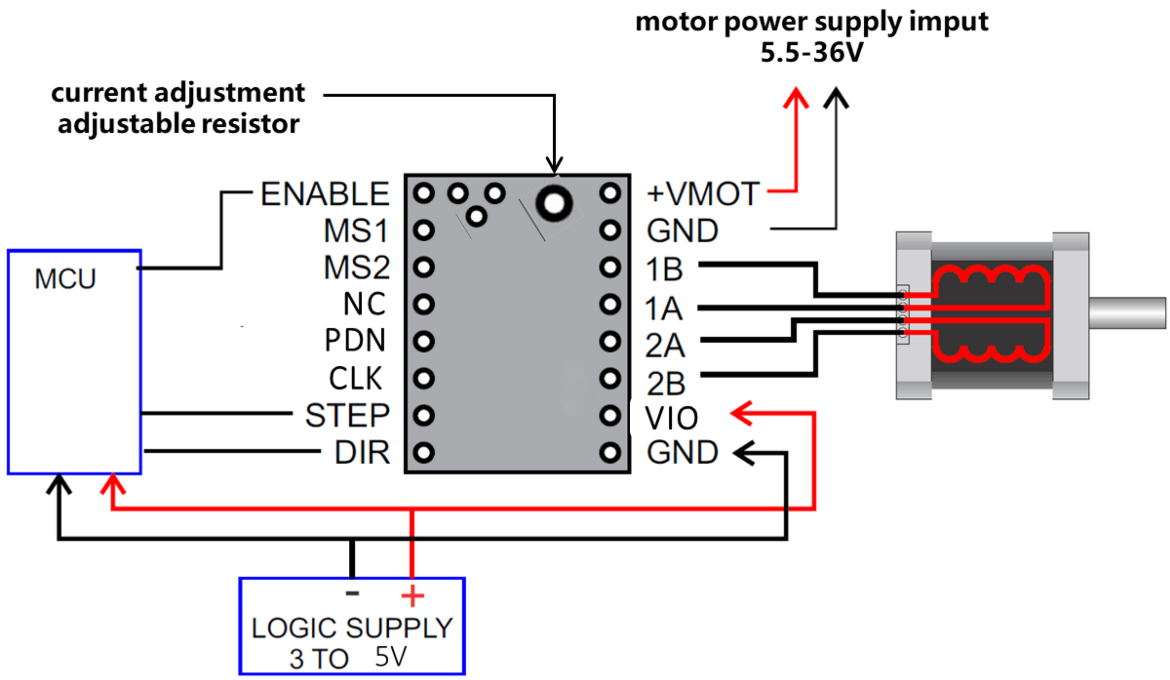

Figure 13: Wire Diagram of TMC2208 (TMC2208 - FYSETC WIKI)

While the TMC2208 was the initial motor driver used, due to it having been the same motor driver used by the ME4320 D term runout measurement team. After more research was conducted the team selected the is motor ks42sth40-1204a motors NEMA 17 motors for actuation of the upper and roller rollers which engage with the endoscope. The KS NEMA 17 motors are 2V with 1.2A per phase stepper motors with a holding torque of 4N.m. The selected stepper for the horizontal movement of the system was the NEMA 23 motor ht23-180-8. Which was an 8 wire 2.5A stepper with 185 N.m holding toque. These stepper motors required a higher output current than the TMC2208 could produce and a higher input current than the TMC2008 could handle which led to one of the modules being damaged during testing. After this the D Term ME4320 switched to using the TB6600 motor driver based on the suggestion of the MQP team members. The power supply was also updated to a 30V 24A switching power supply for the NEMA 17 motors and a 12V 30A power supply for the NEMA 23 motor controlling the horizontal movement of the straightening assembly.

Based on the design that they created the subsystem consisted of 3 stepper motors, two NEMA 17 ks motor ks42sth40-1204a motors and a NEMA 23 motor ht23-180-8. A TB6600 motor controller was used for each motor and that connected to an Arduino Mega. Powering the NEMA 23 motor was a 12V 30A switching power supply while the NEMA 17 motors and driver were powered by a 30V 24A switching power supply. Once again, the Arduino Mega is powered via the USB connected to a laptop. Due to the necessary serial connection between the Arduino Mega and the Python environment of the endoscope correction program, a separate power supply was used.

The motor control program initially created for measurement was expanded to work for multiple motors. The MQP team worked with the ME 4320 B term team to a version of the straightening code which would control the straightening system with direct user inputs for parameters such as the endoscope length and diameter. User inputs were used because the working areas of the measurement subsystem and the prototype straightening system created by the ME 4320 B term team could not be combined. The exact methods in which the program sent data from Python to the Arduino mega are explained in section 7.8.3. The basic function of the program was as follows. The straightening device, mounted on the horizontal carriage, would begin located at the front of the station. The carriage would move the straightening device the length of the system to the beginning of the stem of the endoscope. Once the carriage stops the upper roller would lower while lower roller rises a distance based on the diameter of the endoscope, in order to clamp onto the endoscope. Once the endoscope has been engaged the horizontal carriage will move back and forth along the length of the endoscope a number of times defined by the user. After completing the back and forth motions the rollers will disengage and the straightening devices will be moved back to the front of the system by the horizontal carriage. The straightening devices begins and ends at the front of the system in order to avoid detection by the camera during the measurement process. In the finalized version of the system created by the MQP team the endoscope parameters is be passed to the straightening code from the computer vision based analyses of the measurement code.

This chapter provides an explanation of the significant contributions made by the ME4320 course teams that established the foundation of this project for the MQP team and detailed how they positively impacted this project. The next chapter will discuss this project's general methodology, including the team's mission statement, objectives, requirements, and accomplishments made by term over the academic year.

4 General Methodology

This chapter presents the mission statement, objectives, and requirements of the project and an overview of each term's accomplishments. It also outlines the team's general structure throughout the academic year and the final prototype's guiding principles during its development.

4.1 Mission Statement

This project supports the efforts of Henke Sass Wolf of America to develop innovative solutions in medical endoscopy. The team developed a semi-automated device designed to measure bends in rigid endoscopes and subsequently rectify them based on the data acquired. This was achieved by implementing a participatory design process and developing an innovative measurement and straightening method.

4.2 Objectives

The team strived to accomplish the following objectives throughout this project:

1. Evaluate existing endoscope straightening and measurement procedures to identify areas for improvement.
2. Develop a functional and reliable automated device prototype capable of accurately measuring bends and straightening rigid endoscopes.
3. Utilize stakeholder feedback to refine and adjust the prototype as needed to ensure the device meets user needs and industry standards.
4. Conduct thorough testing and validation procedures to verify the functionality, reliability, and safety of the device under realistic conditions.

4.3 Requirements

The team identified essential design criteria and desired features that would enhance the system, as shown in Table 1 below. All requirements aimed to assist the objective of the project, automating the medical endoscope repair process to enhance accuracy and efficiency. Defining the design requirements provided a structured framework that guided the entire design process.

Table 1: Project Design Requirements

Need	Measure the bends in endoscopes within 10-20 seconds
	Measure the bends in endoscopes with an accuracy of 0.5 mm
	Straighten endoscopes using rollers in under one minute
	Straighten endoscopes using rollers with an accuracy up to 1.0 mm
	Straightening station location must be situated internally
	Ensure compatibility with medical-grade rigid endoscopes ranging in diameter from 2.7 to 5.5 [mm]
	Ensure compatibility with medical-grade rigid endoscopes ranging in length 6.9 to 45.7 [cm]
	Light sources are required on both sides of endoscopes
	Background against which measurements are taken should be white a matte finish
	Cable management solutions to keep the setup organized
	User-friendly interface or software
	The design of the straighening device must not damage the endoscope
	External parts have stable attachment with main station
	Safety features
Want	Ergonomic factors to provide comfort.
	Mounting options available for accommodating different types of endoscopes
	Modular design of station
	All fixtures and included components can be easily cleaned and serviced

The developed station was designed to meet critical requirements for optimal functionality in the research environment. The sponsor, HSWoA, defined that the project should improve the current endoscope straightening process. They requested the measurement to be conducted in 10-20 seconds with an accuracy of 0.5 mm and straightening was completed in under 1 minute with an accuracy of 1.0 mm. The developed station features a designed straightening device that will not damage the endoscope due to spring back calculations. Safety features were integrated to safeguard operators and equipment, while a user-friendly interface promotes ease of use. By adhering to these requirements, the developed station aims to enhance accuracy, productivity, and overall effectiveness.

4.4 Accomplishments Completed by Term

This section outlines the accomplishments the MQP team made by term over the course of the 2023-24 academic year.

4.4.1 A Term

During A term, the team concentrated primarily on reviewing and comprehending the work completed by the D-term 4320 class. The team labeled the endoscopes and devised an initial plan for designing the station. This station would need to be capable of measuring essential information about the bendiness of the endoscopes, as well as straightening them based on the proof of concept developed by the D-term teams, which utilized the cold roller system.

4.4.2 B Term

Over the course of B term, the team was focused on assembling the measurement station using the developed CAD models of all the system's parts and assemblies in SolidWorks to verify measurements during station construction. The team also conducted a large amount of testing on the measurement aspects of the station and validated the team's calibration procedures for the camera system by proving consistency throughout testing. Additionally, the team mentored the B-term ME4320 course team, as they developed a straightening device alongside the MQP team's development of the measurement system and entire research station.

4.4.3 C Term

During C term, the team was focused on preparing for the integration of the straightening device developed by the B-term ME4320 team into the research station. The team worked on additional research for meeting all requirements and performed analysis to prove the system could handle all necessary loads and operate effectively. The team completed the final CAD assembly of the entire station, planned the wiring/electronics system, and made a purchase before beginning re-assembly of the station.

4.4.4 D Term

Throughout D term, the team was focused on completing the integration of the straightening device into the station and testing the system's capabilities to verify its accuracy. The team adjusted the final CAD assembly, reprinted a few parts, and reassembled parts of the station throughout testing. With a new batch of endoscopes, the station was tested to ensure it was measuring the diameters and lengths of all endoscopes correctly. Testing was also performed to ensure the maximum runout of the endoscopes was accurate and to determine how straightened they became (how much the runout decreased). Additionally, the team worked on compiling a combined system code, prepared for the 2024 Undergraduate Research Project Showcase (URPS), and worked on pulling the final report together.

This chapter presents this project's mission statement, objectives, requirements, and an overview of accomplishments completed by the team each term. This chapter outlined the primary goals the team strived to achieve, and the requirements successfully accomplished throughout this project. The following chapter overviews the steps the team took for carrying out endoscope measurement processes including the consideration of using LiDAR, calibration processes, crafting ideal light conditions, endoscope detection methods testing, calculating runout, and creating the final measurement code.

5 Measurement of Endoscopes

The previous team used several tools and methods to calibrate the camera and measure the bends in the endoscope. MATLAB controlled the camera to capture images of the endoscope, which was backlit by LED strips and positioned on diffused acrylic to enhance image clarity. For calibration, they used a checkerboard panel, which allowed the software to adjust the camera settings based on the known dimensions of the checkerboard squares. The resulting data was then converted into a 3D model for the straightening team to use.

The chapter includes detailed information about initial research on using LiDAR, calibration processes, testing for the most optimal light conditions needed within the enclosed prototype, endoscope detection methods testing, calculating runout, camera selection, etc.

5.1 LiDAR Consideration

LiDAR stands for light detection, and ranging is a method for calculating distance. It works by beaming a laser, which will reflect off the target object and return to the sensor; the distance between the target and the LiDAR module is then calculated based on the time of flight of the beam. Time of flight sensors are similar to smaller-scale modules that do the same thing. A method of measuring the runout of endoscopes using LiDAR was initially explored alongside testing for computer vision. For implementation of the LiDAR measurement, the sensors would be positioned so that the laser would hit the center line of the endoscope. The endoscope would rotate 360 degrees while the LiDAR data is recorded. If the endoscope is straight the distance measured by the LiDAR module would be consistent across the rotation time. A larger distance would mean the endoscope is bending away from the sensor and a smaller distance would mean the endoscope is bending towards the sensor. The runout can then be calculated by comparing the maximum distance to the expected distance, had the endoscope been straight.

5.2 Introduction to Endoscope Measurement Processes

In the world of computer vision, calibrating a camera is a critical step that helps to improve the accuracy and reliability of the images it captures. This report outlines the implemented process of camera calibration, which is essential for correcting lens distortions and accurately mapping the pixels in an image to real-world dimensions. The calibration process helps to get more accurate camera readings. The team will walk through each step of this process, starting with setting the calibration criteria, preparing object points, and moving through image acquisition, corner detection of the chessboard, corner refinement, the calibration itself, calculating pixels per millimeter (PPMM), and finally storing the calibration results. Figure 14: OpenCV Calibration Chess Board below shows an example of a chessboard the team used in tests. The goal of this chapter is to provide a clear understanding of how implemented camera calibration is performed and why each step was important, using a practical approach that leverages multiple images of a chessboard pattern. Let’s dive into the details of each phase in the calibration process to see how it contributes to achieving precise and accurate camera calibration [11].

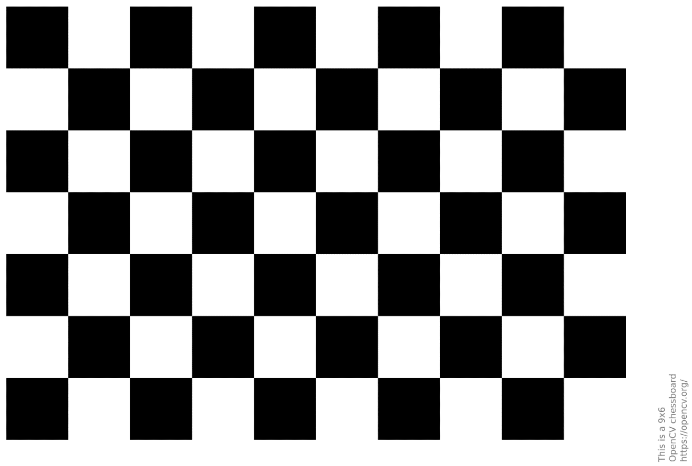

Figure 14: OpenCV Calibration Chess Board

5.3 Calibration Process Steps

Setting Calibration Criteria: At the beginning of the camera calibration process, it is important to establish clear criteria for the accuracy of corner detection. This means making sure that the corners of the chessboard seen in the images are identified with great precision. This step is crucial because accurate corner detection is the foundation of reliable camera calibration. The goal is to ensure that each detected corner of the chessboard in the photographs matches the actual corner as closely as possible, allowing for a high-quality calibration.

Preparing Object Points: In this phase, “object points” are created. These points represent the 3D coordinates of the chessboard corners as they exist in the real world, but in a perfect, idealized form. Think of these points as the exact spots where the corners should be if everything were perfectly measured. These object points are vital for the calibration process because they act as a standard or reference point that the camera’s images can be compared against [12].

Image Acquisition and Pre-processing: During this stage, the system looks through a specific folder for images that match a certain name pattern and file type. Once an image is found:

- It is loaded into the computer’s memory so it can be worked with.

- The image is turned into grayscale, which means it is converted into shades of gray. This step is done because working with one color (gray) makes it easier to spot the chessboard corners than working with full-color images.
- The system notes down the size of the image, which is important for understanding how the camera sees and captures space.

Chessboard Corner Detection: After turning the images into grayscale, the next task is to find the inner corners of the chessboard within these images. These corners are crucial because they are used as “image points” in calibrating the camera. This step is about identifying specific points in the image that correspond to the corners of the chessboard, which are then used to understand how the camera captures these points [12]. The following image, Figure 15: Chessboard Corner Detection, displays this detection process.

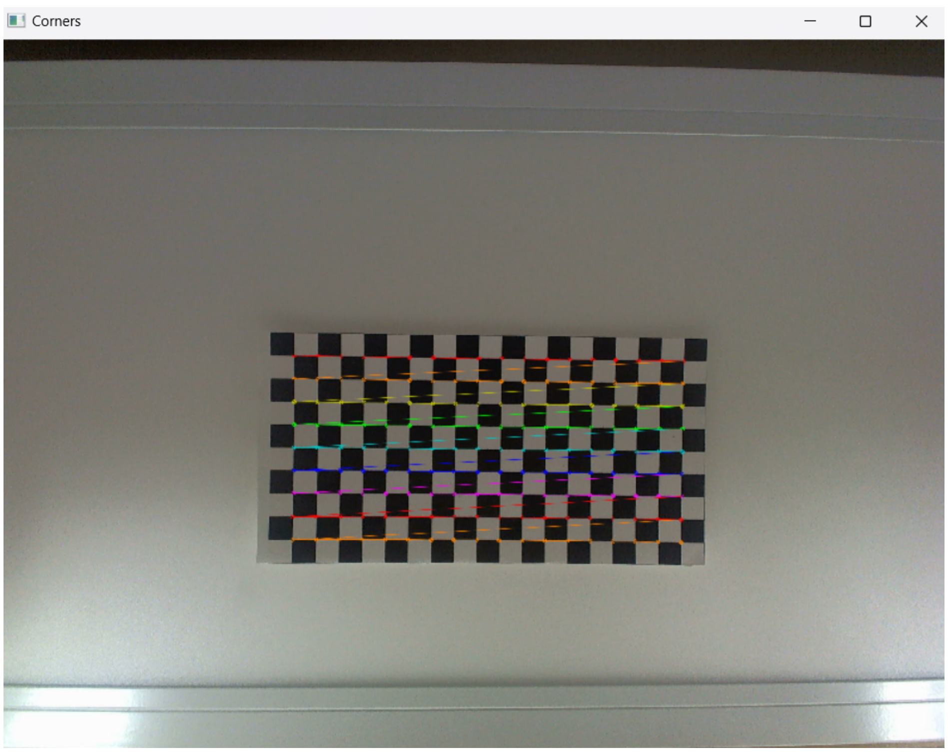

Figure 15: Chessboard Corner Detection

Corner Refinement: If the system successfully finds the chessboard corners in an image, it doesn’t stop there. These detected corners are then made even more accurate through a process called corner refinement. This means adjusting the position of the detected corners to match the actual corners’ positions as closely as possible, down to a fraction of a pixel. This increased accuracy is key to making the calibration as precise as possible.

Camera Calibration: With the chessboard corners identified and refined in all the images, the camera can now be calibrated. This process uses the object points (idealized real-world corners) and the image points (detected corners in the images) to figure out the camera's unique characteristics. These include the camera's intrinsic parameters, such as its focal length and the position of the optical center, as well as distortion coefficients that tell us how the camera lens distorts images, both radially and tangentially.

Calculating Pixels Per Millimeter (PPMM): After calibrating the camera, the system calculates how many pixels in the image represent one millimeter in the real world, for both the horizontal and vertical directions. This measurement, called Pixels Per Millimeter (PPMM), is crucial for translating sizes and measurements from the image (which are in pixels) into real-world units (like millimeters). This is especially useful for tasks that require precise measurements, like mapping or creating 3D models from images [12].

Storing Calibration Results: Finally, the results of the calibration are saved in a JSON file. This file includes the camera matrix, which describes the camera's intrinsic parameters, the distortion coefficients that tell how the lens distorts images, and the PPMM values. Saving this information makes it easy to correct distortion in future images taken with the same camera and from the same viewpoint, without having to recalibrate the camera each time.

5.4 Program Results and Parameters

The camera matrix, also known as the intrinsic matrix, is crucial because it captures the unique characteristics of a camera. It includes details like the focal lengths (fx, fy) along the camera's x and y axes and the optical centers (cx, cy). The focal lengths measure how far the lens is from the sensor that captures the image, and the optical centers point to the exact spot where the main axis of the lens meets the image surface. This matrix is key for converting three-dimensional camera coordinates into two-dimensional ones seen in the image [11]. Cameras often face issues with distortion because of how their lenses are shaped and built. There are two main types of distortion:

- Radial Distortion: This makes straight lines appear curved in photos, getting worse the further you are from the image's center. There are two kinds of radial distortion: barrel distortion, where lines curve inward, and pincushion distortion, where lines curve outward [13].
- Tangential Distortion: This occurs when the lens is not perfectly parallel to the imaging plane, causing some areas in the image to appear closer than they should be. It's as if the image is tilted in some parts [14].

The distortion coefficients are numbers that describe how much and what kind of distortion a camera lens adds to photos. Knowing these coefficients allows us to correct or “undistort” images, helping them represent the real world more accurately. For accurate and meaningful measurements within an image, understanding the conversion between the pixels seen in the image and actual measurements in the real world is crucial. This conversion is expressed as the Pixels Per Millimeter (PPMM) value. The PPMM value essentially translates how many pixels in a digital image represent one millimeter in the physical world. To calculate this value, one examines specific known distances within the image—for instance, the gap between two corners of a chessboard—and compares these distances to their real-world counterparts, such as the actual size of the chessboard squares. This comparison allows for the derivation of the PPMM value. With precise PPMM values for both horizontal (x) and vertical (y) axes, it becomes possible to conduct detailed and accurate measurements of space and distances directly from photographs. This process enables users to extract valuable spatial data from images, facilitating a variety of applications from mapping to 3D modeling [15].

5.5 Light Conditions

Capturing sharp images of reflective items, like an endoscope, presents unique challenges due to their shiny nature, which can introduce unexpected glares and distortions. However, with the right approach and setup, particularly in a controlled environment with consistent light conditions, these challenges can be overcome. In the following sections, the team will delve into the specifics of how to achieve this.

The backdrop serves as the canvas for the subject, an endoscope. A neutral background, especially colors like gray or black, can help in highlighting the intricate details of the endoscope. These colors are less likely to interfere with the natural colors of the endoscope. Moreover, a matte finish is preferred over a glossy one. A matte background diffuses light evenly, reducing the chances of unwanted reflections that can compromise the image’s clarity [16].

The walls of the lightbox, much like the backdrop, play a crucial role in determining the overall quality of the photograph. Neutral-colored walls, such as gray or black, ensure that there are no color casts affecting the image. A matte texture for the walls is again emphasized, as it helps in managing the light effectively, ensuring it spreads uniformly without creating hotspots or uneven shadows [17].

Lighting is the essence of photography. The direction, intensity, and quality of light can dramatically affect the outcome. For reflective objects like an endoscope, backlighting is a recommended technique. By positioning the light source behind the endoscope and directing it towards the camera, the team was able to achieve a silhouette effect. This ensures that the edges and contours of the endoscope are crisply defined against the backdrop, capturing its form and structure effectively [16].

5.5.1 Light Temperature Selection

When capturing images of reflective medical instruments like endoscopes, selecting the appropriate light temperature is paramount, especially for edge detection. Light sources vary in color temperatures, from warm tones around 3,000K (yielding yellowish hues) to cooler ones near 5,500K (producing bluish shades). A neutral light temperature, approximately 4,500K, is optimal for representing an endoscope's true colors. This balanced lighting reduces color deviations, ensuring genuine image representation and accentuating the endoscope's intricate details. While warmer light temperatures might diminish glare on the shiny surface, aiding in edge detection, they may not always capture the object's authentic color. Conversely, cooler temperatures can amplify reflections and glares, potentially obscuring the precise edges of the shiny endoscope surface.

In conclusion, the overarching goal of this research is to meticulously define the edges of the endoscope in photographs, ensuring both clarity and precision. To realize this within a lightbox environment, the team has underscored the significance of using a neutral, matte background—specifically, tests will be conducted using both black and gray backgrounds. Additionally, the walls will be experimented with in gray and white shades, ensuring they are matte to minimize reflections and potential color biases. Strategic lighting, encompassing both its placement and the optimal temperature of around 4,500K, will be pivotal. By integrating these insights and conducting these specific tests, the team aimed to fine-tune the lightbox conditions, ensuring the endoscope's edges are sharply and authentically captured in every photograph.

5.6 Endoscope Detection Methods Testing

Endoscope detection is considered to analyze the deviation points using OpenCV. It is used to measure endoscope information such as endoscope length, diameter, and runout points. The team tried and tested many endoscope detection methods to make sure the measurement was stable and consistent.

5.6.1 Hough Line Transform

The initial idea of the method was trying to capture the endoscopes as different segments and calculated the angle between lines to visualize the angle in real time. The article mentioned about the Hough line transform can detect straight lines [18]. The image below, Figure 16, shows an example of how the straight lines were detected, and the angle between the lines were calculated based on the detected lines.

Calculate Angle Function:

- Video Capture and Processing
- Hough Line Transform for Line Detection

- Angle Calculation and Display
- Real-time Feedback

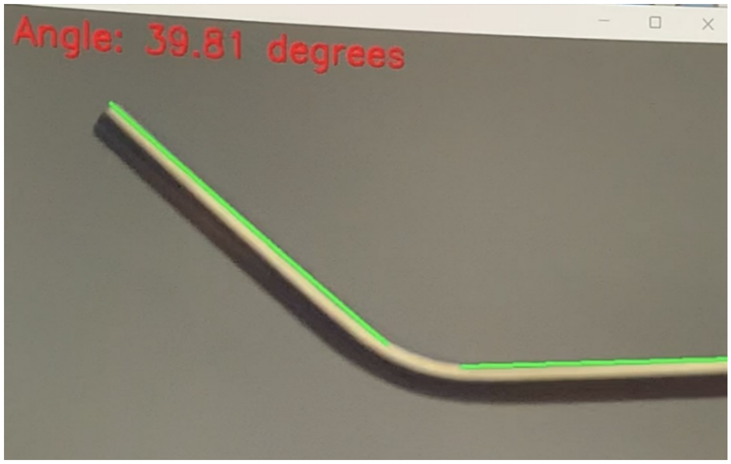

Figure 16: Example of Hough Line Method Output

5.6.2 Curves on Endoscopes

Methods described in section 5.6.1 were abandoned because the bending in an actual endoscope is not very pronounced. Consequently, rather than measuring the angle, the code shifted focus to tracing the contour of the endoscope and identifying the maximum and minimum points of the traced function.

The code recognizes the endoscope's contour by determining the function that fits along it. Viewing this as a function allows for more precise detection of the contour curve. While the code successfully determines the function's equation, it struggles to consistently identify the point of maximum curvature throughout the video. In the example of the output shown in Figure 17, the max point on the endoscope was shown as the blue dot while the max deviation point is on the endoscope of the endoscope.

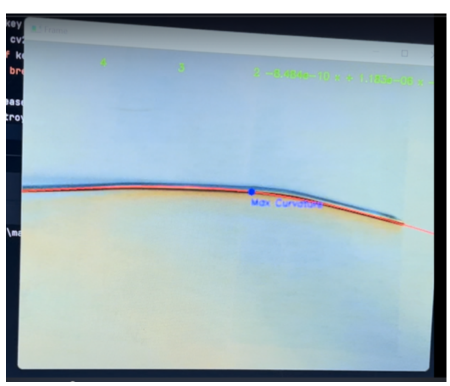

Figure 17: Output of Finding the Curve of the Endoscope

5.6.3 Line Comparison

To enhance the consistency and accuracy of detection, this method employs a background with guiding lines to differentiate the endoscope from the lines. Initially, three lines were used, but this approach often confused the code. After numerous trials, it proved more effective to use just one line to identify deviations in the endoscope's path. The process begins with capturing video footage, which is then subjected to Gaussian Blur and Otsu's thresholding. Following this, the Canny edge detection method is used to identify the edges of the endoscope, which are then compared to the detected straight line. Figure 18 below shows how the test is set up, while Figure 19, also shown below, displays the output comparison between the endoscope contour and a single straight line (the code used for this process is detailed in Appendix E).

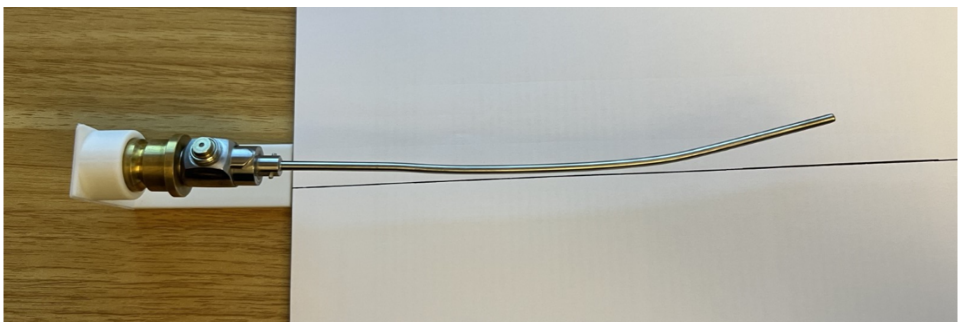

Figure 18: Set-up of the Test

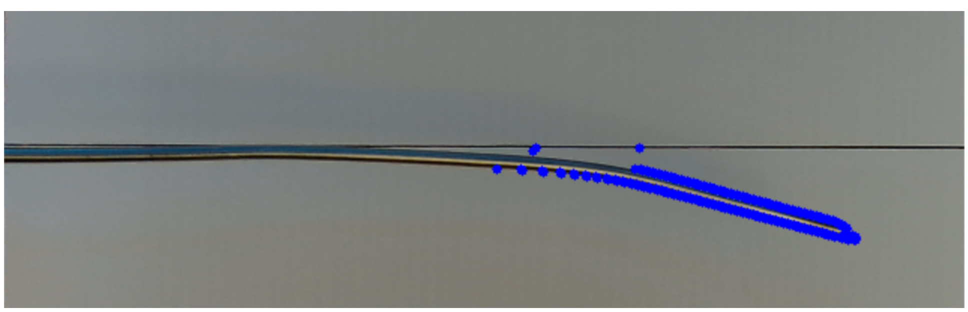

Figure 19: Output of Comparison Between Endoscope Contour and Single Straight Line

Based on the result, to detect smaller bending on the endoscope, a few similar methods were tried and compared.

1. Comparing the endoscope with three background lines, the middle line is aligned directly with the endoscope. For the outer lines, the intention was to check if they are parallel to the endoscope. This approach was largely ineffective due to difficulties in accurately calculating parallelism. (2/5)
2. Three lines are used as a background reference to the endoscope. Initially, the endoscope is compared

directly with the central line. The next step involves ensuring that the distance from the endoscope to each of the outer lines is identical, suggesting symmetry. (4/5)

3. Eliminating the center line, the focus shifts to comparing the distances to the outer lines. Rather than expecting the distances to be exactly equal, a small margin of error is permitted, allowing for slight deviations that are still deemed acceptable. This adjustment yielded satisfactory results. (3/5)

After comparing the results, accuracy, and stability, the second method seems to work best but not very stable. Blue circles indicate places on endoscope where the distance to the top and bottom lines is not symmetrical. Red circles indicate points where the endoscope deviates from the center line. The following images, Figure 20 and Figure 21, show the result of the endoscope comparison between the outer lines and the endoscope contour as well as the centerline and the endoscope contour. The second image, shown in Figure 21, is more accurate since the red dots, which means the endoscope parts were not parallel to the centerline, were detected. However, the top line was detected when it should not have been (the code used for this process is detailed in Appendix F).

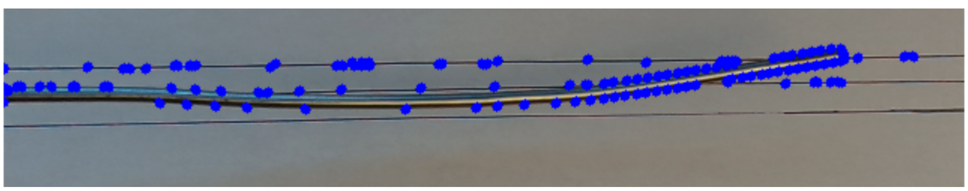

Figure 20: Endoscope Comparison Between Outer Lines to Endoscope Contour

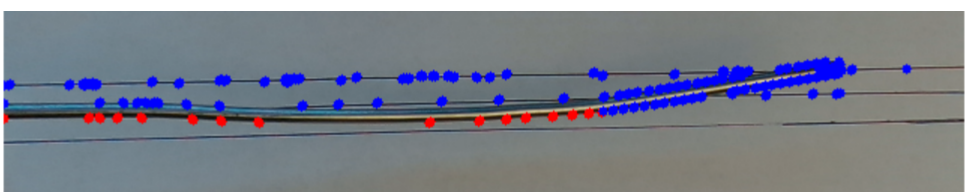

Figure 21: Endoscope Comparison Between Center Line and Outer Lines with Endoscope Contour

5.6.4 New Version Line Comparison

Based on the line comparison test above, an improved method was developed using the central line approach to detect bending in the same test setup as previously used. Instead of manually drawing a line for comparison, this method utilizes a conceptual y=0 line which the left bottom corner as (0,0). This adjustment reduces human error associated with manually drawing lines and aligning the endoscope parallel to the y=0 line, leading to potentially more accurate results. The following image, Figure 22, shows the comparison test result between the endoscope contour and the y=0 line (the code used for this process is detailed in Appendix G).

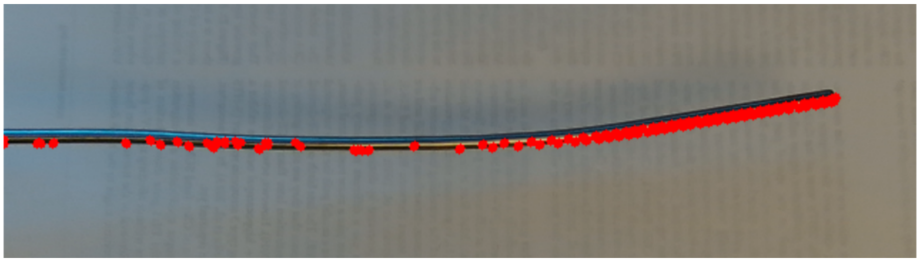

Figure 22: Comparison Test Result Between Endoscope Contour and y=0 Line

Based on the new result, the new code also decided to take images of endoscopes instead of taking videos for a more stable result. In this case, the new code logic is:

1. Display the video, marking the deviations from the line y=0.
2. Stop after 5 seconds.
3. Save the last frame of the video with the marked points as ‘deviation_image.png’.
4. Record pixels coordinates of the points and extract the deviation points and save them to ‘deviation_data.csv.

The following image, Figure 23, displays the output image with the detected deviation points shown by red dots.

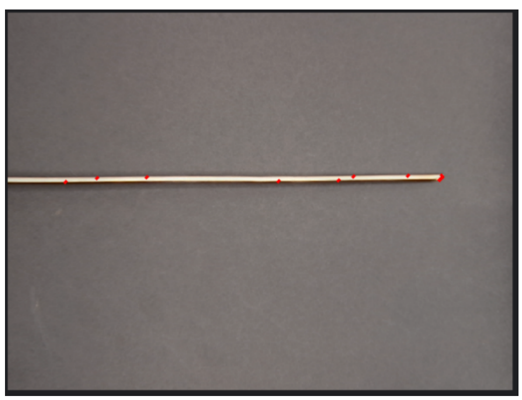

Figure 23: Output Image with Detected Deviation Points

The following screenshot, Figure 24, shows the coordinates of the deviation points for the output image shown in Figure 23 above.

```
342,214
343,213
418,213
419,212
547,212
547,211
549,209
550,209
550,207
549,206
```

Figure 24: Coordinates of Deviation Points

5.6.5 Method from Sponsor

This method, suggested by the team's sponsor liaison, Austin Scott, involves placing 5mm lines along the output image and marking the points where these lines intersect with the endoscope. By connecting these intersection points with multiple lines, the method evaluates the angles formed between consecutive lines. If the angles are within 3-177 degrees, those segments are identified as bent, and the corresponding points are marked (the code used for this process is detailed in Appendix H).

The process involves minimal concerns, primarily requiring the endoscope to remain in a consistent position throughout the procedure. Here are the steps of this method:

1. Capture a frame from the Logitech webcam at 720p resolution.
2. Process the image to detect the endoscope.
3. Draw vertical lines spaced 5mm apart across the width of the frame.
4. Identify intersections between the endoscope and these lines.
5. For each intersection, calculate the angle between lines formed by connecting consecutive points.
6. Mark lines with angles ranging from 0-145 degrees as indicative of bending.
7. Record the intersection points in a CSV file.
8. Save the output image showing the marked points.

The following image, Figure 25, displays an output example of the angle comparison method.

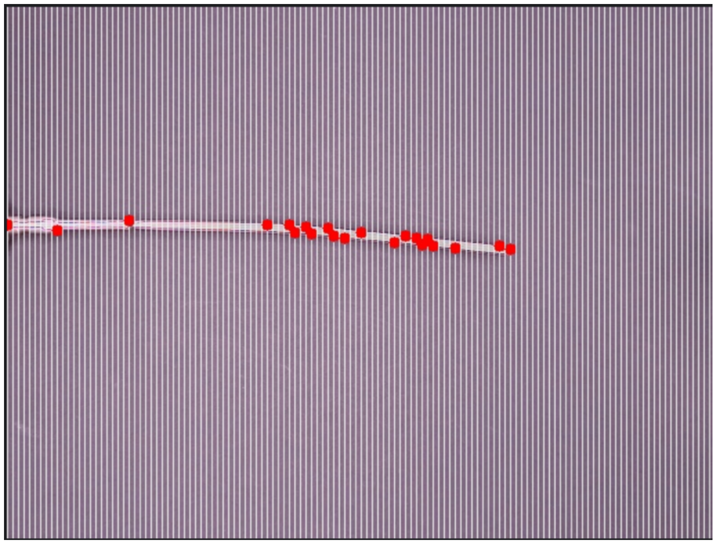

Figure 25: Output Example with Angle Comparison Methods

5.7 Runout Calculator

The initial calculator combines angle comparison and line comparison methods to detect and analyze deviations in the endoscope's contour. It focuses on segment-by-segment analysis, comparing each segment with a theoretical straight line (y=0) to identify any deviations (the code used for this process is detailed in Appendix I). The following steps detail the process for calculating runout within the code:

1. **Load the Image:** Import the picture and apply a Region of Interest (ROI) to focus on the nozzle region.
2. **Process the ROI:** Enhance the nozzle detection by applying blurring, adaptive thresholding, and dilation to the ROI.
3. **Extract Contour:** Identify d extract the contour that represents the nozzle.
4. **Intersection Points:** For each vertical segment in the image, locate the first intersection point with the nozzle starting from the bottom upward.
5. **Reference Point:** Establish the first intersection point as the reference for subsequent comparisons.
6. **Calculate Deviation:** For each intersection point, calculate the deviation from this reference point.
7. **Mark Deviations:** Highlight points on the original image that exhibit significant deviation.
8. **Conversion to Millimeters:** Convert the pixel coordinates of these points into millimeters using a conversion factor that accounts for the resolution (1080p) and the physical height of the camera.
9. **Record Deviations:** Save the coordinates of significantly deviated points into a CSV file for further analysis or reporting.
10. **Display Output:** Show the processed picture, highlighting areas of deviation.

The following image, Figure 26, displays the output of the endoscope deviation points using the initial runout calculator, while Figure 27 shows the output of the endoscope deviation points coordinates with initial runout calculator.

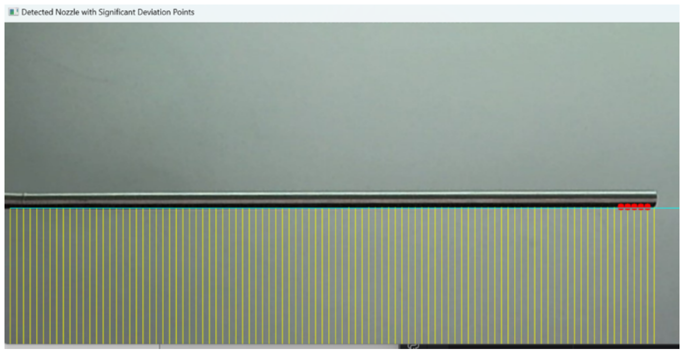

Figure 26: Output of the Endoscope Deviation Points with Initial Runout Calculator

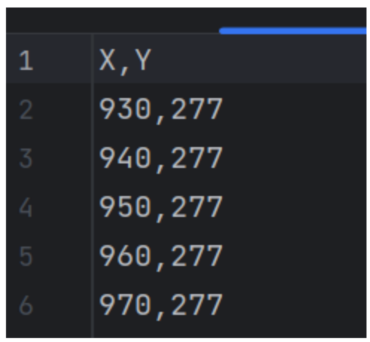

```
X,Y
930,277
940,277
950,277
960,277
970,277
```

Figure 27: Output of the Endoscope Deviation Points Coordinates with Initial Runout Calculator

5.7.1 Runout Calculator Improving and Testing

For improving the initial runout calculator code, particularly focusing on contour detection methods, it's essential to test various images using both Canny Edge detection and Adaptive Thresholding (the code used for this process is detailed in Appendix J). The following list is a structured approach to perform these tests and visually compare the outcomes and includes steps for testing contour detection methods:

1. **Read the Image**
2. **Pre-process the Image:**
    a. Convert the image to grayscale to simplify the analysis.
    b. Apply Gaussian blur to reduce noise and detail in the image, which helps in

highlighting significant edges.

3. **Apply Canny Edge Detection:**
    a. Implement Canny Edge Detection on the pre-processed image.
    b. Visualize the result to assess how well the contours are highlighted using this method.
4. **Apply Adaptive Thresholding:**
    a. Use Adaptive Thresholding on the same pre-processed image.
    b. Visualize the outcome to see how effectively this method detects the contours.
5. **Compare Both Methods Visually:**
    a. Analyze the results side by side to evaluate which method better outlines the contours relevant for runout calculations.
    b. Consider factors such as clarity, continuity of edges, and the capture of relevant details.

The visual comparison layouts, shown in several figures below, consist of the three images detailed here:

1. **Top Image:** The original real picture.
2. **Second Image (Middle):** The result of applying Canny Edge Detection, showing how the contours are defined using this method.
3. **Third Image (Bottom):** The outcome of using Adaptive Thresholding, showing the detected contours with this technique.

The following images, Figures 28, 29, 30 and 31, display the visual comparison layout of endoscopes 1, 2, 3, and 4, respectively.

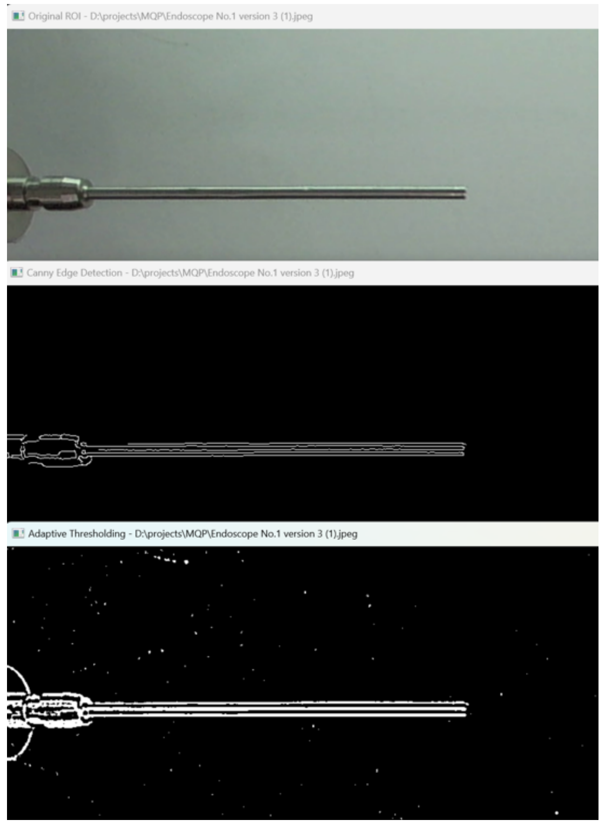

Figure 28: Endoscope 1 Visual Comparison Layout

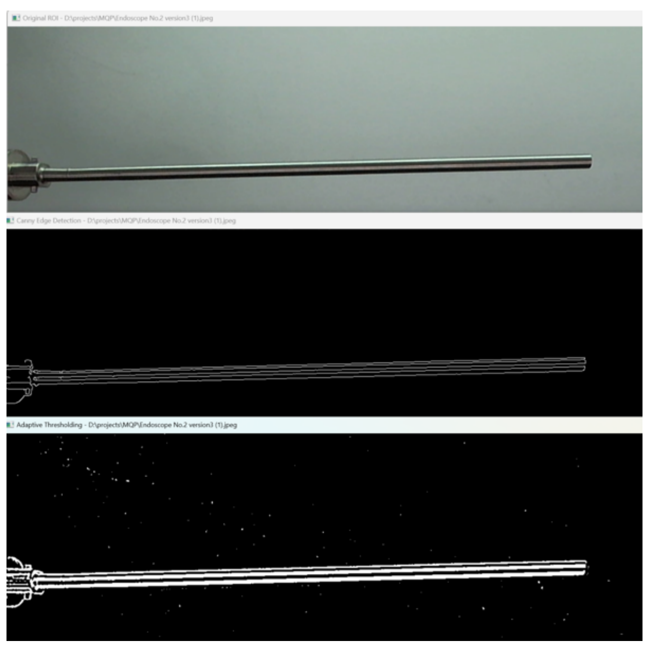

Figure 29: Endoscope 2 Visual Comparison Layout

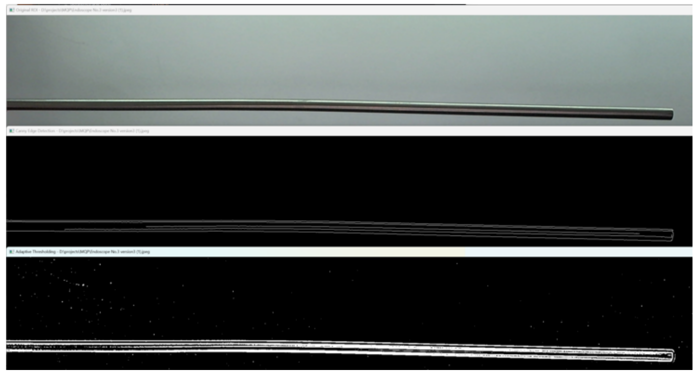

Figure 30: Endoscope 3 Visual Comparison Layout

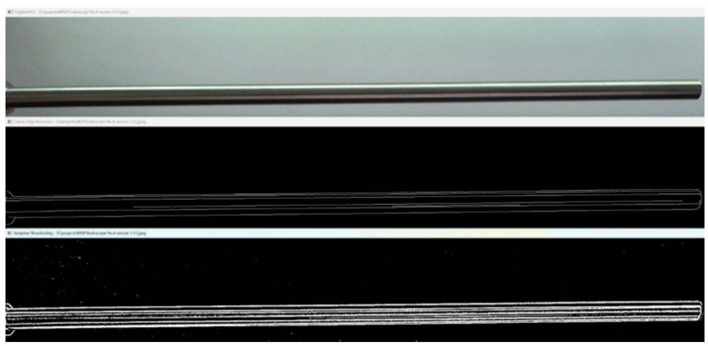

Figure 31: Endoscope 4 Visual Comparison Layout

5.8 Runout Calculator Code Testing Method – Diameter Calculator

Initially, the runout calculator code measured the deviation points of each endoscope successfully. The way to verify accuracy of deviation points is to measure the diameter of the endoscope with the same methods. To be specific, the two codes are both using the same ROI, set up environment, pre-processing contour process and finding distance with pixels difference. The only difference between them is that the diameter code is focusing on finding the distance difference between the upper contour and lower contour, but the runout calculator code is finding the y difference between the initial point and the rest of intersection points along the endoscope.

5.8.1 Light Testing

To determine the most effective lighting environment for the endoscope 5000-watt LED panels were placed at multiple positions around the endoscope. These positions included backlighting, top lighting, side lighting with two panels, and side lighting with one panel. Backlighting is when the panel is positioned behind the endoscope, shining towards the camera. Above lighting is when the light is positioned behind the camera, shining down onto on to the endoscope. Side lighting consists of two LED panels, placed one on each side, ensuring equal lighting on both sides of the endoscopes. One panel of side lighting refers to side lighting with only the LED panel on the left or right side.

All tests took place in a 15-gallon black bin to create a closed lighting environment. The dimensions of the bin were measured at 44cm width, 65mm length, and 30cm height. The webcam was attached to the bottom of the lid of the Webcam bin, shown in Figure 32. It is centered between the left and right sides of the bins top. There is ~20cm between the camera and the endoscope in all tests. The endoscope rig was placed on its side with the bin in a way so that endoscope was centered at a distance 16.5 – 17cm away from each side wall. The lid was on its side to create enough distance between the endoscope and camera for the entire endoscope to be captured within a single image.

Figure 32: Webcam attached to the center of underside of the black bin top

Figure 33: Endoscope Backlighting with white diffuser background

The image above, Figure 33, displays the desired set-up of the endoscope with backlighting and a white diffuser background. Average results from testing backlighting in this configuration measure a 10mm diameter endoscope as 9.15mm.

Figure 34: Endoscope Above lighting, with white diffuser and white background

The average results from testing the above lighting in this configuration, shown in Figure 34 above, measure a 10 mm diameter endoscope as 8.06mm. The following image, Figure 35, shows a similar set-up to the one shown in Figure 33, is lit from one side and the lower LED is used as a background.

Figure 35: Endoscope lighting from one side. Similar setup to Figure 33, the lower LED is used as a background

Using the diameter calculator code that had been created, using the runout calculator as a bases, the accuracy of the various positions was compared. Based on the result from the diameter calculator, light from one side, as shown in Figure 36, gives inaccurate results.

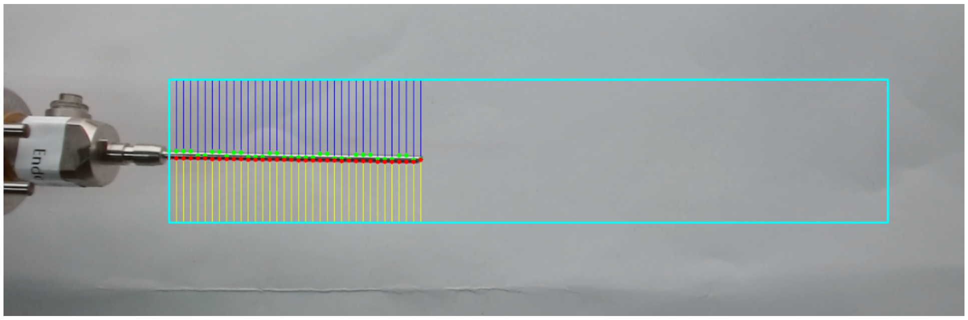

Figure 36: Output of diameter result with light on one side

The red and green dots represent the intersection points of when the edge of the endoscope has been detected. In an ideal reading, there should be a linear progression of these dots following the bend of the endoscope. The diameter is calculated by finding the number of pixels between the green dot representing the top edge and the red dot representing the bottom edge at every intersection. In Figure 36, the inconsistency of the intersection points shown on the contour is caused by shadows of the endoscope from the light side. Therefore, two lights, one from each side, gives a more consistent result, as shown in Figures 37 and 38.

Figure 37: Light set up from two sides

Figure 38: Light set up from two sides

The use of lighting on each side creates a more consistent shadow compared to single side lighting. The results of this are displayed in Figure 39 (two-side output). The green and red dots align with the edge of the endoscope to a much clearer degree when compared to Figure 36 (one-side output) meaning the diameter measurement is more accurate.

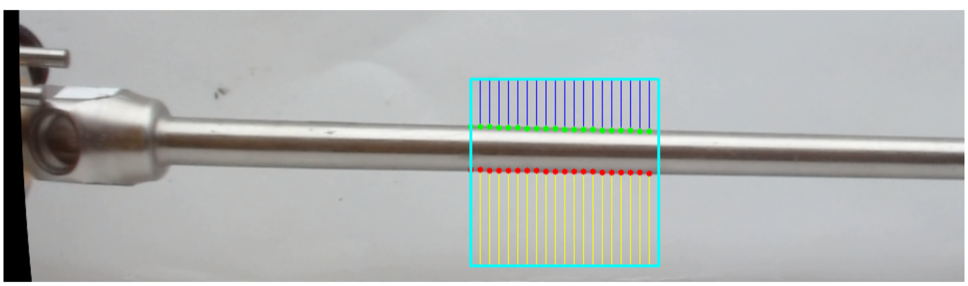

Figure 39: Output of diameter result with light on two sides

5.8.2 Background Testing

With the lights from both sides, the team aimed to get better accuracy with different backgrounds. For endoscope 17 that has a 10mm diameter which the white background had a better result.

Table 2. Measured endoscope diameter with different background

White Background	10.03 mm
Black Background	10.9 mm
Brown Background	12.2 mm

5.8.3 Distorted Image Testing

In the three images below, the team divided the endoscope diameter from three different sections along the endoscope. The first section of the endoscope shown in Figure 40 is measured at 10mm by the program while the actual diameter is also 10mm. The second section, in Figure 41, was 9.66mm and the third section, shown in Figure 42, was 9.1mm. Therefore, the team would know that the measurement was not consistent along the length endoscope which could be caused by image distortion coefficient found from chessboard and camera position.

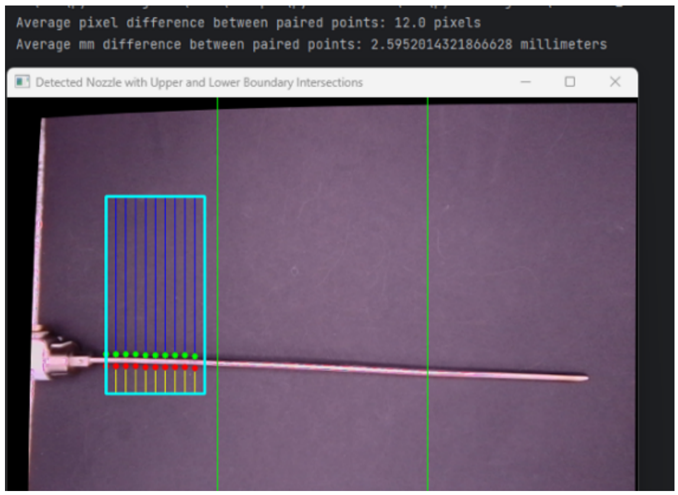

Figure 40: diameter in the first section

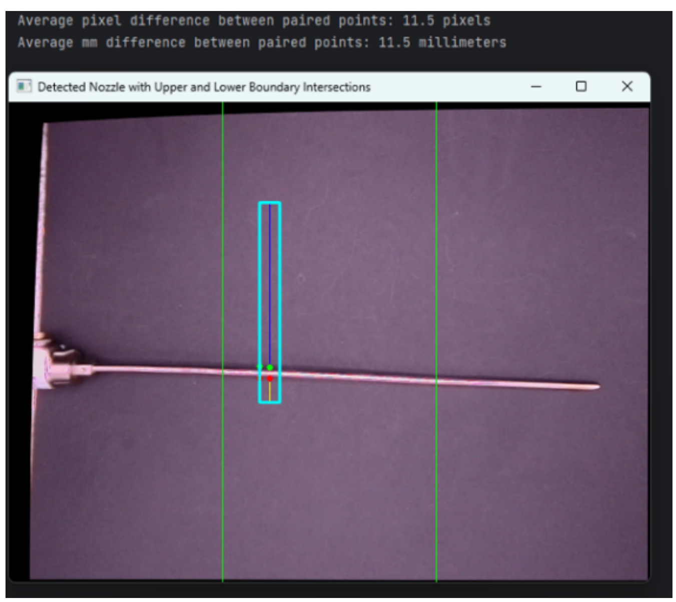

Figure 41: Diameter in the second section

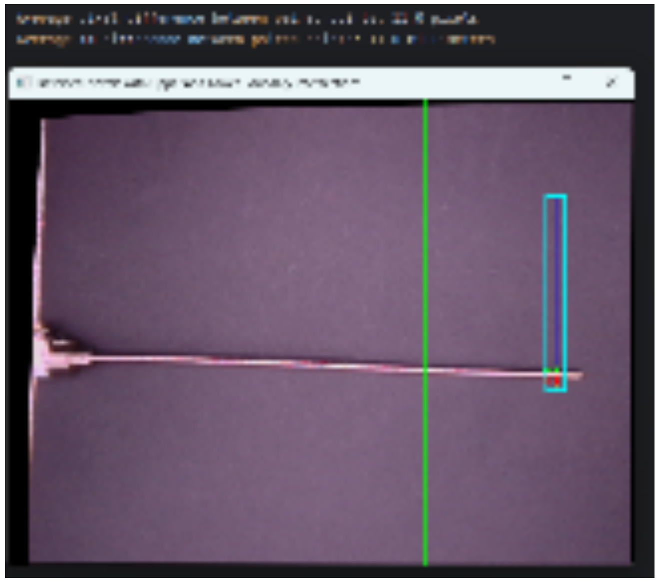

Figure 42: Diameter in the third section

Therefore, the challenges with obtaining consistent diameter values were identified as stemming from the camera's positioning relative to the endoscopes. Proper alignment of the camera in the x-y direction and its tilt in the z-direction are crucial. Adjustments are necessary each time the setup is moved to a new location to account for potential variations in how level the surfaces are.

5.8.3.1 Improvements in Contour Detection

During accuracy tests for measuring the endoscope, issues were encountered with inconsistent results due to the method of contour selection. The existing logic, which selects the largest contour in the image, sometimes incorrectly chose the contour of the image frame itself. This led to inaccuracies in the measurements. The following list consists of proposed changes to the code:

1. **Application of a Mask:**
    1. Use a mask within the ROI to isolate the contour detection process. This approach prevents the algorithm from considering the largest contour of the entire image frame, which often includes extraneous elements and noise from the surrounding environment.
2. **Optimization Benefits:**
    1. By restricting the analysis to the masked ROI, the code becomes more efficient and runs faster due to processing less data. This targeted approach reduces the computational load and enhances the speed of the analysis.
3. **Consistent Camera Setup:**

1. Develop a standard procedure for camera setup each time the station is moved. This may include using leveling tools or predefined settings based on the type of surface to ensure the camera is correctly positioned every time.

The following image, Figure 43, displays a contour shown within the ROI.

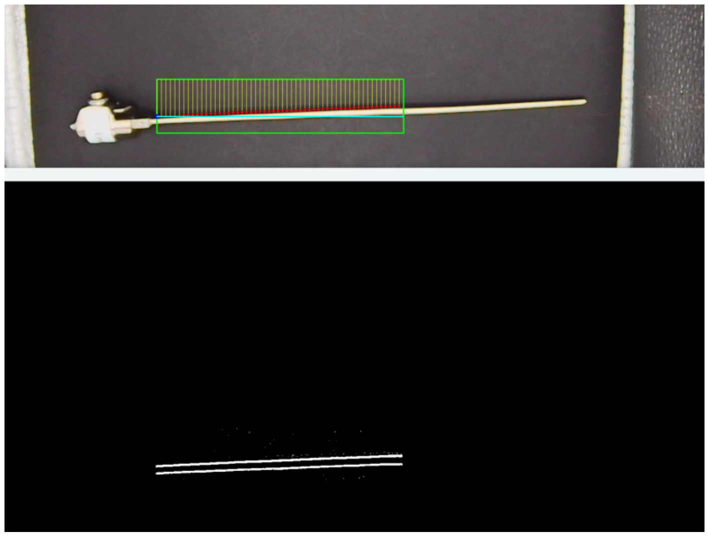

Figure 43: Contour shown within the ROI

5.9 Final Measurement Code

During B-term 2023, it was determined that upgrading to a camera with higher resolution was necessary. The Basler Ace 2, a monochrome 4K camera, was chosen for this purpose. This camera connects to a laptop via USB, offering enhanced image quality essential for precise measurements and detailed image analysis. The following image, Figure 44, shows an example of the output from the new camera.

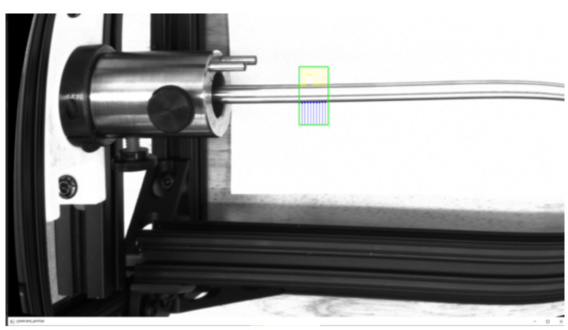

Figure 44: The example of output from the new camera

5.9.1 Integrating Arduino into a Runout Calculator

The same runout calculator code was enhanced by integrating Arduino functionality to manage the number of images captured and the rotation angles of the endoscope. The operational logic is that the endoscope is initially positioned and, as the runout calculation proceeds, it is rotated by the Arduino to acquire new measurements from different angles. The code then compares the maximum deviation results obtained from these various angles and outputs the greatest deviation detected. This integrated system was demonstrated to the sponsor at the conclusion of the B-term. However, a limitation is that the system cannot guarantee that the largest deviation will occur at predetermined angles.

5.9.2 Rotation Method for Finding Maximum Runout

To make sure the code can find the largest runout of the endoscope, a new method was developed and tested instead of measuring and comparing the largest deviation at multiple angles. This method developed by the team will rotate the endoscope 360 degrees while capturing a video. The highest point of runout will be determined by comparing the video frame and the time point of the rotation. Using this method, the algorithm will only need to run the edge detection program on a single image, greatly reducing processing time and improving the consistency.

5.9.3 Find Highest Point Test

In the example provided below, shown in Figure 45, within the defined Region of Interest (ROI), the code can detect points on the contour where the y-value is the highest within the ROI. As a result, both the runout calculator and the diameter calculator can focus on this specific angle—where the highest point occurs—allowing the system to analyze the endoscope just once from a single angle. This approach streamlines the process, enabling efficient and precise measurements without the need for multiple analyses from different angles (the code used for this process is detailed in Appendix K).

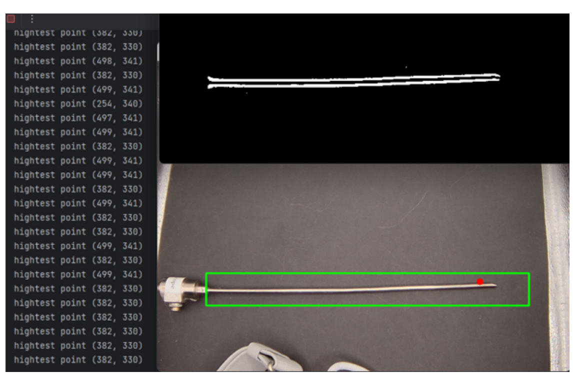

Figure 45: Highest point method test

5.9.4 Implementing Rotation and Final Measurement Code

The new function is designed to identify the highest point while the endoscope rotates 360 degrees. To determine the degree at which the highest point is located, the system incorporates timing measurements. These measurements calculate the angle based on the duration of the rotation. The complete code logic now includes the following steps: adjust the Region of Interest (ROI), then rotate the endoscope to find the highest point, and finally rotate to that specific angle to analyze the runout (see Appendix B for more detail).

Here are the revised steps of the code that outline the process for analyzing the endoscope's runout:

1. **Capture an Initial Image:** Take a single image of the endoscope in its starting position.
2. **Adjust the ROI:** Based on the captured image, adjust the Region of Interest (ROI) to focus on nozzle of the endoscope.
3. **Rotate and Record:** Rotate the endoscope 360 degrees, recording the angle at which the highest point of deviation occurs.
4. **Reposition the Endoscope:** Rotate the endoscope back to the angle identified as having the highest point.
5. **Capture and Distort a New Image:** Take another image of the endoscope at this angle and apply necessary distortions.
6. **Analyze the Contour:** Process the distorted image to analyze the contour of the endoscope. Calculate metrics such as diameter, length, and deviation points along the endoscope.

The following image, Figure 46, provides an example of the final output.

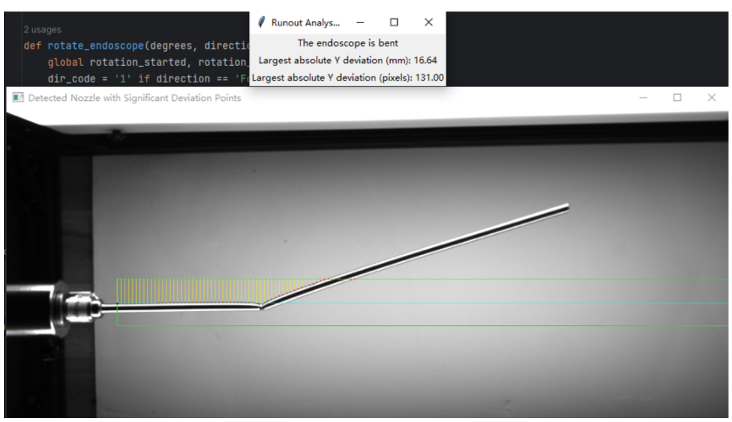

Figure 46: Example of Final Output

5.10 Camera Selection

Table 3. Camera selection decision matrix

Camera	Weight	a2A3840-45ucPRO	LogiTech
Cost	3	3	8
Durability	8	7	3
Size	5	7	6
Sensor	9	9	3
Compatibility	9	7	7
Customization Options	8	8	7
Total		41	34
Weight Total		308	224

The weighted scores and implications mentioned in the table above, Table 3, are further explained as:

Cost (Weight 3): Relative expense, weighted lower because cost is not considered a limiting factor in for camera selection.

Durability (Weight 8): How durable the camera is, highly weighted due to the importance of reliability.

Size (Weight 5): The amount of space required to properly house the camera. Medium weighting because while not overly important the camera should be of a reasonable size to not over burden the system.

Sensor (Weight 9): The resolution and quality of the picture, highest weighted section due to the importance of detecting minute details of the endoscope.

Compatibility (Weight 9): Compatibility of the camera's system with the open cv software. Highest weighted because OpenCV has already been selected as the team's method of computer vision analysis

Customization Options (Weight 8): Options for user customization offered both when ordering the camera as well as the adjustable parameters physically and within the camera's software. Includes parameters such as focal length, exposure, and aperture.

Based on the weighted totals of 308 and 224 in Table 3 above, it was determined that the a2A3840-45ucPR (Basler Pro Ace 2) [19] would capture the images for the measurement system's algorithm. The

Basler Pro Ace 2 led in important areas such as sensor quality and durability.

Figure 47: Basler Pro Ace 2: a2A3840-45ucPR

This chapter consists of detailed information about initial considerations of using LiDAR, calibration processes, testing for the ideal light conditions needed within the station, endoscope detection methods testing, calculating runout, and camera selection processes. The next chapter provides an overview of the components of the station, outlines the station requirements, describes the team’s endoscope mount selection, and explains additional station parts specifications.

6 Station Overview

This chapter gives the station overview of the provided station requirements and decision matrices for different station components, as well as outlining the endoscope mount selection process and additional parts specification. Figure 48: Station Components below is a labeled overview of the developed station. The main labeled parts are the camera holder, sliding panel door, LED panel, lead screw and rails, background mount, endoscope, straightening device, and endoscope mount.

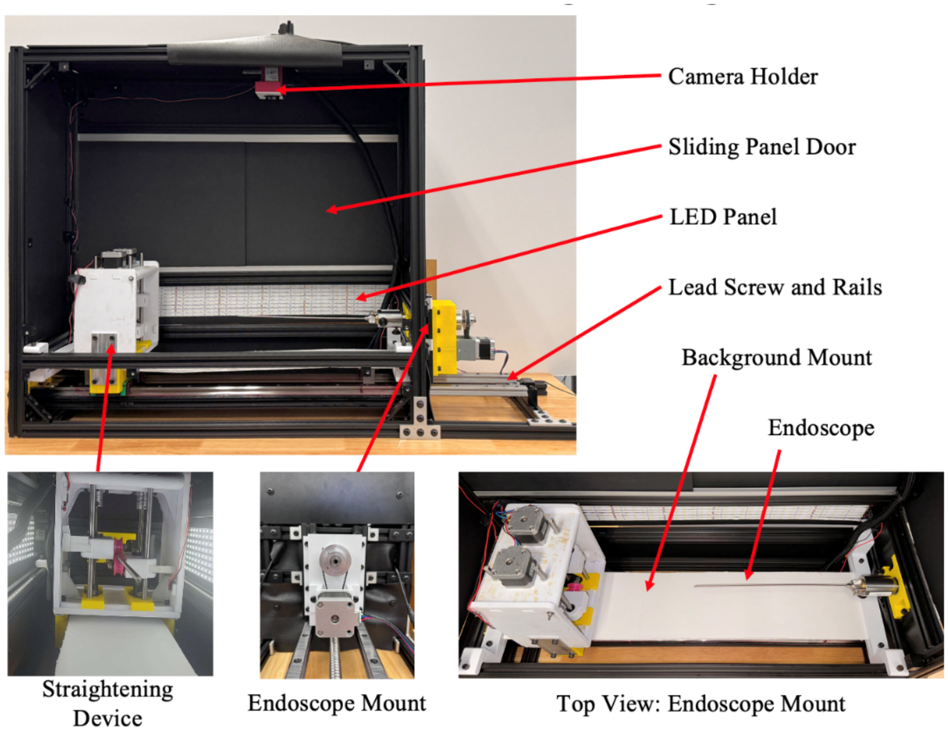

Figure 48: Station Components

6.1 Station Requirements

Upon review of the essential parameters based on various factors for the research station, particularly focusing on the measuring station, the team has identified several critical requirements based on the decision matrices provided next. These requirements, shown in the following list, ensure the optimal functionality and efficiency of the measuring station within the research environment:

1. Measurement Endoscopes Lengths: The measuring station must be able to measure endoscopes with length ranging from 6.9 cm to 45.7 cm to facilitate diverse research activities.
2. Straightening Station location: it must be situated internally, within the research station, to use station space efficiently.

3. Light source location: Light sources are required on both sides of endoscopes based on light source tests. This dual-sided lighting is crucial for consistent illumination, which is vital for accurate edge detection and precise measurements.
4. Background: The background against which measurements are taken should be white a matte finish to avoid reflections and ensure the best edge detection.
5. Camera Adjustment: The camera system should feature 2 Degrees of Freedom (DOF) to allow for adjustments in positioning and focus, which are essential for capturing data.
6. Camera Distance Range: The station height should be enough to be capable for cameras operation distance ranging from 21 cm to 48.3 cm, giving it the flexibility to capture various endoscope sizes.
7. Reconfiguration: The station must have a modular design, enabling easy reconfiguration to adapt to different experimental setups and requirements.
8. Mounting Endoscopes Flexibility: There should be mounting options available for accommodating different types of endoscopes, which increases the station's applicability across various research scenarios.
9. Wire Management: The station should include cable management solutions to keep the setup organized and prevent interference with measurement and straightening processes.
10. Controlling/Monitoring: A user-friendly interface or software is necessary for the controlling and monitoring station to facilitate ease of use and efficient data management.
11. Safety: The design must incorporate features to ensure the safety of the operator and the protection of the equipment.
12. Comfort: Ergonomic factors should be considered to provide comfort to the operator during extended periods of use, which can help maintain focus and accuracy.

In translating the identified critical requirements into a CAD model for the research station's measuring station, careful consideration was given to each parameter to ensure optimal functionality and efficiency within the research environment. These requirements are tailored to meet the unique demands of the measuring station in the research setting. A modular design facilitates easy reconfiguration to adapt to different experimental setups, and mounting options cater to various endoscope types, increasing applicability across research scenarios. Safety features were incorporated to protect operators and equipment, and ergonomic considerations were considered to ensure operator comfort during prolonged use, enhancing focus and accuracy. By adhering to these requirements in the CAD model, the team aimed to elevate the accuracy, productivity, and overall effectiveness.

6.1.1 Measuring Station Light Position Decision Matrix

A set of design matrices was employed to systematically prioritize and quantify the design requirements for the device. Design matrices were used for light position, frame selection, interior part station access, camera, diffusor, and endoscope mount. All matrices use scales from 1 to 10, where 1 means worst or less important, and 10 means the best applicable.

Table 4. Measuring station light position matrix

Light Position	Weight	Backligting (Testing)	Single Side lighting	Backlighting (Concept 1)(Not based on testing)	Dual Side lighting	Top Lighting
Spec						
Camera Height	5	7	6	10	8	4
Camera stablity	8	4	6	8	4	4
Background (Behind endoscope)	6	3	7	4	7	7
Diffuser Positioning	6	1	5	7	3	1
Wall Panel color	4	4	4	8	4	4
Endoscope insertion	7	6	6	8	6	1
Endoscope roatation	4	3	3	9	3	3
Endoscope stablitly	3	5	5	8	5	5
Measurement Consitency	9	7	3	0	8	6
Measurement Accuracy	7	6	7	0	6	6
Total		46	52	62	54	41
Weight Total		281	311	328	331	246

The compared lighting positions are those specified in the lighting test section, 5.8.1. Backlighting is pictured in Figure 33: Endoscope Backlighting with white diffuser background. Single side lighting in Figure 35: Endoscope lighting from one side. Similar setup to Figure 33, the lower LED is used as a background, dual side lighting in Figure 38: Light set up from two sides, and top lighting in Figure 34: Endoscope Above lighting, with white diffuser and white background. Backlighting concept 1 is based on a theoretical, more refined testing area, as opposed to the black box testing that was used.

The weighted scores and implications mentioned in the table above, Table 4. Measuring station light position matrix Table 4, are further explained as:

Camera Height (Weight 5): For testing, there needs to be as many controlled variables as possible, so the camera height should be consistent between trials as well as between lighting configurations. This criterion is how easy it is to change the height of the camera, should need to be when testing. Weighted at 5 because the best camera height for a specific light configuration can be established once the results of the comparison tests are determined.

Camera Stability (Weight 8): This criterion evaluates how stable the camera was during the testing process for each configuration. It is extremely important that the camera is stable because changes in how it is mounted will result in parameters, such as pixel per millimeter, defined by the calibration code no longer being correct for the picture that is taken.

Background (Weight 6): This criterion elevates how easy it is to place/change a background that will be behind the endoscope, thus appearing on camera. The team's initial tests on different backgrounds show this had a very noticeable effect on the runout and diameter measurement results, so being able to easily change/retest the backgrounds once a light configuration is chosen is very important for controlling the variables.

Diffuser Positioning (Weight 6): This criterion evaluates how easy it is to set the diffuser in its required position and how easy it is to adjust the diffuser while the team performed tests.

Endoscope Insertion (Weight 7): This criterion evaluated how much replacing the endoscope during testing affected the measurement system including the camera's position and LED configuration.

Endoscope Rotation (Weight 4): This has a weight of 4. It shows how well the design allows for the rotation of the endoscope.

Endoscope Stability (Weight 3): This criterion evaluated how stable is the endoscope within this design. Weighted lower because all testing has been done with the same endoscope holding frame.

Measurement Consistency (Weight 9): This criterion evaluated, based on testing so far, what lighting positioning has produced the most consistent results (each trial is approximately within 0.05mm of each other). It is weighted higher an accuracy, because the optimal conditions of the chosen LED configuration will be further explored. If the given configuration cannot produce consistent results, the accuracy of the results cannot be trusted.

Measurement Accuracy (Weight 7): This criterion evaluates ow close were any of the trails to the actual diameter of the endoscope.

Upon evaluating the weight totals, 'Dual Side Lighting' emerges as the top choice with a weighted total of 331. This option stands out for its high scores in camera stability, endoscope insertion, and measurement consistency, which are among the most heavily weighted criteria, hence having a significant influence on the overall score. The 'Single Side Lighting' and 'Backlighting (Testing)' options, despite their merits, do not achieve the same balance of highly weighted criteria as the 'Dual Side Lighting' does. 'Top Lighting', while advantageous in terms of weight, significantly underperforms in categories that are crucial, such as measurement consistency and accuracy. Therefore, based on the weighted scores and the prioritized criteria, 'Dual Side Lighting' was recommended for selection. Its superior performance in critical areas such as camera stability, measurement consistency, and accuracy made it the most suitable option for ensuring high-quality measurements in the research station.

6.1.2 Decision Matrix Measuring Station Frame Selection

Table 5 was used as a design matrix for frame selection.

Table 5. Frame Decision Matrix

Frame Selection	Weight	Steel Welded Frame	Aluminum Frame	Wooden Frame
Cost	6	7	5	8
Durability	8	5	9	2
Weight	4	4	9	6
Customization Options	8	6	9	8
Total		22	32	24
Weight Total		146	210	152

These weight scores and implications are further detailed as follows:

Cost (Weight 6): This criterion was given a moderate weight because the frame should not be changed frequently. As a result, cost played the most important role.

Durability (Weight 8): A high weight was placed on durability, showing a strong preference for a frame that will withstand use over time without significant wear.

Weight (Weight 4): This has the lowest weight among the criteria, suggesting that the physical weight of the frame is a less critical factor in the decision-making process because the station is stationary and should not be moved during its operation.

Customization Options (Weight 8): This was also given a high weight because it was the team's prototype and it was important to be able to integrate new features when it was needed.

The scores of these various categories can be further defined as:

Cost (1 to 10): Scores measure the relative cost, with a higher score indicating a more cost-effective option.

Durability (1 to 10): Scores indicate the expected longevity of the frame, with a higher score pointing to more durable materials.

Weight (1 to 10): Scores represent the heaviness of the frame, with a higher score denoting a lighter frame that may be easier to handle and install.

Customization Options (1 to 10): Scores assess how well the frame can be tailored to specific requirements, with a higher score reflecting greater customization possibilities.

Upon reviewing the weighted scores in the Table 5, the ‘Aluminum Frame’ option emerged as the clear choice, with a weighted total of 210. This selection stood out, particularly for its Durability and Customization Options, which are among the highest-weighted criteria and thus had a significant impact on the overall score. The ‘Wooden Frame’, despite scoring well on cost, fell short on Durability, which is a highly weighted criterion, resulting in a less favorable overall score. The ‘Steel Welded Frame’ offered a balanced cost and durability but was outperformed by the aluminum option in terms of weight and customization options. Given these considerations, the ‘Aluminum Frame’ was recommended for selection. Its combination of high durability, lightweight, and extensive customization options aligned well with the prioritized criteria and offered a versatile and long-term solution for frame needs.

6.1.3 Measuring Station Interior Part Station Access

Table 6 was used to define the best way to access the internal environment of the station.

Table 6. Interior Part Station Access

Interior Part Station Access	Weight	PVC Strip Curtain	Side Hinge Door	Bottom Hinge Door	Sliding Door Up	Partially Sliding Door Side
Cost	6	8	7	7	4	6
Durability	8	10	6	7	5	6
Efficient Space Usage	9	7	3	4	8	10
Ease of Access	10	4	6	7	8	5
Maintenance Requirements	5	8	7	7	6	8
Safety	7	2	7	7	7	8
System Complexity	8	10	6	6	2	6
Total		49	42	45	40	49
Weight Total		365	309	336	311	368

These weighted scores are furthered detailed as follows:

Cost (Weight 6): Given moderate importance, suggesting a balanced consideration between price and other factors because this part should have a price/quality balance.

Durability (Weight 8): High weight, emphasizing the long-term durability because the station was opened frequently.

Efficient Space Usage (Weight 9): Very high priority, reflecting the necessity to maximize space efficiency in the operational area. In the case of station plants, it saves warehouse space and money.

Ease of Access (Weight 10): The highest importance, underscoring that accessibility is a critical driver of productivity and operational fluidity. The operators open the door each time to change the endoscope, so it is important to provide a convenient work environment.

Maintenance Requirements (Weight 5): Moderate importance, indicating maintenance is a consideration but secondary to more critical factors.

Safety (Weight 7): High importance, ensuring that the chosen method does not compromise on safety while considering that all options meet a basic safety standard.

System Complexity (Weight 8): High weight, preferring systems that are user-friendly and reduce the likelihood of errors or extensive training.

These category scores can be further defined as:

Cost (1 to 10): Scores measure relative expense, with 10 indicating cost-effectiveness.

Durability (1 to 10): Scores reflect the expected lifespan of the access method, with 10 being most durable.

Efficient Space Usage (1 to 10): Scores represent how well the space is utilized, with 10 being the most space efficient.

Ease of Access (1 to 10): Scores assess the smoothness of operation, with 10 offering the least resistance to workflow.

Maintenance Requirements (1 to 10): Scores indicate the frequency and cost of maintenance needed, with 10 being low maintenance.

Safety (1 to 10): Scores gauge the level of safety provided, with 10 being the safest.

System Complexity (1 to 10): Scores assess operational simplicity, with 10 being the most straightforward and easy to use.

Based on the weighted totals in the Table 6, the ‘Partially Sliding Door Side’ option scored the highest with a weighted total of 368, closely followed by the ‘PVC Strip Curtain’ with a weighted total of 365. The ‘Partially Sliding Door Side’ option excelled particularly in Efficient Space Usage and Safety, which are among the most heavily weighted criteria. Although the PVC Strip Curtain had a high score in Durability, its lower scores in Ease of Access and Safety, which are crucial criteria, made it slightly less favorable. Considering all factors, the ‘Partially Sliding Door Side’ was the recommended choice for interior part station access due to its optimal balance of space efficiency, safety, ease of access, and overall fit with the weighted criteria. This option aligned with the operational priorities and was expected to offer the best long-term value and performance.

6.2 Endoscope Mount Selection

Table 7 was used as a design matrix for endoscope mount selection.

Table 7. Endoscope mount decision matrix

Endiscope Mount	Weight	Single hole insertion	Clamping Mechanisim
Endoscope roatation	8	8	8
Endoscope stablitly	8	8	9
Ease of Access	7	4	8
Cost	3	3	4
Durability	6	6	5
Total		29	34
Weight Total		201	234

These weight scores are furthered detailed as follows:

Endoscope Rotation (Weight 8): Highlighting the importance of precise rotation for optimal viewing angles during procedures.

Endoscope Stability (Weight 8): Emphasizing the need for stable positioning to ensure clear visualization and procedural accuracy.

Ease of Access (Weight 7): Underscoring the importance of easy access for smooth workflow and efficiency.

Cost (Weight 3): Balancing affordability with performance and reliability considerations.

Durability (Weight 6): Stressing the importance of long-term resilience to withstand frequent use.

These category scores can be further defined as:

Endoscope Rotation (1 to 10): Scores assess the ease and precision of endoscope rotation, with 10 indicating optimal control.

Endoscope Stability (1 to 10): Scores reflect the reliability and steadiness of the endoscope during operation, 10 noting minimal movement or vibration.

Ease of Access (1 to 10): Scores evaluate the ease of accessing and maneuvering the equipment, with 10 representing minimal hindrance to workflow.

Cost (Weight 3): Scores measure relative expense, with 10 indicating cost-effectiveness.

Durability (Weight 6): Scores reflect the expected lifespan of the access method, with 10 being most durable.

Based on the weighted totals in Table 7, the ‘Clamping Mechanism’ option scored the highest with a weighted total of 234, closely followed by the ‘Single Hole Insertion’ with a weighted total of 201. The ‘Clamping Mechanism’ option excelled particularly in Ease of Access and Endoscope Stability, which are among the most heavily weighted criteria. Considering all factors, the ‘Clamping Mechanism’ is the recommended choice for the endoscope mount due to its optimal balance of endoscope stability, cost, ease of access, and overall fit with the weighted criteria. This option aligns with the operational priorities and is expected to offer the best long-term value and performance.

6.3 Measurement Station Parts Specification

A variety of custom parts were required to ensure proper station activity. The background mount and endoscope mount were custom parts developed during this process.

6.3.1 Background Mount

A background was installed to provide a solid, white backdrop for the measurement system to capture images of endoscopes in optimal conditions for the clearest images possible. The background, which is a matte white foam board, runs along the entire width of the station through the slot in the straightening device to cover the lead screw and rails underneath and shield them from view of the camera mounted at the top of the station. Background brackets, or mounts, were designed in SolidWorks and 3D printed, shown on both ends of the station in Figure 48 below (white PLA), to stabilize the background as the straightening device moves back and forth across the station. The background mounts, consisting of two narrow pieces with screws holding them together, were designed to compress the background from the top and bottom and hold it in place. Both mounts screw in and firmly attach to the T-slot aluminum profiles on the front and back of the station to keep the background still and ensure it remains at the necessary height.

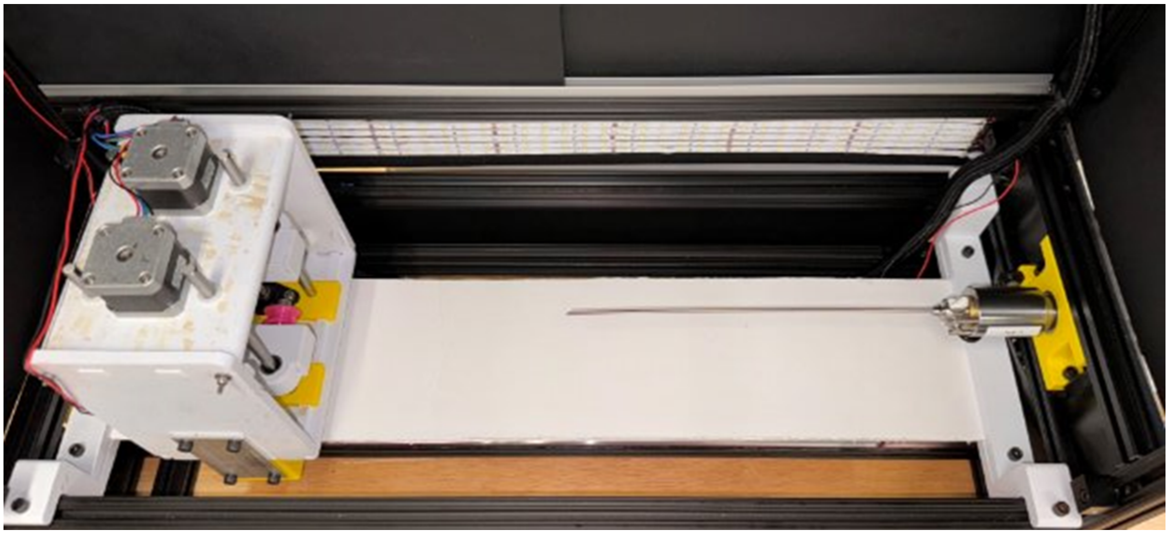

Figure 49: Top View of Inside of the Station Displaying the Background Mount

6.3.2 Endoscope Mount

An endoscope mount is a device or fixture designed to securely hold an endoscope in place during procedures or measurements. The mount provides stability and precise positioning of the endoscope, allowing for optimal visualization and manipulation during procedures. The endoscope mount utilizes a belt and pully system with a NEMA 17 motor. This motor type is used in precision equipment due to its ability to move in precise increments, making it well-suited for tasks requiring accurate positioning. The 3:1 gear ratio signifies that for every three rotations of the motor shaft, the output shaft completes one rotation. This gearing arrangement effectively increases torque while reducing speed, providing the necessary power to support the weight of the endoscope and ensure smooth, controlled movements. Endoscopes can be inserted through the sliding panel doors in the station. The team applied HSWoA current endoscope insertion method to retain familiarity and ease of use. To insert the endoscope, users place the knob of the endoscope through the designated slot, ensuring a precise fit within the station. Once positioned, the endoscope is firmly secured in place using screw knobs located on the station’s surface. These screw knobs provide users with tactile feedback.

The ME4320 B-term teams design was unstable and induced heavy vibrations. The mount’s design failed to incorporate additional supports or reinforcements to counteract the vibrations induced during operation. Without adequate stabilization, the mount was susceptible to excessive movement, amplifying the instability of the overall system. The absence of proper alignment mechanisms or adjustment features hindered the team’s ability to fine-tune the positioning of the endoscope effectively. This limitation constrained their ability to achieve optimal alignment, leading to runout errors and decreased accuracy of the imaging process.

This design was improved in several ways, one of which was creating an adjustable endoscope mount, which offers versatility and precision in positioning endoscopes. Its autonomous rotation capability, facilitated by an attached motor, allows for smooth and controlled movement, enabling operators to easily navigate the endoscope to desired angles and orientations. This autonomous rotation not only enhances procedural efficiency but also reduces the risk of unwanted movements that could compromise the accuracy of observations or measurements. All rotation of the endoscope is controlled by the NEMA 17 motor. This system is adjusted remotely. The endoscope mount was securely affixed to the station using two 8-inch T-slot aluminum profiles to ensure robust stability and minimize the risk of vibrations. The motor's location was calculated to ensure optimal tension on the belt pulley system. Figure 50 shows the motor and transmission system. The belt drive is located 5.5 mm apart ensuring proper tension and smooth and reliable rotation of the endoscope. Maintaining optimal tension is crucial to prevent any potential slack in the belt, which could compromise the precision and accuracy of the endoscope's movements. If too much slack is present in the belt drive system, the belt may slip on the pulleys, resulting in erratic or incomplete rotation of the endoscope. This loss of control can impede the operator's ability to manipulate the endoscope, affecting straightening of endoscopes. Moreover, elevating the endoscope mount station serves to prevent interference with the lead screw and rails.

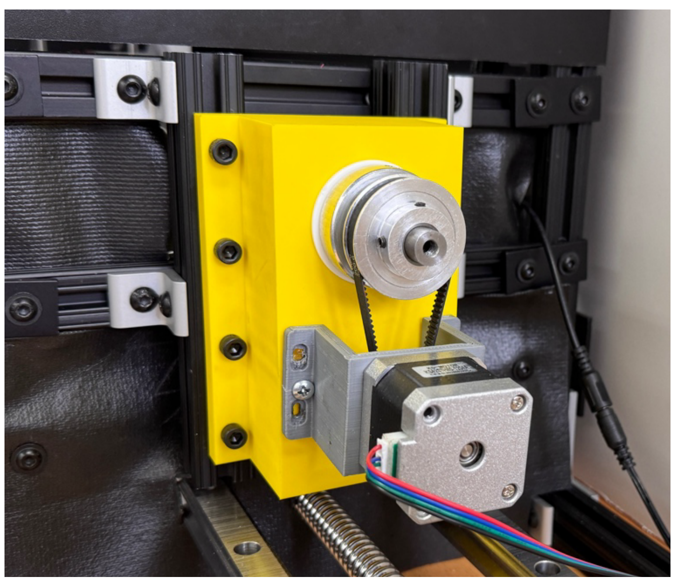

Figure 50: Endoscope Mount Motor and Transmission System

This chapter overviewed station requirements, endoscope mount selection processes, and parts specifications for several main components of the station. The next chapter details the straightening device's parts, performed analysis, and several component specifications.

7 Straightening Device

This chapter gives the straightening device overview and explains how the team defined the required force to straighten the endoscopes and how the team verified the basic calculations with FEA software. Then, the selection of stepper motors and lead screws as couplers to achieve the force and velocity requirements is discussed. Additionally, the team details individual parts and verifies that they have the desired factor of safety.

7.1 Straightening Device Overview

These straightening device updates outline the principal design modifications undertaken on the current project. The revisions are based on the team's discussion of improving functionality and efficiency with HSWoA based on the previous team's results. The design changes were considered during the revision process, and engineering concepts were applied parallel with Finite Element Analysis (FEA), leading to the final decisions described below. Figure 51: Straightening Device Components shows the integral components of the straightening device. Roller adapters move up and down where the flanged nut is fixed into the roller adapter, which converts rotational motion from vertical stepper motors into linear motion. Vertical lead screw and stepper motor are engaged through the flexible shaft. Stepper motors are fixed to the top plate. Direction yellow rods prevent rotation about the vertical lead screw axis. Rollers are fixed to the roller adapter and can rotate about their central axis. The background covers the horizontal lead screw and can go through the slot in the H-shaped part.

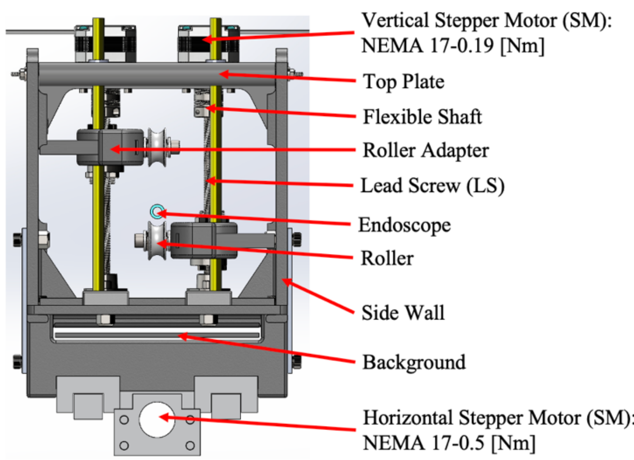

Figure 51: Straightening Device Components

7.2 Required Straightening Force

Since the endoscope's bendiness is caused by plastic deformation, this has a significant impact on the selection of the stepper motor and lead screw. It was essential to ensure that the application of force did not lead to localized plastic deformation on the endoscope's surface. The straightening device operates with a three-roller mechanism, where two rollers are positioned below the endoscope and one above it. The previous team provided some stress-strain curves for stainless steel, but the team used the material parameters from the SW library to get the most accurate estimation in basic calculations. Additionally, the applied force should be considered as a force applied not only on stainless steel tubes but with a layer of glass fiber.

The core of the team's analytical approach involved a detailed static analysis to determine the precise force each roller set (top/bottom) must apply to achieve the desired straightening effect without compromising the endoscope's integrity. Given that the movement of the rollers was predefined, allowing for a controlled displacement, the safety factor of the endoscope was not a primary concern in this context. Instead, the focus shifted to preventing surface-pointed plastic deformation, which can be addressed by selecting an appropriate material for the rollers.

This analysis will assess the stress distribution across the endoscope when subjected to the straightening force, treating the endoscope as a beam under bending stress, as illustrated in Figure 52: Static Roller Diagram. The material composition of the first and last layers of the endoscope, particularly its construction from 304 stainless steel, along with its geometric dimensions—such as the outer and inner diameters of its layers—will significantly influence the analysis outcomes. The aim was to calculate the force necessary to surpass the yield strength of the endoscope's composite material, assuming the endoscope has not undergone hardening from previous deformations and that its yield strength remains constant.

Following a general discussion on the methodological approach, the team will employ Excel, which can be found in step 7, for detailed calculations across different endoscope models. This step was critical for tailoring the straightening force to the specific requirements of each endoscope type, thereby ensuring the device's effectiveness and the endoscope's structural integrity post-straightening.

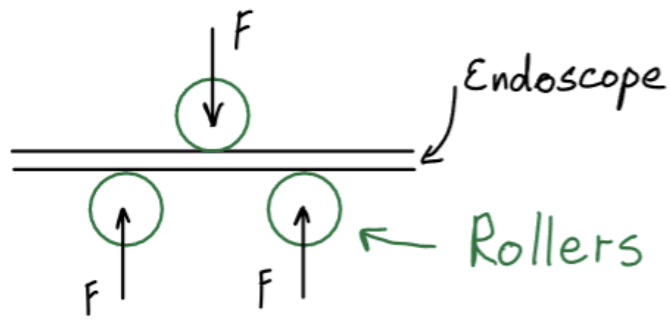

Figure 52: Static Roller Diagram

In the team's development of a model for the static analysis of the endoscope straightening device's roller mechanism, we've employed specific simplifications and assumptions to facilitate the analysis. These are critical for understanding the behavior of the system under load and ensuring accurate and reliable predictions of the forces required to correct the deformation of endoscopes. The assumptions are as follows:

1. Modeling the two bottom rollers as fixed supports: The team treated the two bottom rollers as pin supports. This assumption simplifies the analysis by providing a stable and immovable base against which the top roller can apply force.
2. No slip condition between layers: The assumption of a no-slip condition between the layers of the endoscope was crucial. It implies that the layers reinforce each other, acting as a single composite structure rather than individual layers sliding over one another. As a result, the maximum force required should be the sum of the forces acting on each layer, acknowledging their combined resistance to deformation.

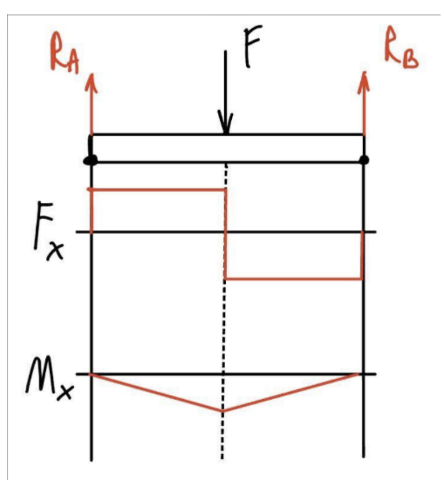

Figure 53: Simplified Statics Roller Diagram

The team followed a systematic approach to derive a solution using the general formula, considering the specified parameters and the setup of the endoscope straightening device. Given that the material of the endoscopes is 304 stainless steel and fiber type A is between SS layers, the team can outline the steps necessary to define the maximum beam bending moment within this framework. The forces were illustrated above in Figure 53: Simplified Statics Roller Diagram:

Ra, Rb – Reaction forces at the locations of the bottom rollers, which are considered simple supports.

F – The resultant force applied by the top roller is the force applied by a single roller due to the simplification.

L – The effective length between the two bottom rollers.

Step 1: Reaction Forces

The team needed to establish equilibrium conditions for the system to solve for the reaction forces (Ra and Rb). The team assumed a symmetric setup, Ra and Rb can be found by balancing the moments around any one of the fixed supports and ensuring the sum of vertical forces equals zero.

$$R_a + R_b = F$$

$$R_a = R_b = \frac{F}{2}$$

Step 2: Defining the Maximum Bending Moment

The maximum bending moment (*Mmax*) in the beam (endoscope) subjected to a uniform distributed load or a concentrated central load occurs at the midpoint of the span (*L*/2) or at the location of the concentrated load. In this scenario, the team considered *F* as a concentrated load applied at the midpoint:

The bending moment at any point *x* along the length of the beam was calculated using the formula $M_x = -R_a * x + F_3 * \left(x - \frac{L}{2}\right)$

As a result, $M_{max} = \frac{F * L}{4}$

Step 3: Maximum Stress

Given the adjustment of the Factor of Safety (FoS) to 1, based on the understanding that the predefined displacement would exceed the elastic region anyway, the calculation of maximum stress became a direct function of the material's yield strength. This simplification was based on ensuring that the operational parameters intentionally allowed for plastic deformation, which was necessary for the straightening process.

$\sigma_{max} = \frac{YS}{FoS}$

Where,

YS – yield strength

FoS – factor of safety

Step 4: Second Area Moment of inertia

In the context of the endoscope straightening device, accurately calculating the second area moment of inertia for each layer of the endoscope was essential for understanding how it would resist bending. Given that endoscopes could be modeled as cylindrical shells or tubes, the moment of inertia for each layer needed to be determined based on its outer and inner diameters.

Parameters:

D: Outer diameter of the any layer (stainless steel or glass fiber)

d: Inner diameter of the layer (stainless steel or glass fiber)

The moment of inertia (*I*) for a cylindrical shell or tube layer can be calculated using the formula for a hollow cylinder, which is particularly relevant for tubular structures like endoscopes:

$$I = \frac{\pi}{64} * (D^4 - d^4)$$

Step 5: Maximum stress

After determining the moment of inertia for the stainless steel layers of the endoscope, the next step involved calculating the maximum bending stress experienced by the endoscope during the straightening process. The bending stress formula gave the bending stress in a beam subjected to a bending moment.

Bending Stress Formula:

The formula for calculating bending stress (σ) in a beam is:

$$\sigma_{max} = \frac{M * c}{I}$$

M: Maximum bending moment (determined in earlier steps)

I: Moment of inertia for the layer (calculated in the previous step)

$c = \frac{D}{2}$: Distance from the neutral axis to the outermost fiber.

Step 6: Combining the Formulas to Calculate Maximum Force per Layer and Total Resultant Maximum Force

In this step, the team integrated the previous steps to calculate the minimum force that should be applied to each stainless steel layer of the endoscope during the straightening process. Then, the team determined the stress in the fiber layer and found the force, where (Fl1, Fl2, ...) are the minimum force for each layer.

$$\frac{YS}{FoS} = \frac{M * c}{I} = \frac{8 * F * L * D}{\pi * (D^4 - d^4)}$$

$$F_{min} = F_{max} = \frac{YS * \pi * (D^4 - d^4)}{24 * FoS * L * D}$$

Maximum force is the force that can be applied from a perspective to avoid plastic deformation; however, the team used this as the minimum force to initiate plastic deformation in the straightening process. In adapting the team's analysis to account for the distinct material properties of the fiber layer in the endoscope, a direct application of the same formula used for the stainless steel (SS) layer was not feasible. This was due to the significant difference in the yield strength (YS) of the two materials. Specifically, the YS of Type A fiber is approximately 1700 MPa, which is about eight times higher than that of stainless steel, which has a YS of 207 MPa. To accurately estimate the force required to deform the fiber layer, the team's approach leveraged the strain experienced by the stainless steel layer as a reference point.

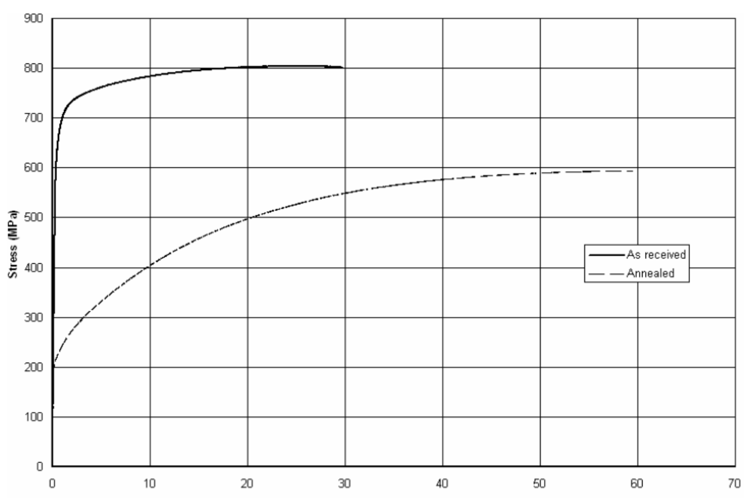

Figure 54: Stress-Strain curves for AISI 304 (Reproduced as is from [20])

Given that the YS of the SS layer is known from Figure 54, the team examined the stress-strain curve for stainless steel to determine the corresponding strain at this yield point, which equals 0.1% [21]. Under the assumption of a no-slip condition between the layers, it was reasoned that the fiber layer undergoes an equivalent strain due to the uniform distribution of deformation forces across the endoscope's structure. The stress of glass fiber at 0.1% strain equals 130 MPa [22]. This assumption allowed us to surmise that the fiber layer, despite its higher YS, would experience the same strain as the SS layer under applied forces.

To compute the force necessary to induce deformation in the fiber layer, the team then utilized the identified strain to find the corresponding stress for the fiber layer. Instead of using the YS directly as the team would for a material's initial yielding point, this stress value—derived from the strain experienced by the stainless steel and assumed for the fiber—is used in the formula for calculating bending stress and, subsequently, the required force. This method provided a more accurate representation of the forces needed to achieve plastic deformation across the different materials comprising the endoscope.

To calculate the total resultant minimum force that should have been applied from one roller:

$$F_{\min(total)} = Fl_1 + Fl_2 + Fl_n$$

Where n = number of layers

Next, an Excel, Table 9 shown below, will be used to input these calculations for concentric endoscopes. This will facilitate the determination of minimum forces applicable in the straightening device for different endoscope models, ensuring they can start plastically deforming to go back to their initial shapes. The endoscope models are provided in Figure 55: Endoscope Models Sheet 1 and Figure 56: Endoscope Models Sheet 2, which the team used to define glass fiber and stainless steel diameters.

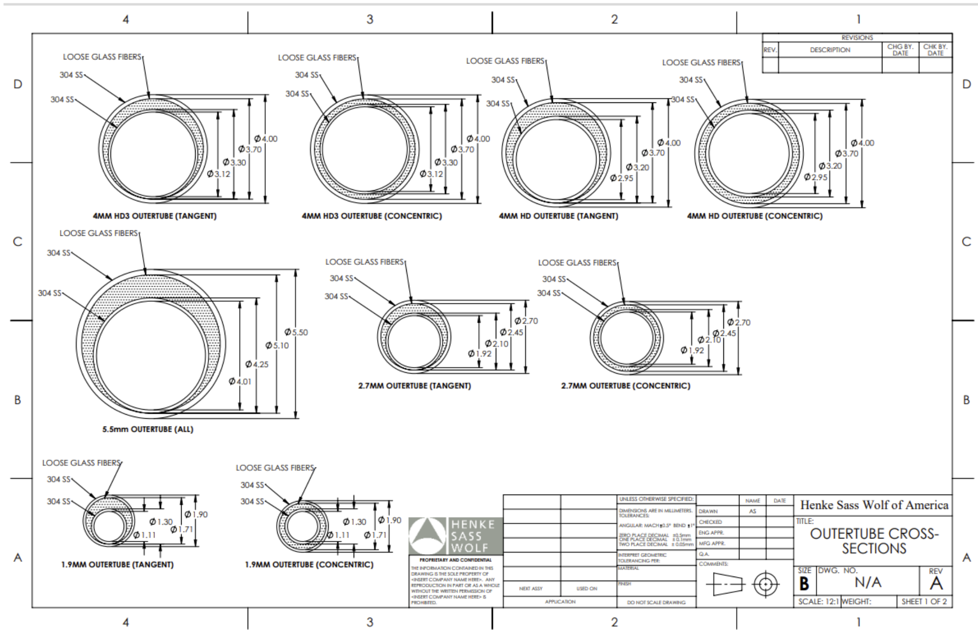

Figure 55: Endoscope Models Sheet 1

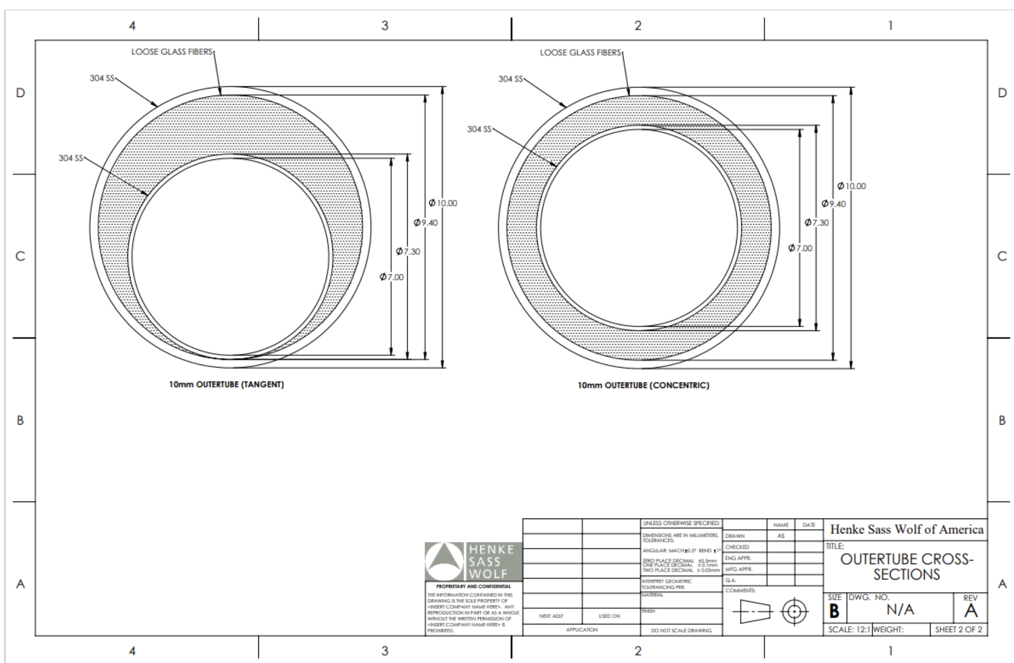

Figure 56: Endoscope Models Sheet 2

Step 7: Excel calculations

The Table 8. Endoscope Known Data was filled with known geometric parameters and material properties for different endoscopes and materials of endoscope layers. Then, it was used to calculate the minimum force for different layers (1, 2, 3) and the total force needed to be applied.

Table 8. Endoscope Known Data

Known Data Parameters								
Endoscope models (Concentric)	Diameters [m]				Geometric Parameters	Material Properties		FactorOfSafety
	d1	D1	d2	D2	RollerDistance "L" [m]	Stress Fiber Type-A [Pa]	Yield strength AISI304 [Pa]	
10mm	7.00E-03	7.30E-03	9.40E-03	1.00E-02	6.00E-02	1.30E+08	2.07E+08	1
4mm HD3	3.12E-03	3.30E-03	3.70E-03	4.00E-03				
4mm HD	2.95E-03	3.20E-03	3.70E-03	4.00E-03				
2.7mm	1.92E-03	2.10E-03	2.45E-03	2.70E-03				
1.9mm	1.11E-03	1.30E-03	1.71E-03	1.98E-03				

Table 9. Minimum Required Calculated Force

Endoscope models (Concentric)	Calculated Forces [N]			Calculated Stress [Pa]			Total Force MAX [N]
	Layer 1 (SS)	Layer 2 (Fiber)	Layer 3 (SS)	Layer 1 Stress	Layer 2 Stress	Layer 3 Stress	
10mm	81.366	449.652	296.767	2.07E+08	1.30E+08	2.07E+08	827.785
4mm HD3	9.776	15.827	23.208	2.07E+08	1.30E+08	2.07E+08	48.810
4mm HD	12.319	18.985	23.208	2.07E+08	1.30E+08	2.07E+08	54.512
2.7mm	3.776	5.759	8.580	2.07E+08	1.30E+08	2.07E+08	18.114
1.9mm	1.393	2.833	4.662	2.07E+08	1.30E+08	2.07E+08	8.888

7.3 FEA Minimum Force Verification

In this project, the team used finite element analysis (FEA) as an important step to check the team's math on how much force would be needed to straighten endoscopes. By using the FEA tool in SolidWorks, the team could closely look at stress, shape changes, and the forces needed in real-life situations. This section outlines the boundary conditions, initial conditions, and mesh information applied across all endoscope models within the FEA framework, leading to a summarized presentation of key findings.

Endoscope models:

The team used cross-section area dimensions from the drawing provided previously, and the distance between the bottom rollers defines the endoscope model length equal to 60 mm.

Boundary Conditions:

1) Fixed Geometry: The end faces of the top layer of the endoscope are fixed in position, replicating the stabilizing effect of the straightening device's support. The green arrows in Figure 57: Fixed Geometry show the fixed geometry.

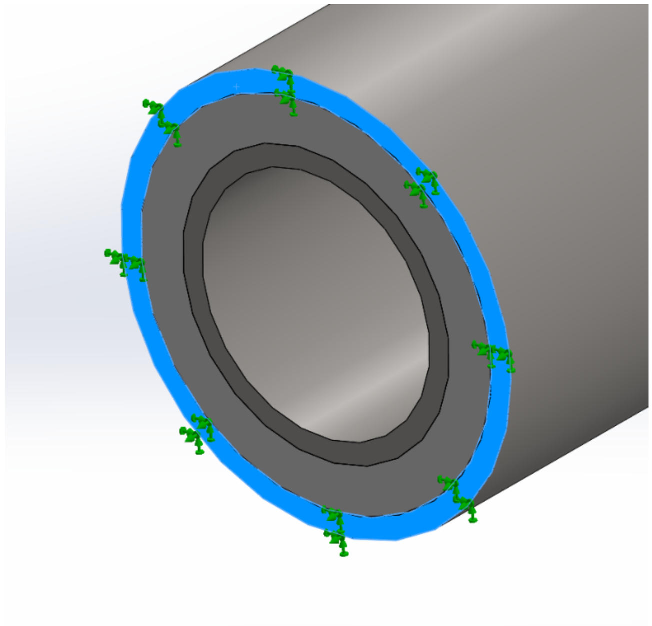

Figure 57: Fixed Geometry

2) Global Interaction: Surface-to-surface contact interaction is employed to accurately model the complex dynamics between different components of the endoscope, ensuring realistic simulation of their mechanical interactions.

Initial Conditions

Force Application: The contact area between the roller and the endoscope was simplified to a fixed dimension and shape, focusing on minimizing localized surface deformation. An elliptical contact area of 5.25 mm^2 was chosen, representing the maximum possible contact area for the smallest model of the endoscope. This area is critical in simulating the concentrated force application by the roller. The area is shown in Figure 58. The force magnitude, derived from theoretical calculations and detailed in an Excel sheet “EndoscopesForceAnalysis,” is applied centrally to this area to mimic the real contact scenario.

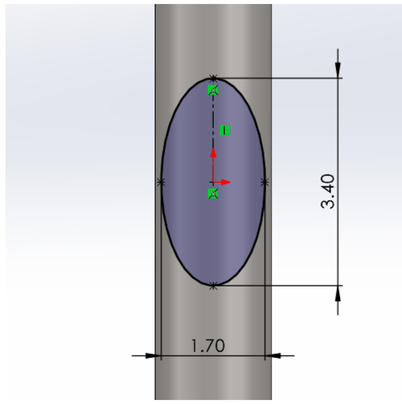

Figure 58: Area of Contact

Mesh Information from the SolidWorks mesh setup included several key details. The mesh type chosen was a solid mesh utilizing a blended curvature-based approach to accurately capture the intricate geometrical features of the endoscope. To ensure a high-quality mesh conducive to precise FEA results, 16 Jacobian points were utilized which enhanced the mesh's accuracy. The element size of the mesh was set with a maximum of 0.41 mm and a minimum of 0.14 mm. This range was optimized to balance computational efficiency with the need for detailed analysis in areas of high stress concentration. The mesh is shown in Figure 59: Mesh Example.

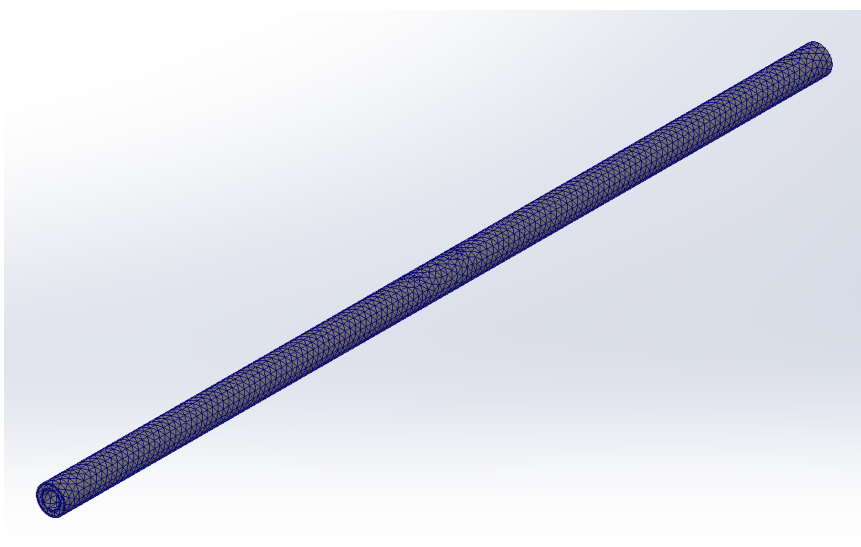

Figure 59: Mesh Example

In the context of finite element analysis (FEA) for the endoscope straightening device, the use of color-coded stress maps is a common technique to represent different levels of stress visually across the endoscope's structure during the simulation. When discussing the results of an FEA simulation, mentioning a "pink region" typically indicates areas where the material has undergone plastic deformation. This is based on a predefined color scale where each color corresponds to a specific range of stress values, with pink often denoting stress levels that exceed the material's yield strength, leading to permanent deformation.

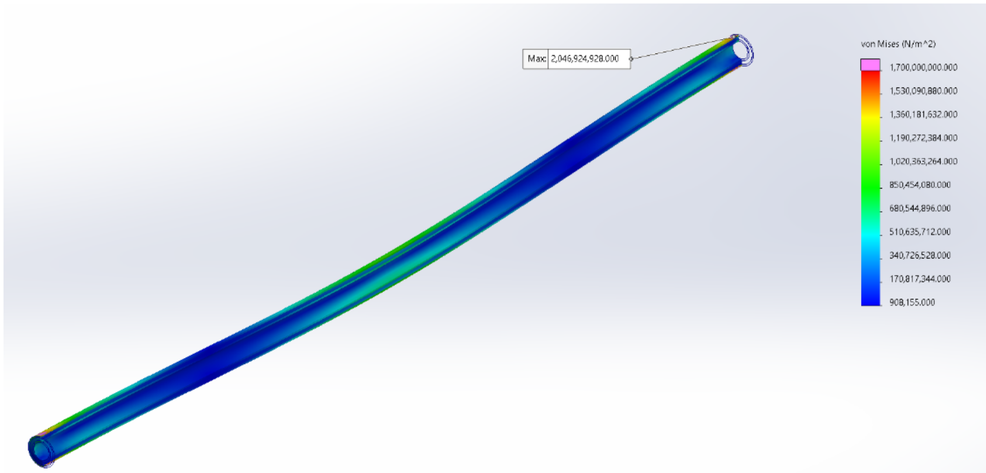

Figure 60: Example 1.9mm Endoscope Diagram

In the next table, the minimum forces are found through FEA for each endoscope model using the same model conditions described above, and the second column has previously estimated forces through static analysis.

Table 10: FEA vs Basic Estimation

Endoscope models (Concentric)	FEA Min Forces [N]	F Calculations Min Force [N]
10mm	750	828
4mm HD3	62	49
4mm HD	70	55
2.7mm	25	18
1.9mm	10	9

Table 10 presents the comparative outcomes derived from both Finite Element Analysis (FEA) and preliminary calculations for various endoscope models. The data indicated that the endoscope with the largest diameter displayed the largest discrepancy between the basic calculated force and the force found from Finite Element Analysis (FEA) for straightening. This variance is attributed primarily to the thicker stainless steel fiber layers inherent to the larger endoscope model, which inadvertently contribute to the observed inaccuracies in the force estimation. Specifically, the model of the endoscope measuring 10mm in diameter necessitates a force application that is significantly higher—tenfold, to be precise—than that required for the next largest model. During a consultation with the team's project sponsors, a collective decision was made to set aside the development efforts concerning the 10mm endoscope model temporarily within the current phase of the project. This strategic pivot aims to streamline the prototyping phase and circumvent the additional complexities associated with this particular model, especially considering that only a marginal fraction, precisely 0.5%, of all bent endoscopes encountered in practice correspond to the 10mm variant. This focused approach was anticipated to facilitate a more efficient allocation of resources and expedite the overall development timeline.

In the subsequent stage of the team's investigation, attention shifts towards evaluating a 5.5 mm endoscope characterized by its non-concentricity. This analysis specifically targets the endoscope weakest point, with the experiment structured around a predefined separation of 60mm between the rollers and a contact area dimensioned at 5.25 mm2, as previously outlined and shown in Figure 61: Force Application Point. The designated point 'A' on the endoscope symbolizes this frail section, where an applied force of 75 N has been identified as the minimum necessary to commence the straightening procedure under the current conditions shown in Figure 63: 160 N force applied 5.5 Non-Concentric. This force threshold was determined through prior calculations for concentric endoscopes and is deemed critical for initiating corrective action without compromising the structural integrity of the endoscope.

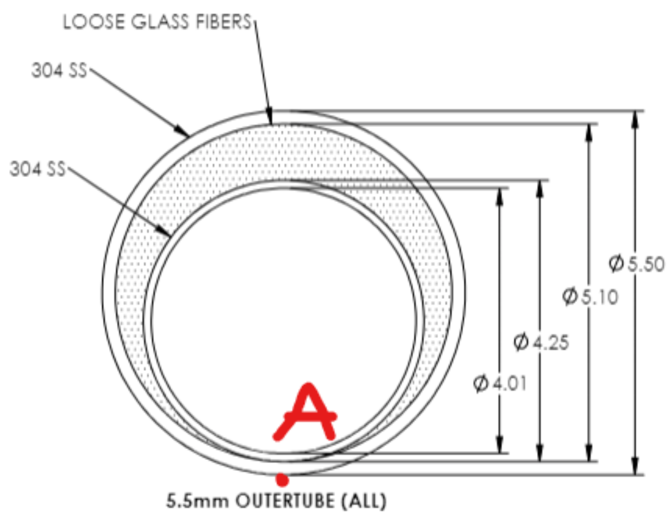

Figure 61: Force Application Point

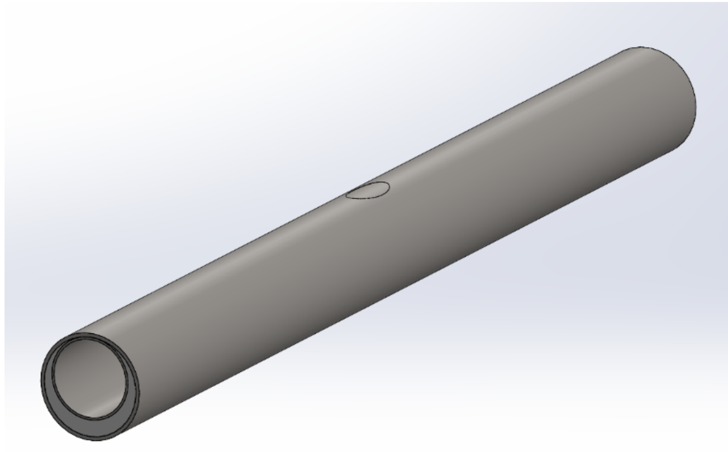

Figure 62: 5.5mm Non-Concentric Endoscope CAD Model

160 N force is enough to initiate plastic deformation for a 5.5 mm Non-Concentric endoscope. The 5.5 mm endoscope model is shown in Figure 62: 5.5mm Non-Concentric Endoscope CAD Model.

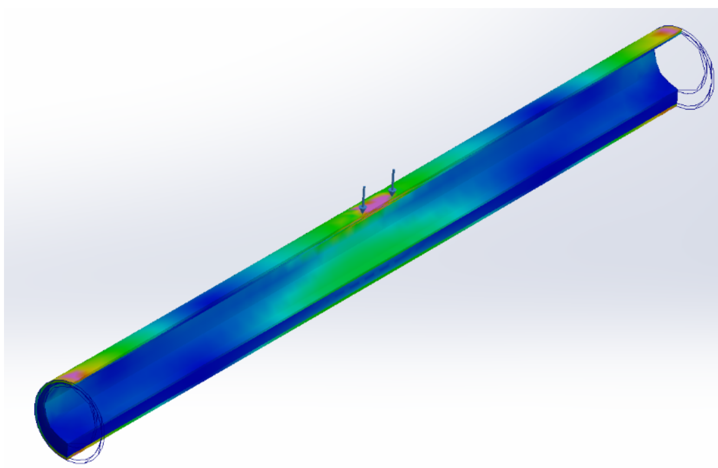

Figure 63: 160 N force applied 5.5 Non-Concentric

Initial estimates were recognized to possess a degree of inaccuracy, primarily due to the limited information on the specific material properties involved. Consequently, the precision of the finite element analysis (FEA) remains uncertain without further empirical validation. To address this, real-world testing was deemed necessary. Despite these limitations, based on the data available from general material property libraries, it is apparent that the force required to initiate straightening is greater than initially calculated, with a minimum of 160 N identified as necessary. The FEA diagram is shown in Figure 63. To account for potential inaccuracies in the team's calculations and ensure a margin of safety, a Factor of Safety (FoS) of 2 will be applied to the force exerted by the rollers.

7.4 Vertical Stepper Motor/Lead Screw

This sub-chapter talks about selection of vertical stepper motor and vertical lead screw of the straightening device as a coupler to get desired force and velocity parameters.

7.4.1 Introduction

In the team's latest analysis, the team has determined that the total force required to be exerted by the stepper motors and lead screw couplers should amount to 320 N, which means each set of rollers, top and bottom, needs to apply 160 N. It is vital to understand the forces involved with the lead screw to select a suitable screw assembly for the team's equipment. Since the team's references provide measurements in imperial units, the team has converted the team's metrics accordingly.

There are several important parameters to consider regarding the stepper motor and lead screw coupler specifications such as:

Weight of Assembly: The lead screw is responsible for moving a weight of 1.8 N.

1) External Forces: Each roller set, both top and bottom, needs to exert a force equivalent to 35.96 lbs, which is 160 N in the metric system.
2) Desired Linear Velocity: The target speed is 15 inches per minute, which translates to 6.35 mm per second.
3) Time to Reach Desired Velocity: The system should take 0.5 seconds to achieve the desired speed.
4) Type of Linear Bearing: The assembly has a specific plastic bearing with a friction coefficient of 0.05.

Following the identification of these parameters, the team adopted a formula-based approach to estimate the required power of the stepper motor, and all calculations were done in Excel for ease of future estimations.

Step 1: Calculation of Total Force on Lead Screw [23]

1) $F_t = F_a + F_e + F_f$

Where:

Ft = Total Force

Fa = Force due to acceleration

Fe = External Forces equals 36.37 [lbs]

Ff = Force of friction

2) Let's calculate the force of acceleration:

$$a = \frac{v}{60} * \frac{1}{t}$$

Where:

V = velocity (IPM) or (in/minute)
T = time to reach velocity (s)

$$F_a = \frac{a}{12} * \frac{W}{g}$$

Where:

W = weight of assembly being accelerated (lb)

G = gravity = 32.174 (ft/s/s)

A = acceleration (in/s/s)

3) Next, the team found friction force using friction coefficient between lead screw and flanged bearing type:

$$F_f = \mu * w$$

Where:

W = weight of the assembly

$\mu =$ coefficient of friction

All these components were meticulously calculated using an Excel spreadsheet, "VerticalStepperMotorAnalysis," with the inputs requiring user specification highlighted for clarity and ease of modification.

Table 11: Excel Calculations Step 1; Vertical Stepper Motor

Step 1: Calculate total force on lead screw								
Initial SI values	Units	Value				Calculation	Units	
Roller reaction force	N	160						
Assembly mass	kg	0.183			1)	a		0.5
Assembly weight	N	1.79523				Fa		0.000522658
Parameters					2)	Ff		0.020179193
Name	Units	Value						
Roller reaction force	lbs	35.96944			3)	Ft	lbs	36.39372571
w - Weight of assembly	lbs	0.403583861						
Fe - external force	lbs	36.37302386						
Velocity	in/min	15						
Time to reach velocity	s	0.5						
Friction coefficient based on linear Bearing type	none	0.05						

Step 2: Define minimum lead screw diameter [24]

According to the source calculator referenced, the minimum diameter required for the lead screw is 0.08 inches for this team's application. However, to ensure a margin of safety and account for any unforeseen loads or stresses, the team decided to utilize a lead screw with a diameter of 0.25 inches. Choosing this lead screw puts us in a great spot—it does not just meet this project's needs; it goes above and beyond. Therefore, the straightening device will be both more reliable and built to last longer.

Step 3-4: Select the stepper motor/lead screw based on the required torque and linear velocity output.

In the third step of the team's process, the team focused on selecting the ideal combination of a stepper motor and lead screw to ensure the device achieves the desired torque and linear velocity. The team's investigation centered around two primary options. The first option involved retaining the team's existing stepper motor while introducing a new lead screw. Conversely, the second option proposed replacing the current motor with a new one but keeping the existing lead screw. The goal for both scenarios was to meet this project's specific requirements for coupling to achieve the necessary linear speed and torque.

Initially, the team assessed the current stepper motor, available from McMaster-Carr, which offers a torque output of 27 in-oz. This motor was considered in conjunction with a lead screw featuring a ¼"-40 thread (Part No: 6350K694) from McMaster, which translates to a 0.025-inch movement per screw revolution ("McMaster-Carr," n.d.). To determine the required torque, which was calculated to be 14.56 ozf*in, the team applied the total force calculated in Step 1 and the lead of the screw in the team's formula:

$$Torque = F_t * Lead$$

Furthermore, the team explored the potential linear velocities using the relationship:

$$V = RPM * Lead$$

This exploration was supported by examining the torque curve for the NEMA 17, 27 in-oz motor in Figure 64.

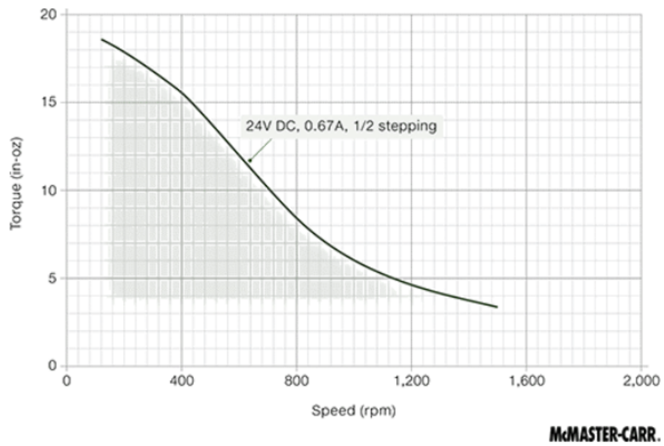

Figure 64: NEMA 17 27 in.-oz; Torque curve (Reproduced as is from [25])

Subsequently, the team evaluated an alternative stepper motor, another NEMA 17 variant (Part No: 6627T65) from McMaster, notable for its higher torque capacity of 39 in-oz. The torque-speed diagram is shown in Figure and paired with the team's pre-existing ¼"-20 thread lead screw (Part No: 6350K696), [25]. This setup required a stepper motor torque of 29.11 ozf*in. However, upon review, the team identified that adapting the system to accommodate these components would incur higher costs.

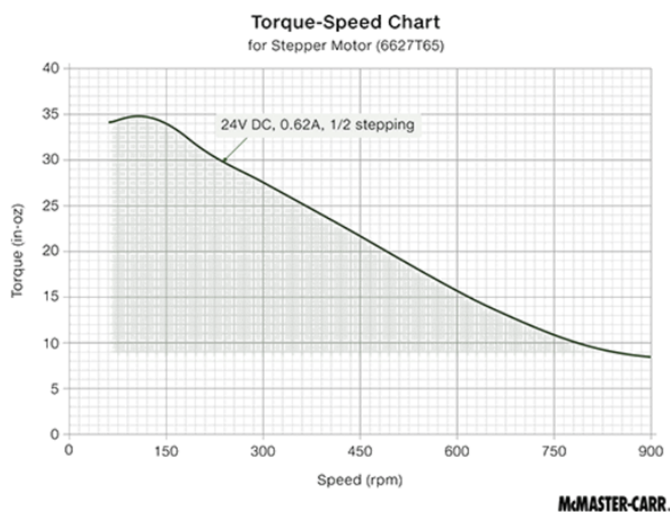

Figure 65: NEMA 17 39 in.-oz; Torque curve (Reproduced as is from [25])

After thorough consideration and analysis, highlighted by the green indicators in the team's Excel

"HorizontalStepperMotorAnalysis" spreadsheet for clarity, the team decided to go ahead with Option 1. This decision was made by balancing performance outcomes and cost-effectiveness, ensuring the straightening device efficiently meets its operational requirements.

Table 12. Step 3; define the required torque of stepper motor based on lead screw parameters

Step 3: Define the required torque of Stepper motor based on lead screw parameters								
Lead screw model	1/4"-20 Thread Size	Units						
Link:	https://www.mcmaster.com/6350K696/							
Option 2	Travel distance per turn (lead)	inch	0.05		5)	Torque	lbs*in	1.819686286
							ozf*in	29.11498057
Lead screw model	1/4"-40 Thread Size							
Link:	https://www.mcmaster.com/6350K694/							
Option 1	Travel distance per turn (lead)	inch	0.025		*	Torque	lbs*in	0.909843143
							ozf*in	14.55749028

Table 13. Step 4; define the appropriate stepper motor based on the required torque; options cost

Step 4: Stepper Motors		
Stepper motor model	NEMA 17, 27 in.-oz. Maximum Holding Torque	
Link:	https://www.mcmaster.com/6627T64/	
Option 1	RPM	
	min	max
	200	1300
Stepper motor model	NEMA 17, 39 in.-oz. Maximum Holding Torque	
Link:	https://www.mcmaster.com/6627T65/	
Option 2	RPM	
	min	max
	70	900

Options				
Option 1:	Use existing stepper motor with new lead screw	Linear velocity range [inch/min]		Cost of two lead screws
		min	max	$
		5	32.5	54.73
Option 2:	New stepper motor with existed lead screw	Linear velocity range [inch/min]		Cost of two stepper motors
		min	max	$
		3.5	45	158

7.5 Straightening Device Components Specification

7.5.1 Introduction

The device previously used for straightening had several notable weaknesses, which were created by team ME4320. First, it tended to shake and bend while straightening, which made it less effective and accurate. Additionally, the design included many unique parts which could have been replaced with symmetric parts. Another issue was the lack of direction pins, which made assembly more difficult. Furthermore, it used heavy steel plates, but these could have been swapped for 3D-printed parts that are lighter yet still strong.

The goal of the updated design changes was to improve the straightening device. In the following sections, the team went into the specific changes the team suggested for the straightening device, and the team showed the math needed to prove these changes could make the device more efficient and practical to use. The parts the team discussed later were shown in Figure 66.

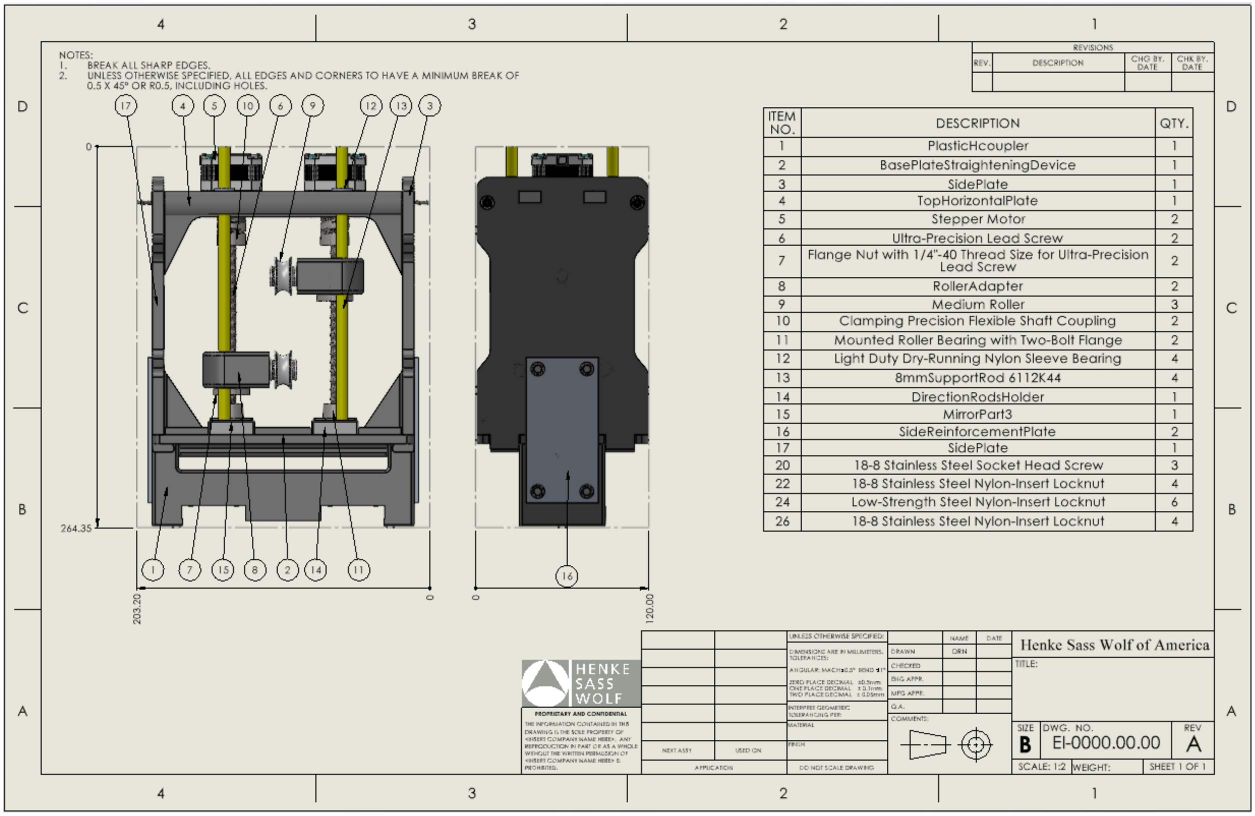

Figure 66: Straightening Device Main Components

7.5.2 Machined Parts

7.5.2.1 Side Reinforcement Plate

The objective of integrating a side reinforcement plate was to strengthen the joint where it connects to the Plastic H coupler component. This reinforcement was crucial as the primary load applied to this part emanated from the force exerted by the rollers, quantified at 160 N. In the team's Finite Element Analysis (FEA), the team used this force to simulate the stress and assess the durability of the reinforcement plate. The CAD model is shown in Figure 67.

In the FEA setup, the team treated the two lower holes of the plate, which bolt directly to the H coupler, as fixed support—this represented the fixed geometry in the team's model, Figure 68. The team then applied the 160 N force to the top holes of the plate to mimic the real-world application of the roller force, Figure 69. The team found that the side reinforcement plate was indeed capable of withstanding these forces based on FEA, Figure 70. The overall part's dimensions are provided in Figure 71.

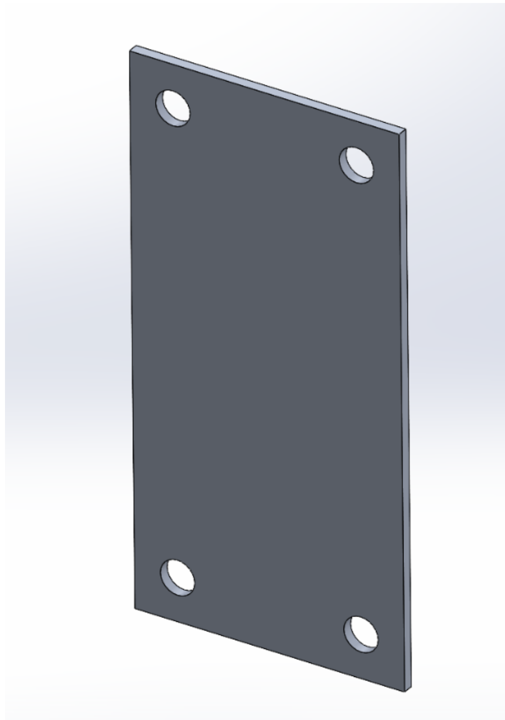

Figure 67: Side Reinforcement Plate CAD model

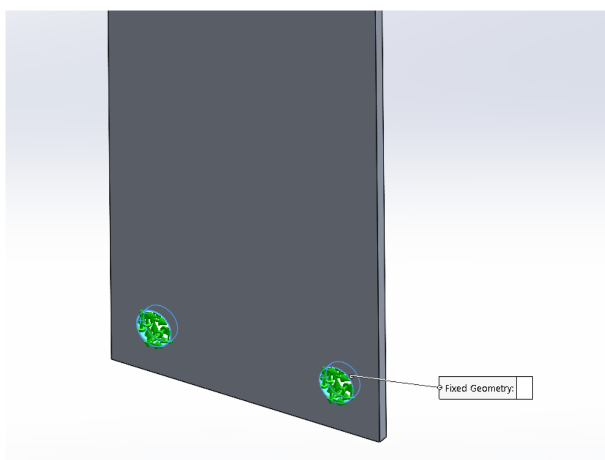

Figure 68: Side Reinforcement Plate; FEA; Fixed Geometry

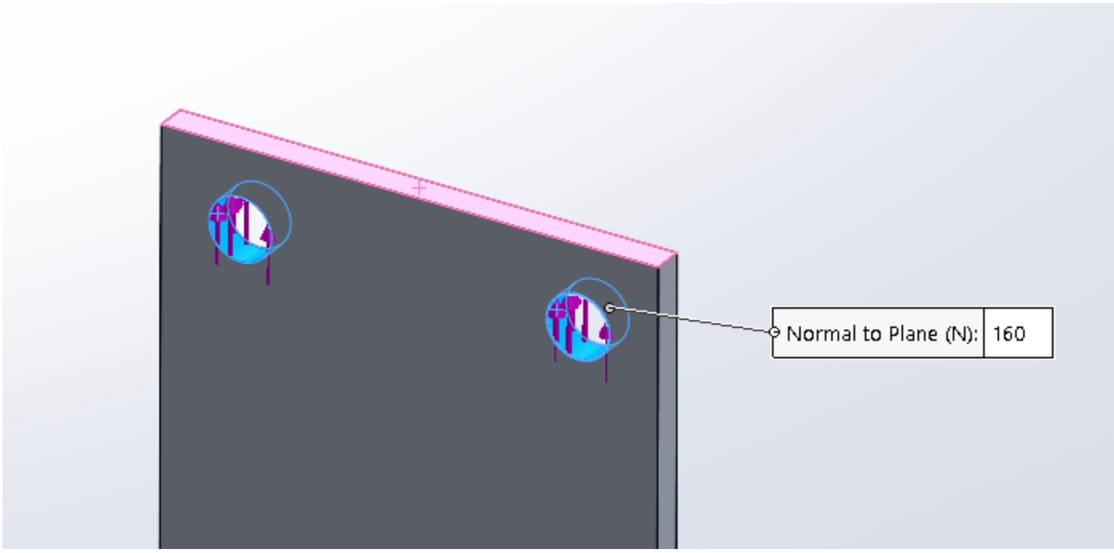

Figure 69: Side Reinforcement Plate; FEA; Applied Load

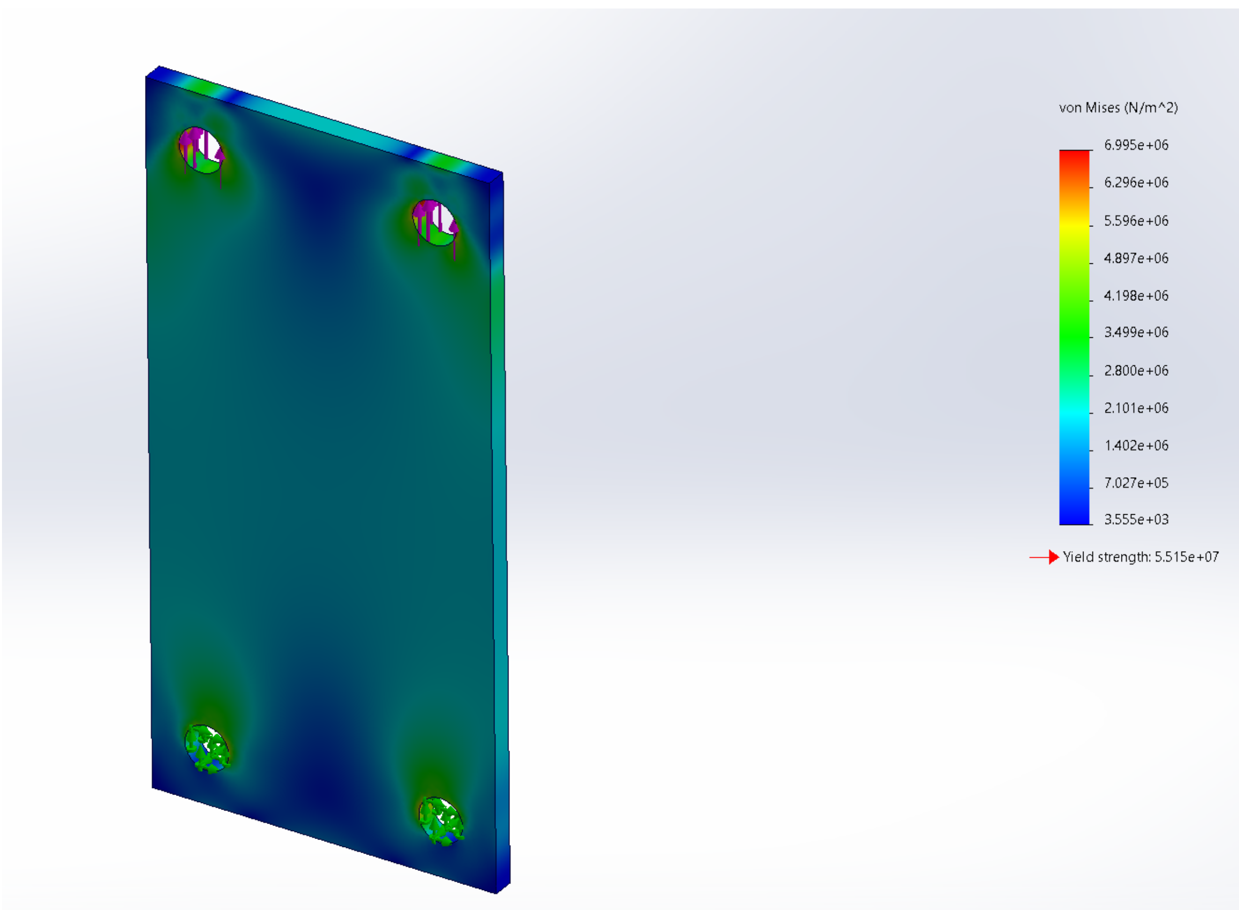

Figure 70: Side Reinforcement Plate; FEA; von Mises Stress Results

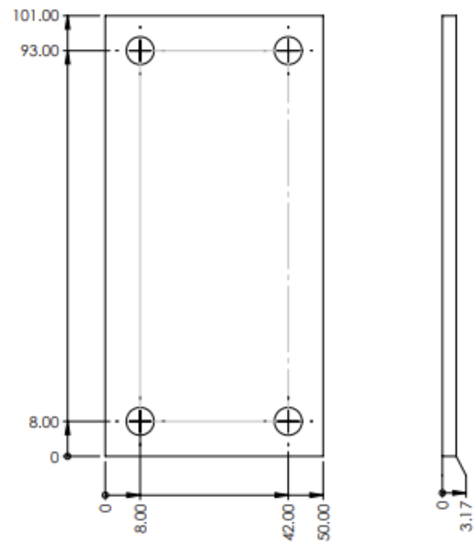

Figure 71: Side Reinforcement Plate; Overall Dimensions

Side Reinforcement Plate Specification is provided in Table 14

Table 14. Side Reinforcement Plate Specification

Raw Material Part No. (McM)	9057K118
Material	6061 Alloy
Applied Load	160 [N]
Max Stress (FEA stress)	7 [MPa]
Safety Factor	7.8
Dimensions: length, width, height	101, 50, 3.17 [mm]
Mass	0.042 [kg]

7.5.2.2 Vertical Lead Screw

The team procured the lead screw for this project from McMaster, and upon receipt, the team proceeded with machining it to meet the team's specific requirements. As McMaster provides certified parts with clear material specifications regarding load capacities, there was no necessity to conduct Finite Element Analysis (FEA) for the lead screw, and the minimum lead screw diameter was found in previous chapters. The CAD model is provided in Figure 72.

Following the cutting of the ordered lead screw into two separate pieces, each piece underwent a lathing process at one end. This machining step was executed in strict accordance with the technical drawings to ensure a precise fit, provided in Figure 73. Once lathed, each piece was then carefully aligned and pressed to fit the mounted roller bearings, securing them in place and completing the assembly process.

Figure 72: Vertical Lead Screw CAD model

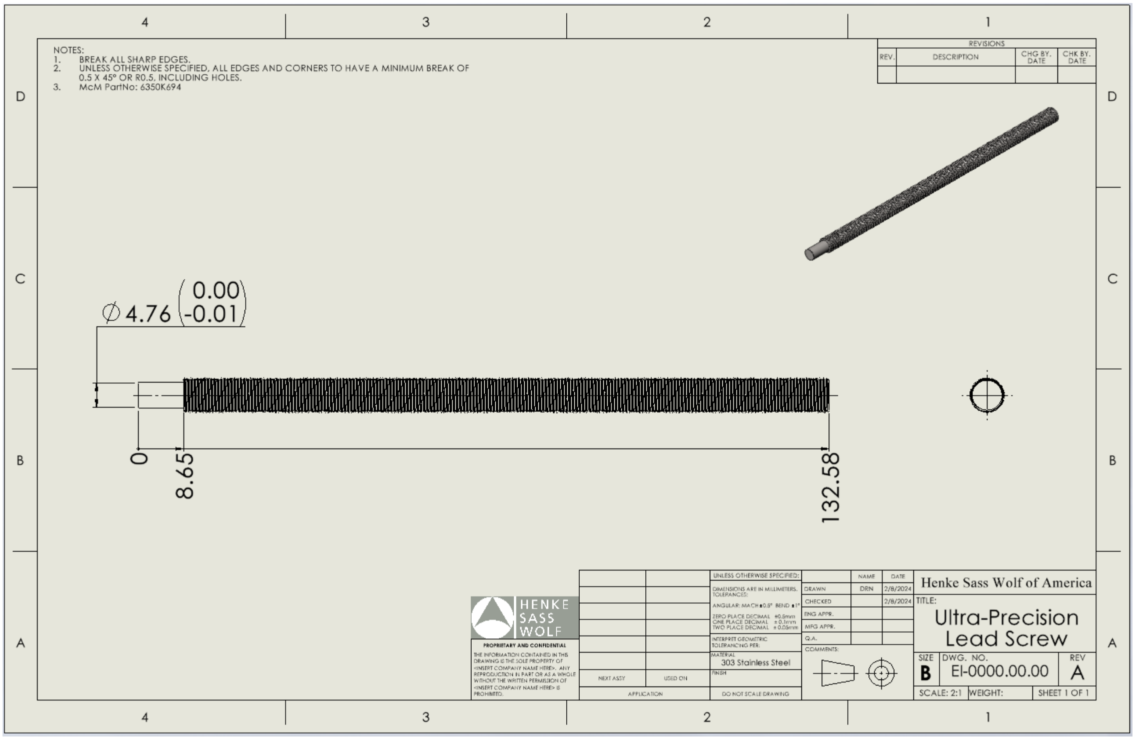

Figure 73: Vertical Lead Screw; Overall Dimensions

Vertical Lead Screw specification is provided in Table 15:

Table 15. Vertical Lead Screw Specification

Raw material Part No. (McM)	6350K694
Material	303 Stainless Steel
Applied Load	160 [N]
Min required Diameter	2.03 [mm]
Actual Diameter	6.35 [mm]
Dimensions: length	132.58 [mm]
Mass	0.03 [kg]

7.5.3 3D Printed Parts

7.5.3.1 Top Horizontal plate

Redesigning the top horizontal plate was a crucial change the team made to increase the stiffness of both this part and the whole straightening device. The CAD model is shown in Figure 74. Significant improvements were made to the part's structure to achieve this goal:

1. Through Side Holes: The team incorporated two through side holes at the top of the assembly for the insertion of compression rods. The addition of these rods played a crucial role in minimizing the assembly's tendency to fluctuate, thereby contributing to enhanced stability during operation.

2. Reinforcing Ribs: To increase the plate's resistance to the forces exerted by the rollers and the torque generated by the stepper motors, the team added two ribs on the bottom face of the plate.

3. Side Legs: Four side hooks were integrated into the design. These hooks rested against the side plates, serving as additional stabilizing points and simplifying the assembly process.

The fixed geometry feature was applied at the points where it connected with the side plates, Figure 75. During the simulated stress tests, a force of 160 N was applied to both the left and right sides of the plate, representative of the compression exerted by the rollers, Figure 76. The stress diagram is show in Figure 77. The overall "Top Horizontal Plate" dimensions are presented in Figure 78.

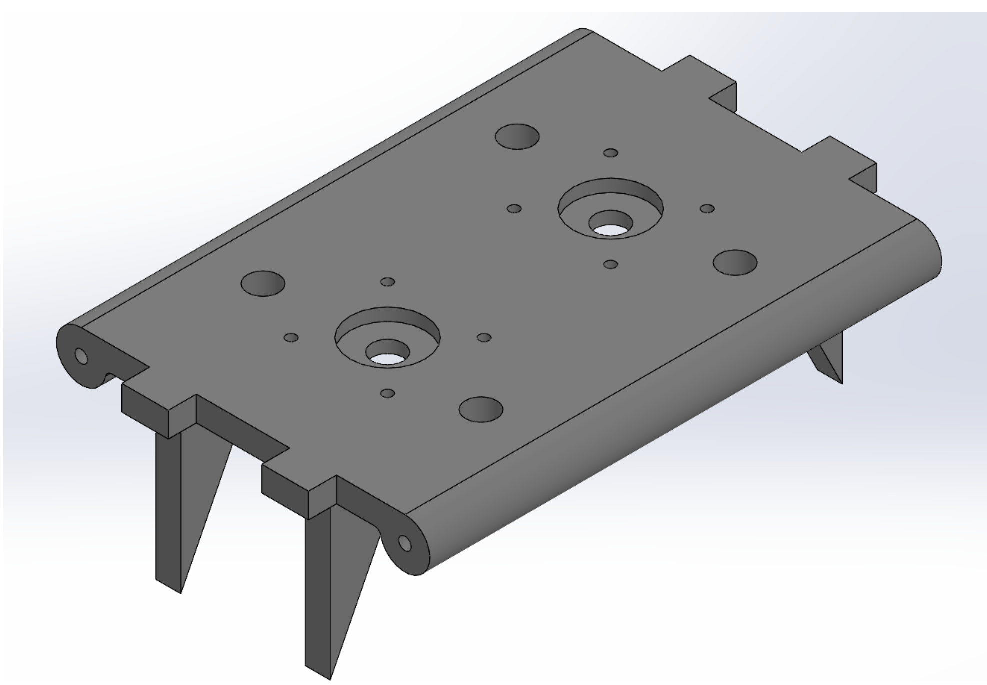

Figure 74: Top Horizontal Plate; CAD model

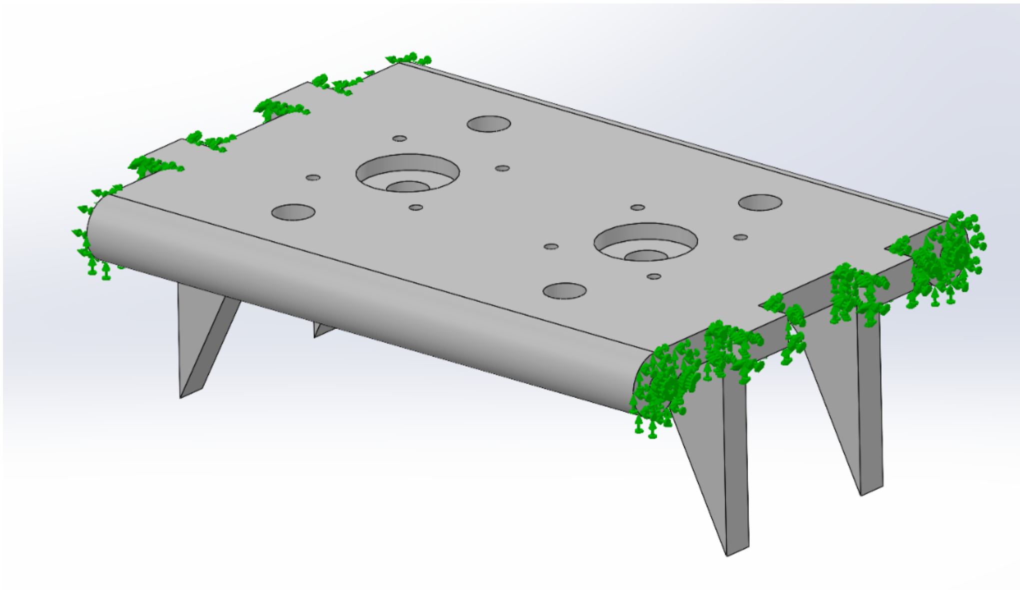

Figure 75: Top Horizontal Plate; FEA; Fixed Geometry

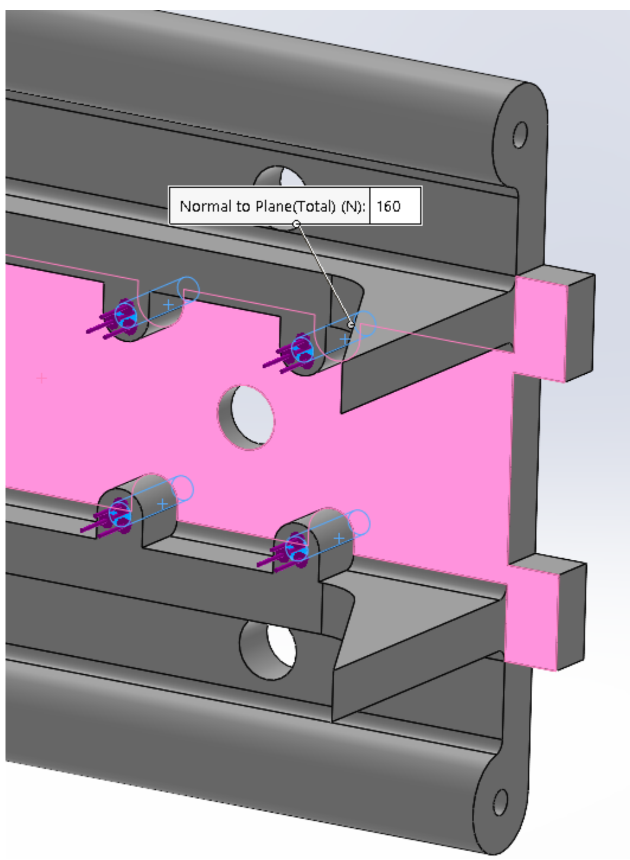

Figure 76:Top Horizontal Plate; FEA; Applied Load

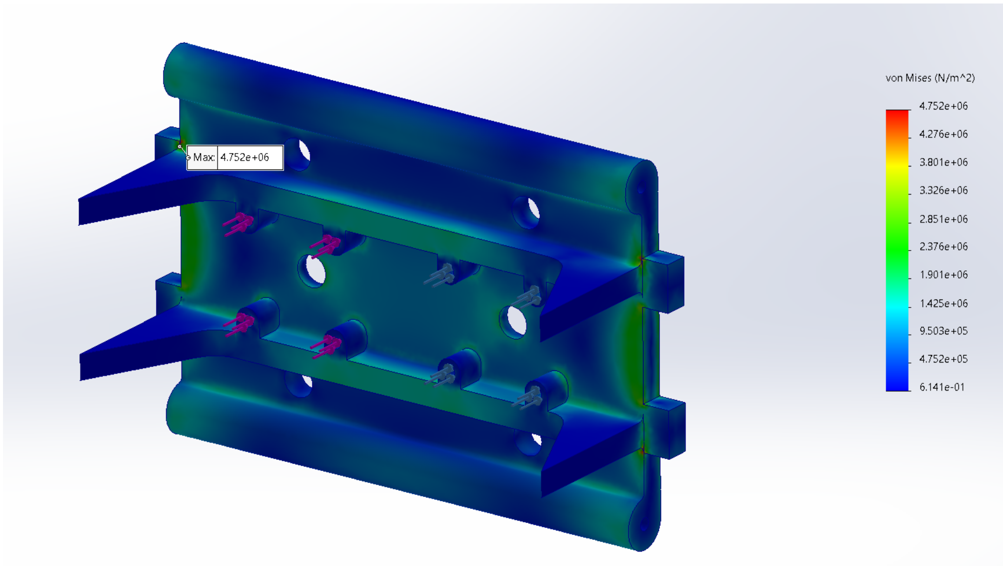

Figure 77: Top Horizontal Plate; FEA; von Mises Stress Results

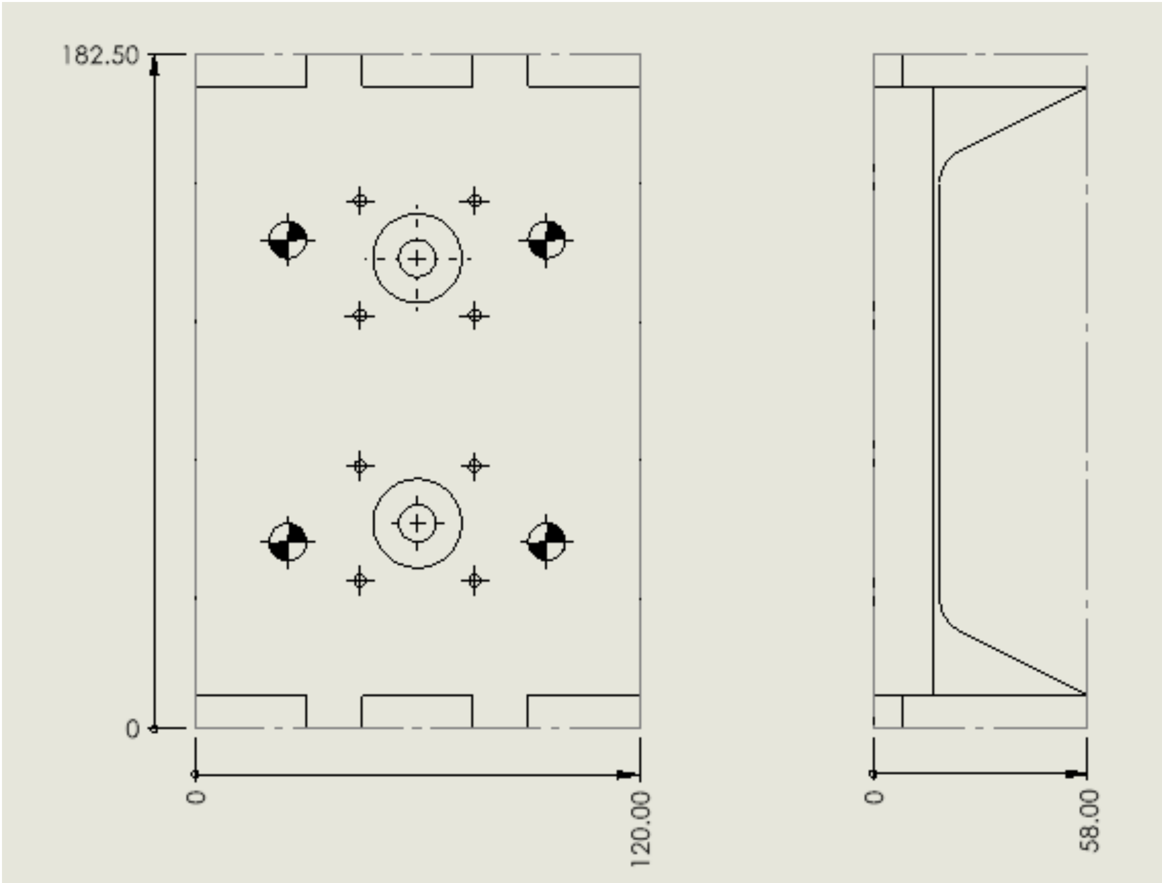

Figure 78: Top Horizontal Plate; Overall Dimensions

Top Horizontal Plate specification is provided in Table 16:

Material	ABS
Applied Load	300 [N]
Max Stress (FEA stress)	4.7 [MPa]
Tensile Strength	30 [MPa]
Safety Factor	6
Dimensions: length, width, height	182.5, 120, 58 [mm]
Mass	0.23 [kg]

Table 16: Top Horizontal Plate

7.5.3.2 Side Plate

The team revised the design of the side plate component to enhance its stability and assembly process. The CAD model is shown in Figure 79. The changes include:

1. Increased Thickness: The team increased the thickness of the side plate to provide greater strength and stiffness, ensuring the component could better resist deformation and stresses during operation.
2. Bottom Hooks: Bottom hooks were integrated into the design. This addition aimed to streamline the assembly process by allowing parts to be initially positioned and secured without the immediate need for screws, which were added later to fully secure the assembly.
3. Side Leg: A side leg was incorporated and designed to rest against the bottom plate. These hooks served as an extra contact point, and the bottom plate provided additional support to the overall structure.

The fixed geometry feature was applied at the points where it connected with the side plates and the hook surfaces, Figure 80. During the simulated stress tests, a force of 160 N was applied in total on the top square cuts where the top plate was connected, Figure 81. This force was representative of the rollers. The changes to the plate improved the overall assembly's stability. The FEA diagram is shown in Figure 82. These adjustments also made the assembly process more efficient, as components could now be temporarily secured by the bottom hooks. This allowed for simpler handling and alignment of parts before they were all permanently attached together. The overall side plate dimensions are shown in Figure 83.

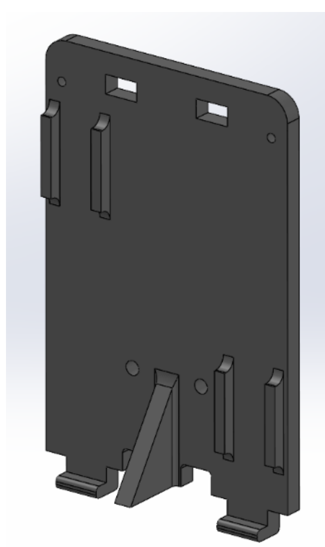

Figure 79: Side Plate; CAD model

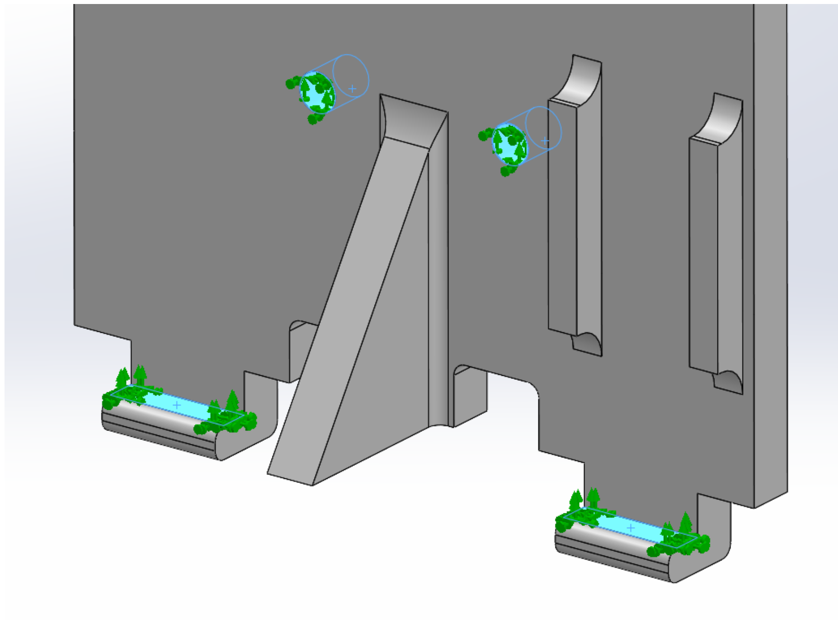

Figure 80: Side Plate; FEA; Fixed Geometry

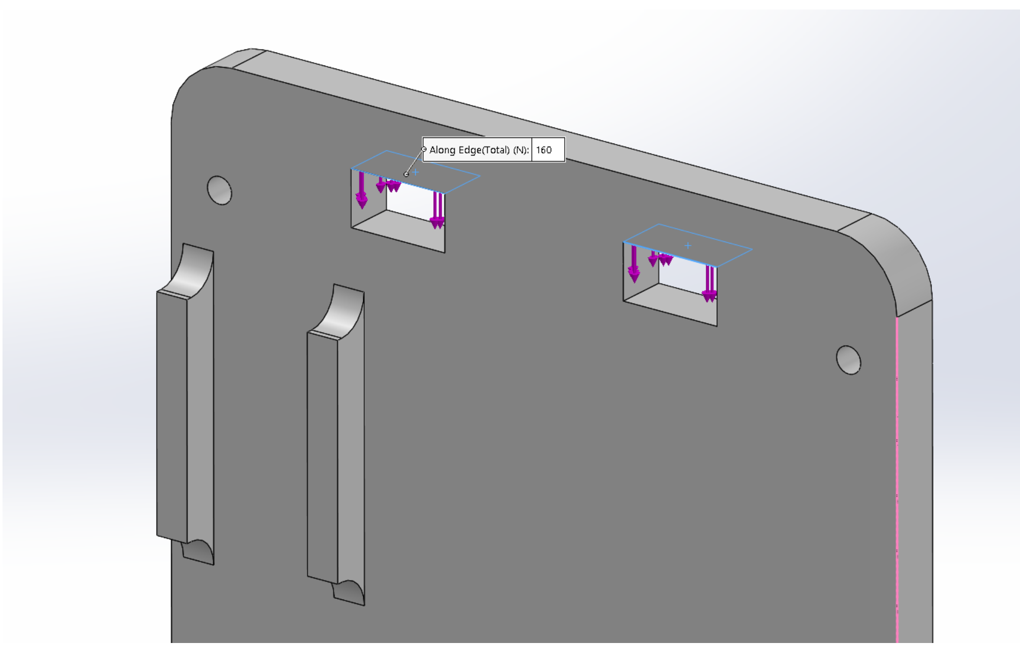

Figure 81: Side Plate; FEA; Applied Load

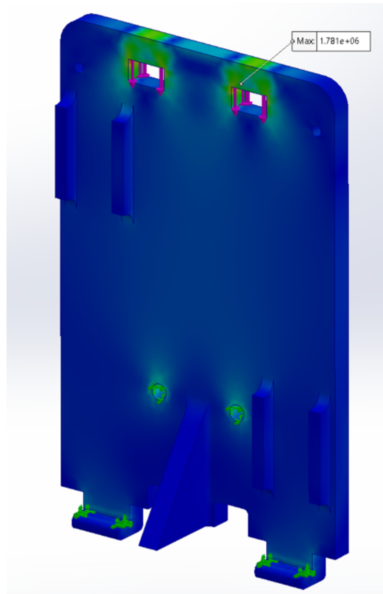

Figure 82: Side Plate; FEA; von Mises Stress Results

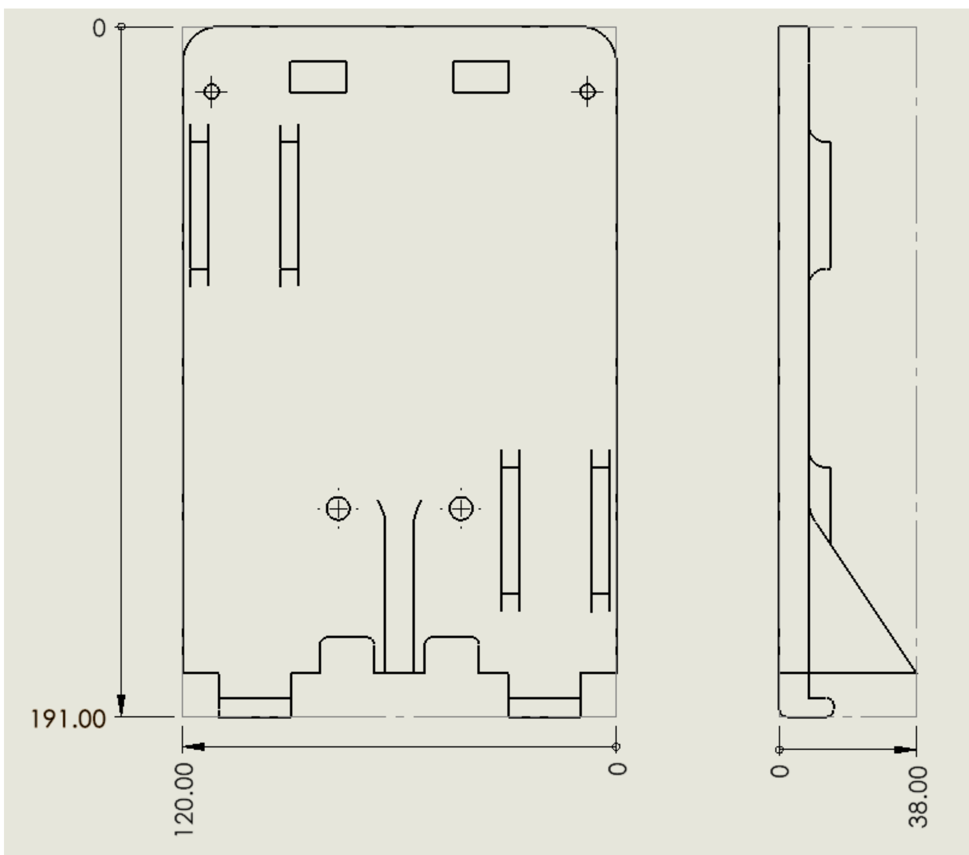

Figure 83: Side Plate; Overall Dimensions

The Side Plate specification is shown in Table 17le 17:

Material	ABS
Applied Load	160 [N]
Max Stress (FEA stress)	1.8 [MPa]
Tensile Strength	30 [MPa]
Safety Factor	17
Dimensions: length, width, height	185, 120, 38 [mm]
Mass	0.185 [kg]

Table 17. Side Plate Specification

7.5.3.3 Baseplate of Straightening Device

The team opted to replace the stainless steel previously used for the base plate with ABS plastic to reduce the device’s weight while maintaining sufficient strength to handle the operational loads. ABS offered a favorable balance of rigidity, toughness, and impact resistance, making it a suitable alternative for this application. The key design features the team implemented in the ABS base plate included reinforcing ribs. The Base Plate CAD model is shown in Figure 84. The team added a central reinforcing rib to the underside of the base plate to increase its stiffness and load-bearing capacity. Additionally, the team featured two reinforcing ribs on the top surface. These served to strengthen the plate and functioned as guide ribs, simplifying assembly.

In the team’s Finite Element Analysis, the load specifications showed that the base plate had been designed to accommodate a force of 160 N, which was the maximum expected load exerted by the rollers. The fixed geometry is shown in Figure 85. The team applied this force at the specific location on the plate where the vertical lead screw needle bearing was fixed, as this point was anticipated to experience the highest stress during operation, Figure 86. The team secured the part in the area where it contacted the H-shaped part, using the fixed geometry feature.

Following these modifications and the material switch, the team’s assessments revealed that the ABS base plate possessed the requisite durability to endure the applied forces. FEA diagram is presented in Figure 87. The overall Base Plate dimensions are presented in Figure 88.

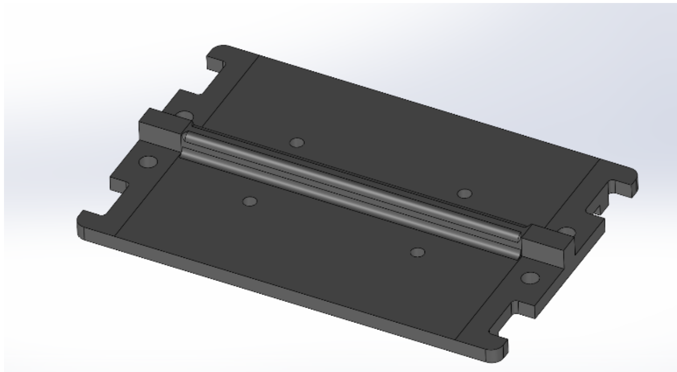

Figure 84: Base Plate; CAD model

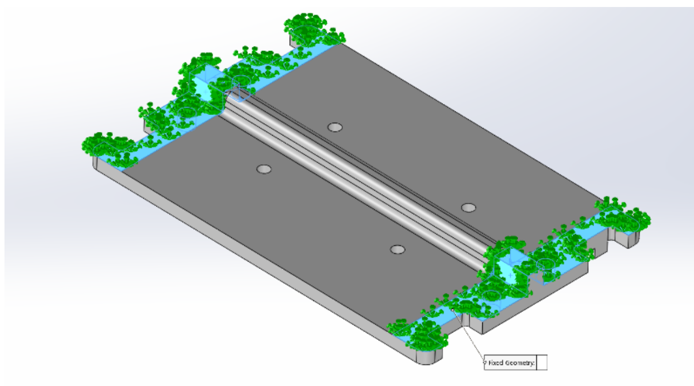

Figure 85: Base Plate; FEA; Fixed Geometry

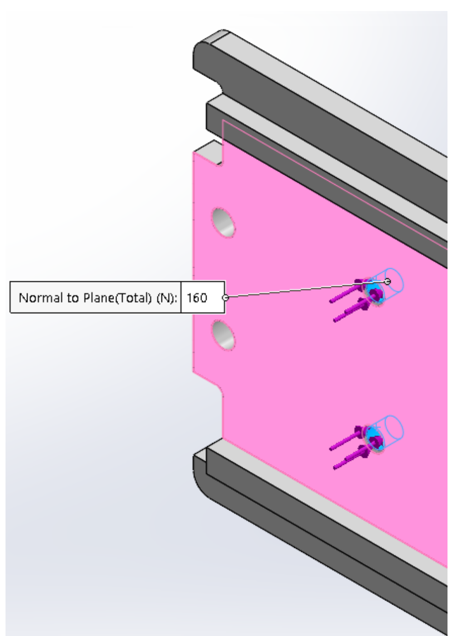

Figure 86: Base Plate; FEA; Applied Load

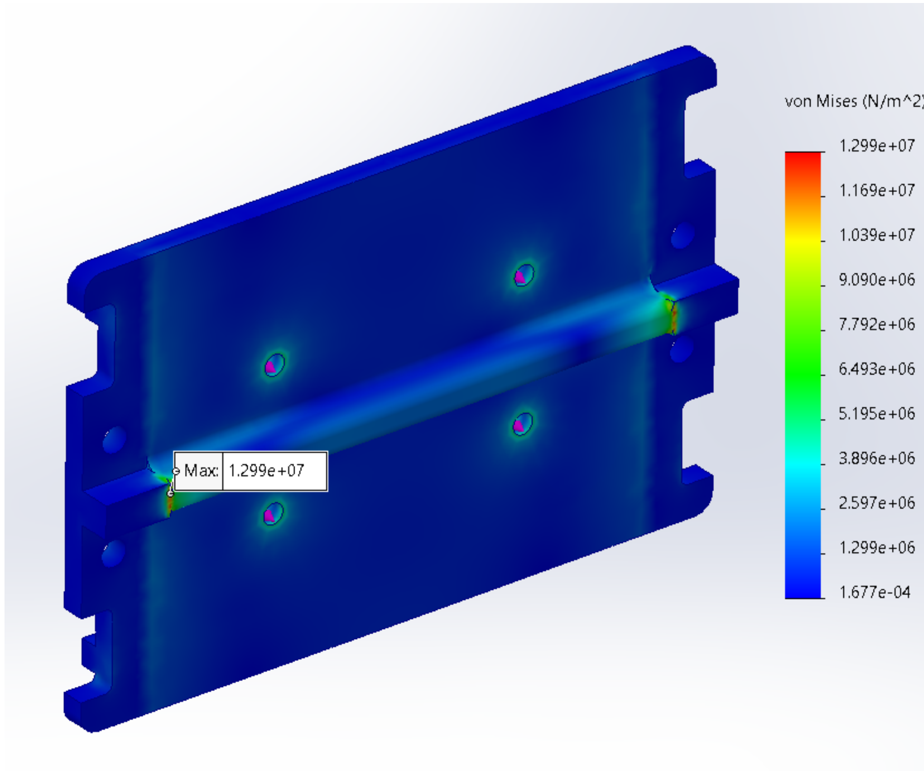

Figure 87: Base Plate; FEA; von Mises Stress Results

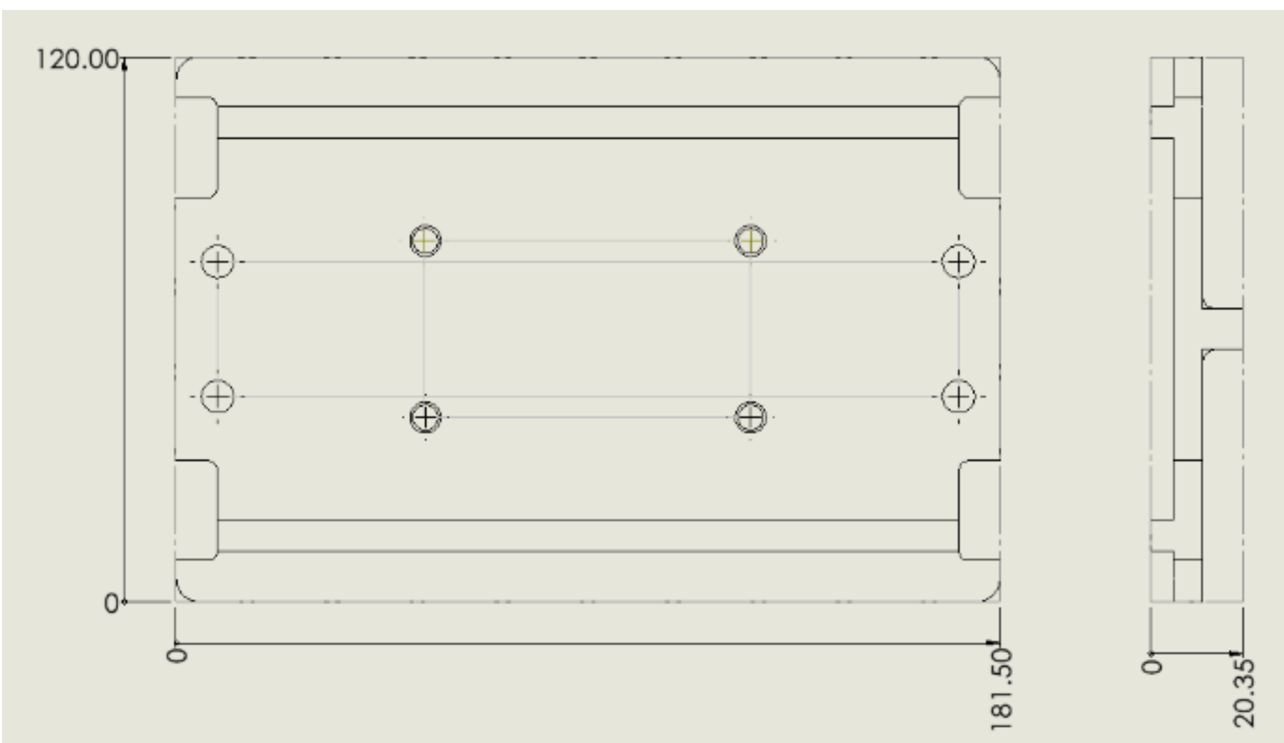

Figure 88: Base Plate; Overall Dimensions

The Base Plate Specification is presented in Table 18:

Table 18. Base Plate Specification

Material	ABS
Applied Load	320 [N]
Max Stress (FEA stress)	13 [MPa]
Tensile Strength	30 [MPa]
Safety Factor	2.3
Dimensions: length, width, height	181.5, 120, 16.35 [mm]
Mass	0.16 [kg]

7.6 Roller Adapter

The team standardized the roller adapter design for use on both the left and right sides. By combining parts into unified assemblies, the team reduced the number of unique pieces to produce and simplified replacements in case of breakage. Improvements to the roller adapter included the incorporation of a flanged nut mounted internally within the adapter where the vertical lead screw goes. This nut was secured through the component's round surface instead of relying solely on flanged bolts. The CAD model is shown in Figure 89.

To assess the impact of forces acting on the roller adapter, the team introduced virtual pins in the team's model to simulate the application of force. These pins emulated the bolts that would typically be used, and the team applied a maximum force of 160 N to each pin in the simulation, Figure 91. It is important to note that the team's analysis focused on the roller adapter part itself and not on the stress in the modeled bolts. This is because the bolts, made of stainless steel, are already known to possess a strength capacity well beyond the applied force.

The simulations accounted for the fixed geometry at the points where the adapter would be attached to the rest of the assembly, ensuring the analysis reflected the true operational conditions, Figure 90.

The results of the team's analysis indicated that the newly designed roller adapter could comfortably withstand the applied loads, Figure 92. It is also worth noting that under typical operating conditions, the force experienced by each pin is likely to be around 80 N, which is well within the safety margin of the design. This reassured us that the roller adapter would perform reliably within the straightening device, even under repeated use.

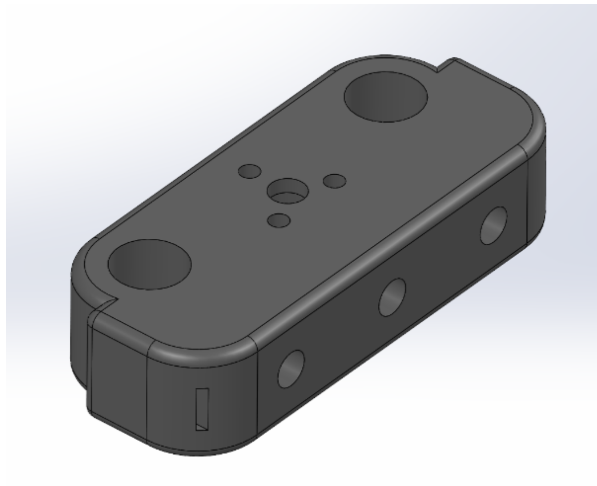

Figure 89: Roller Adapter; CAD model

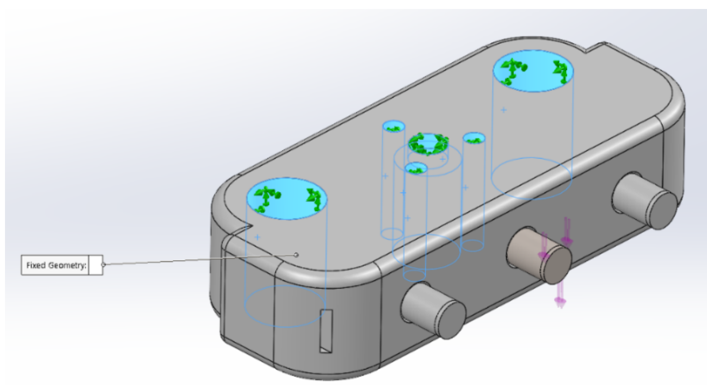

Figure 90: Roller Adapter; FEA; Fixed Geometry

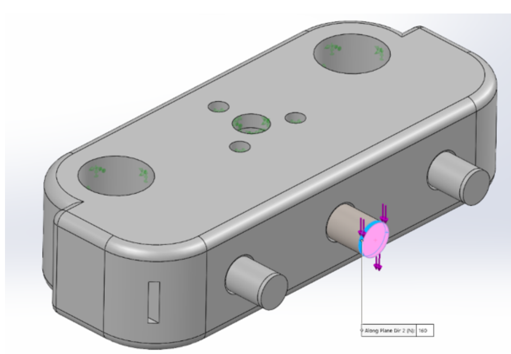

Figure 91: Roller Adapter; FEA; Applied Load

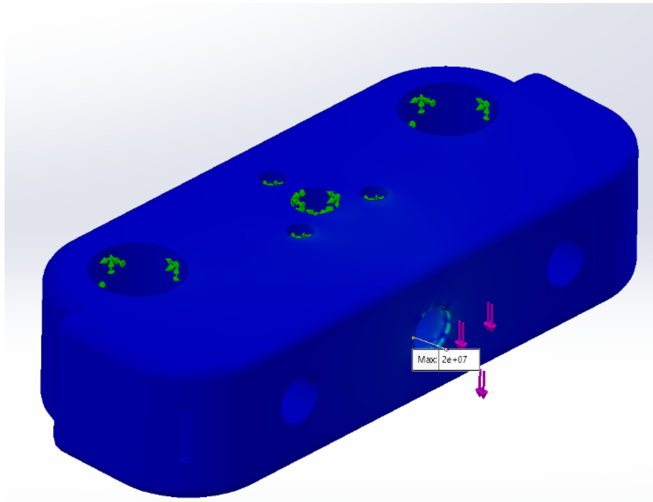

Figure 92: Roller Adapter; FEA; von Mises Stress Results

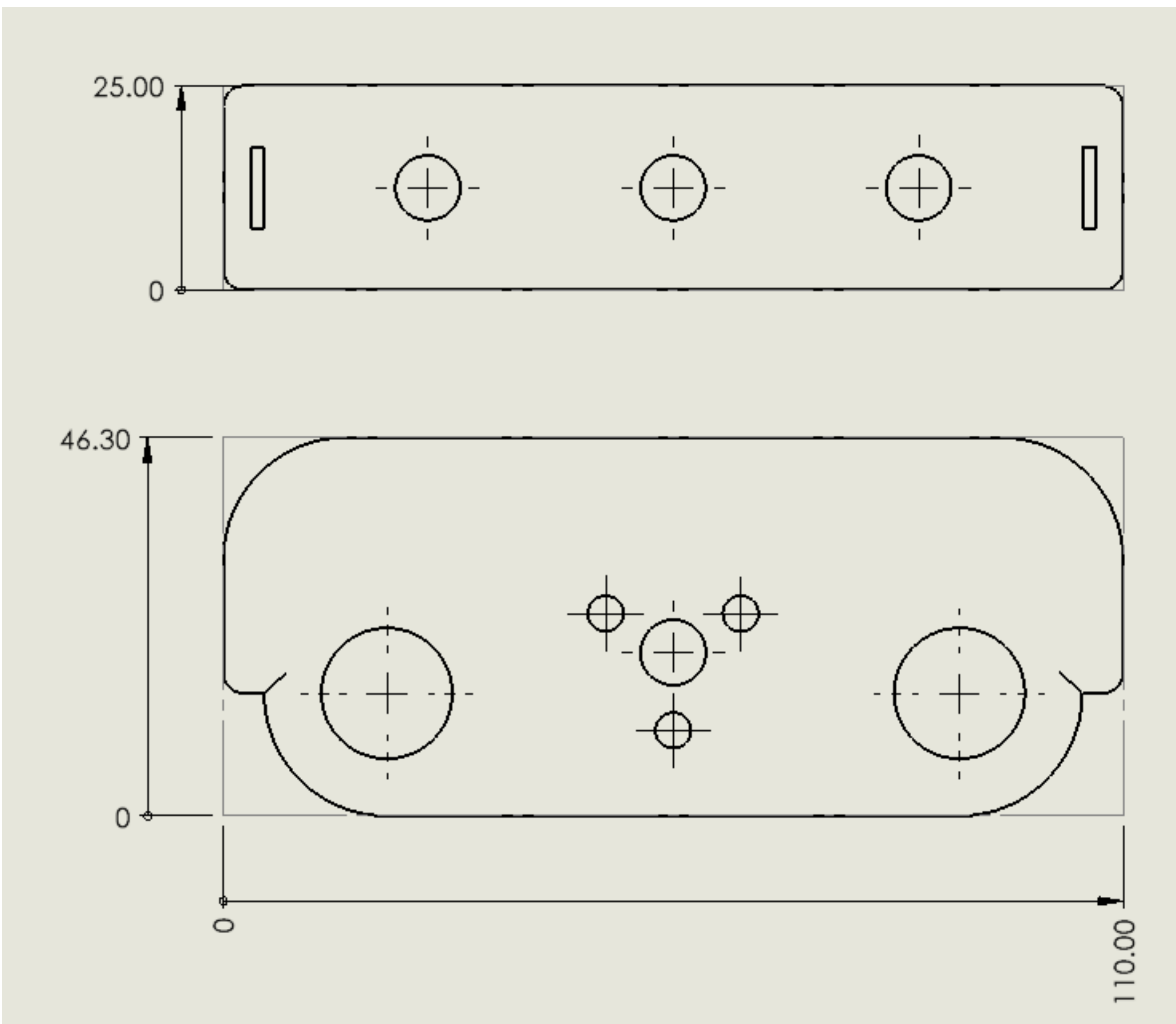

Figure 93: Roller Adapter; Overall Dimensions

The Roller Adapter specification is shown in Table 19:

Table 19. Roller Adapter Specification

Material	ABS
Applied Load	160 [N]
Max Stress (FEA stress)	20 [MPa]
Tensile Strength	30 [MPa]
Safety Factor	1.5
Dimensions: length, width, height	100, 46.3, 25 [mm]
Mass	0.1 [kg]

7.6.1 Direction Rods Holder

The updated design features a Direction Rods Holder, specifically designed to firmly hold the 8mm direction rods and the roller bearing for the vertical lead screw. The ability to rigidly fix the direction rods enhanced the structural assembly stability. Key features of the Direction Rods Holder part included direction grooves for easier assembly. Additionally, the part had two grooves that simplified the assembly process with the Base Plate. The CAD model is shown in Figure 94.

The part was fixed with a fixed geometry function, specifically at the points where the grooves were located and where the needle bearing of the vertical lead screw was positioned. The fixed geometry is shown in Figure 95. These were positioned within the reinforcement ribs of the base plate. The torque was applied at the place of the 8 mm rods, Figure 96.

Upon evaluation, it was clear that the Direction Rods Holder was well-equipped to easily withstand the anticipated loads. The diagram is presented in Figure 97. The overall dimensions of “Direction Rods Holder” is shown Figure 98.

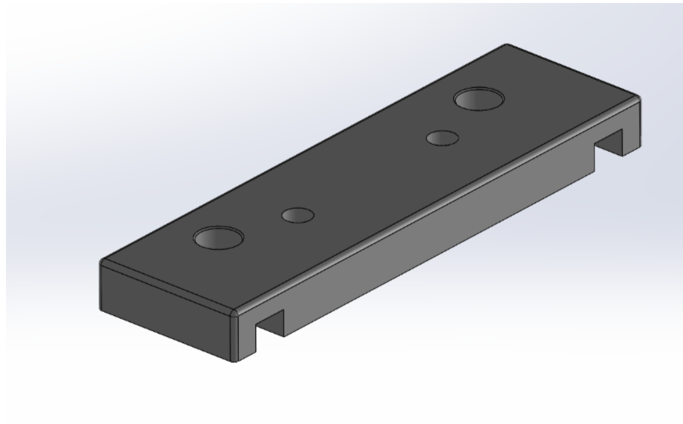

Figure 94: Direction Rods Holder; CAD model

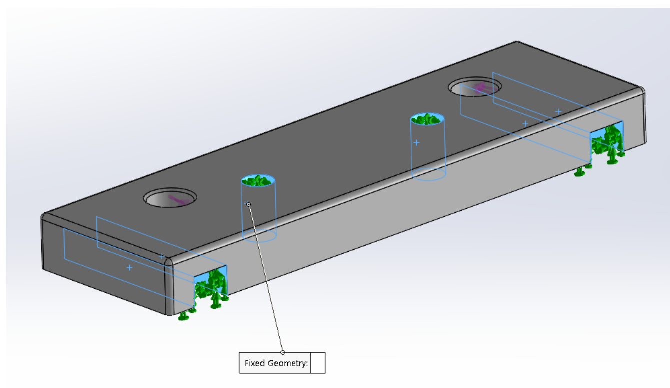

Figure 95: Direction Rods Holder; FEA; Fixed Geometry

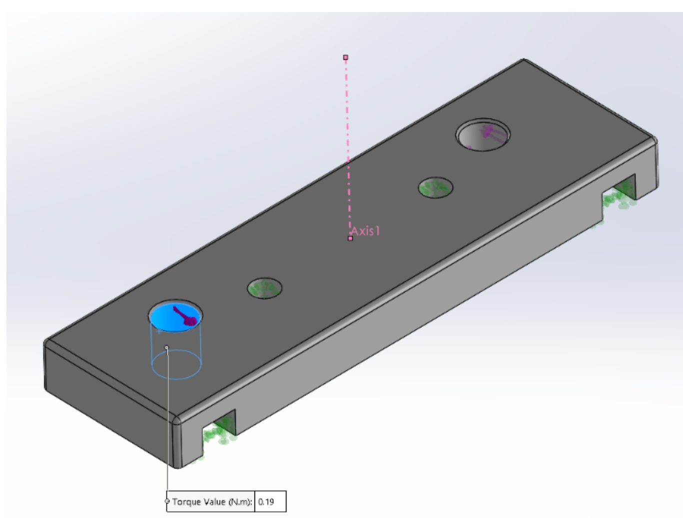

Figure 96: Direction Rods Holder; FEA; Applied Load

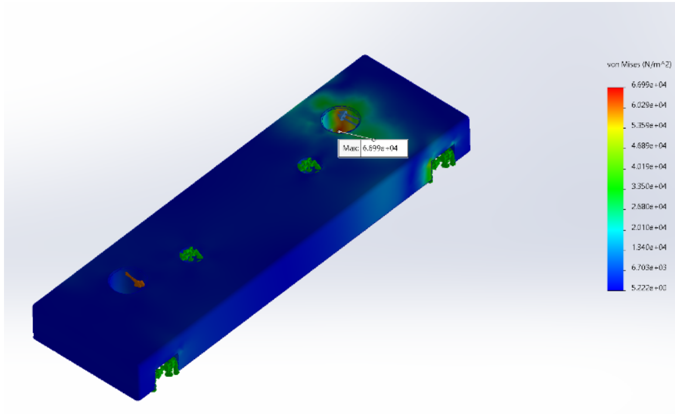

Figure 97: Direction Rods Holder; FEA; von Mises Stress Results

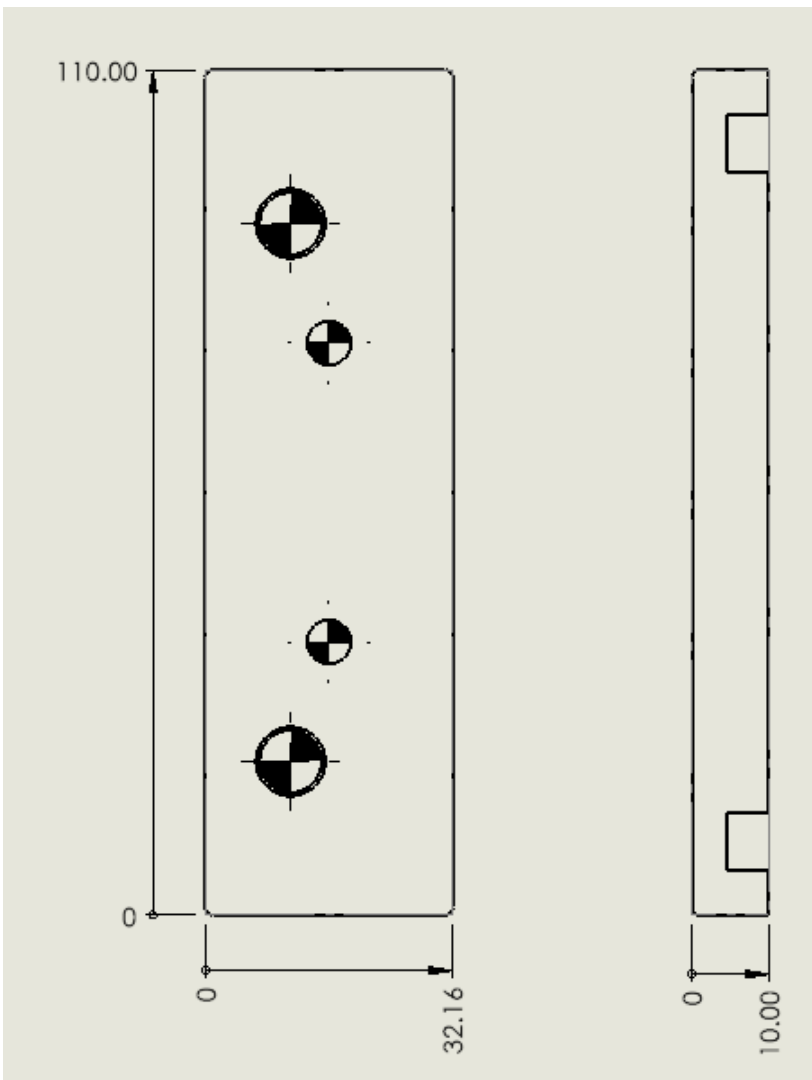

Figure 98: DirectionRodsHolder; Overall Dimensions

The specification of “DirectionRodsHolder” parts is presented in Table 20.

Table 20. Direction Rods Holder Specification

Material	ABS
Applied Torque (Axis 1)	0.19 [Nm]
Max Stress (FEA stress)	0.07 [MPa]
Tensile Strength	30 [MPa]
Safety Factor	429
Dimensions: length, width, height	110, 32.16, 10[mm]
Mass	0.032 [kg]

7.7 Horizontal Stepper Motor/Lead Screw

In the team’s pursuit to optimize the performance of a straightening device operated by a horizontal lead screw system, the team moved to a suitable stepper motor selection by considering the required linear velocity of the straightening device, acceleration, and the assembly’s mass. The team leveraged a reputable online calculator alongside the team’s previously developed Excel sheet for precise calculations, ensuring the stepper motor’s torque and the system’s linear velocity range aligned with the device’s requirements.

The mass of the straightening device, determined via SolidWorks, needed to be accounted for in the team’s calculations, which necessitated converting SI units to empirical units for compatibility with the calculator:

1. Straightening device weight which should be moved: 5.5 [lb], 2.5 [kg].
3. Target Linear Velocity: 189 [in/min], 8 [cm/s]
4. Time to Reach Velocity: 1 [s].
5. Bearing Type: Ball bearing.

7.7.1 Calculator 1 - Total Force Acting on Lead Screw

With the assembly set to move horizontally, the total force acting on the lead screw was evaluated, factoring in the weight of the assembly, the desired velocity, the time to reach this velocity, and the type of bearing system (ball bearing system). Remarkably, the calculated total force was 0.0531 lbs (0.236 N), indicating minimal external force influence due to the efficient carriage with ball bearings.

The calculator input included several elements, Figure 99. The orientation of the assembly travel was horizontal. The weight of the assembly was 2.5 kg. The velocity was 189 inches per minute (8 cm/s). The time to reach the velocity was 1 second. The bearing type was a ball-bearing system. The external forces included the carriage with ball bearings, which had no friction force and was recorded as 0 lbs. The output from the calculator, presented in Figure 99, showed the following results: The total force was 0.0531 pounds, equivalent to 0.236 Newtons.

This input demonstrates that the design was effective in minimizing resistance and optimizing movement, highlighting the effectiveness of the chosen bearing system.

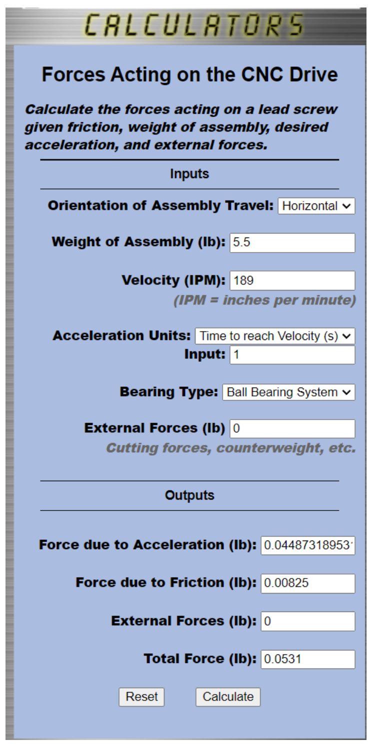

Figure 99: Horizontal Lead Screw; Acting Total Force; Calculator 1

7.7.2 Calculator 2 - Minimum Lead Screw Diameter

Further analysis involved assessing factors such as the lead screw's support distance, the load it bore, the type of end supports, and the safety factor. The analysis determined that the minimum required diameter for the lead screw was 0.46 inches. The team's existing lead screw, with a diameter of 0.63 inches, comfortably exceeded this requirement, ensuring structural integrity.

The calculator inputs included several elements, presented in Figure 100. The distance between the nut and support was measured in SolidWorks and found to be 30 inches or 76.2 cm. The load on the lead screw was the weight of the straightening device, recorded as 5.5 lbs. The type of end support was supported-supported. The safety factor was set at 2.

The calculator output indicated that the minimum diameter of the lead screw needed was 0.46 inches, while the team's existing lead screw measured 0.63 inches.

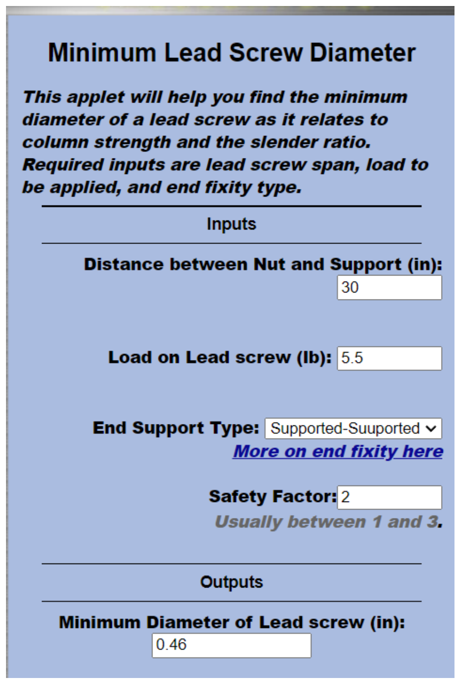

Figure 100: Horizontal Lead Screw; Minimum Lead Screw Diameter; Calculator 2

7.7.3 Calculator in Excel - Torque, Linear Velocity

For the horizontal lead screw, calculations mirrored those used for the vertical lead screw to ascertain the linear velocity and the requisite torque of the stepper motor. The outcome indicated a minimum torque requirement of 0.1699 [ozf*in] at 950 RPM or higher. The team's selection of a NEMA 17, 71 motor was based on its favorable torque characteristics, offering ample torque at the start with high RPM capabilities. The torque/speed diagram is presented in Figure 101. This choice allows velocity experimentation, as the team's target was 189 in/min, yet this motor can achieve speeds up to 600 in/min. The motor's theoretical torque at peak RPM stands at 8 [ozf*in], far surpassing the minimum requirement.

A potential challenge identified relates to the quality of the carriage ball bearings and the flanged ball screw, which were sourced from Amazon. There is concern these components may exhibit a higher friction force than expected, impacting the system's efficiency.

Table 21. Horizontal Lead Screw; Excel; Torque; Linear Velocity

Step 1: Calculate total force on lead screw								
	Velocity	in/min	189			Calculation	Units	
	Time to reach velocity	s	1			F(total)	lbs	0.0531
Step 2: Define min lead screw diameter								
						Min Lead screw Diameter	in	0.46
Step 3: Define the required torque of Stepper motor based on lead screw parameters								
Lead screw model	Travel distance per turn (lead), [inch]		0.2			Torque	lbs*in	0.0106
							ozf*in	0.1699
							N*m	0.0012
Step 4: Stepper Motors								
Stepper motor model	NEMA 17, 71							
Link:	https://www.mcmaster.com/6627T67/							
	RPM							
	min	max						
	70	3000						
Linear velocity range								
			Linear velocity range [inch/min]					
			min	max				
			14	600				

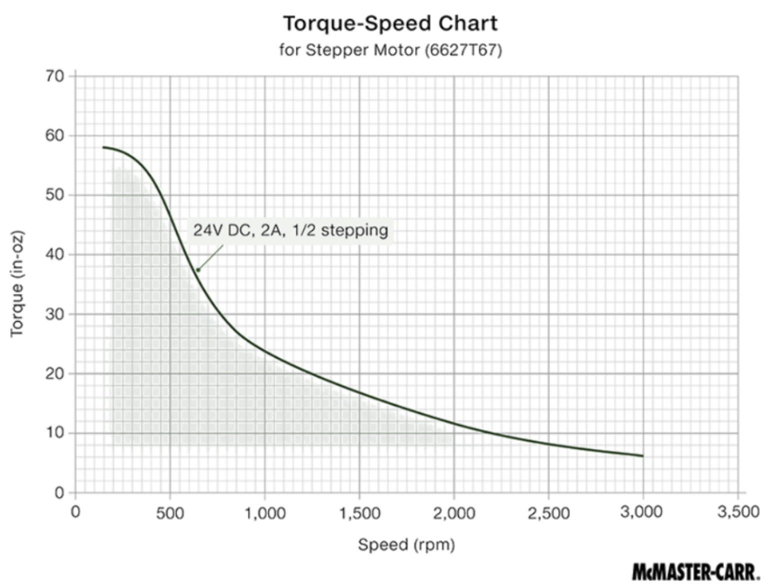

Figure 101: NEMA 17, 71; Torque Curve

7.8 Summary of Straightening Device Changes

The enhancements made to the straightening device include increased rigidity of the entire assembly and a reduction in unique parts, as well as the application of a puzzle assembly concept for easier integration. The device demonstrated excellent stability and reliability during straightening tests, which is explained in Chapter 6.9. An exception occurred when the roller adapter part broke due to the upper roller failing to stop correctly, damaging the lower roller adapter. Additional limit switches or sensors could be installed to prevent similar failures in the future, as discussed in section 8.3.2. Considering different manufacturing methods, such as using SLA printers, could also enhance surface finishing and material properties in future iterations.

7.8.1 Straightening System Code

Using the previously mentioned rotational code developed as a base for the straightening system code, which would later expand to become the motor control code, including functions to facilitate measurement and straightening. Following this version of the could have expanded functionally based on the expanding requirements of the system.

7.8.2 Arduino Code

Due to a lack of a viable method to directly control stepper motors with Python, it was determined that the motors would receive command signals from an Arduino Mega, which will further connect to Python to receive commands. The straightening code was developed in sections based on the functioning portions of the overall system. The initial Arduino code simply rotated the endoscope at a rate of 1/4 rotation per 10 seconds allowing for image and LiDAR evaluation. The second version of the code was created with the ability to receive data from the partner python code. When the signal was received, the endoscope would rotate the same ¼ rotation initial version. This simple code used in the measurement system served as the base for the creation of the straightening code used by the B-Term ME4320 team, mentioned in section 3.2.1.

In the finalized version of the Arduino motor control code the main function there are several important functions. The first this the setup function, which is automatically run once upon startup by the Arduino. In this function the pin are defined as inputs or outputs, high and low and variables are initialized. The serial port is also set to begin reading data. In the main loop of the Arduino code the serial port is checked for data every 10 milliseconds. If data is found it is saved by adding it to a buffer. Should the length of the buffer exceed a certain size it is determined that a complete signal has been received and the Arduino beings parsing. The signal from the Python code is a numeric value which is received as a string. This string is subdivided into smaller strings then these smaller strings are converted to integers. A string is a sequence of characters while a integer is a number value. When a function is created it is only able to use specific data types. The function for controlling the stepper motors via the Arduino was created to accept only integer values, as such the values strings from the python code are converted to integers. An example of this is the Arduino program receiving a single of “12345”, which is divided into 3 strings “12” , “34” and

“5”. When converted the string “12” becomes the integer 12. In this example the integers 12, 34 and 5 are used command the stepper motors. Once the integer variable’s have been created the Arduino motor conrols function is called. After the motor control function is executed the data buffer is reset and the main loop begins again, waiting for more data.

7.8.3 Python Code

Using the python library PySerial The initial python code was a function that sent a signal to the Arduino code which then rotated the endoscope clockwise or counterclockwise depending on a 0 or 1 bit. The main logic begins with establishing a serial connection between the Arduino Mega and the python program. Once the connection established made the Arduino is continuously polling, checking the serial connection for data from the Python code. Once data, in the form of a string, has been received the Arduino executes the given commands.

The main function of the python code sends the Arduino a string of numbers with each number representing various attributes of the motors. The string is a minimum of 8 digits with a maximum equivalent to 7 digits plus an unsigned long integer which is 4 bytes, which is equal 4,294,967,295 bits. An example of what Python code can send a signal of 21130002 which is 8 digits, the minimum signal length to send all relevant data or a signal of 41199994294967295, which is the largest possible signal value and length. The reason for this limitation is due to the processing of the Arduino Mega. values larger will cause a computation error. This limit is fine for the purposes of the project. What these digits represent is as follows. The 1st digit specifies the motor which ranges from 1 to 4, each value representing a specific motor. Motor 1 actuates the stepper motor controlling the upper rollers, motor 2 is the lower rollers, motor 3 is horizontal movement of the straightening assembly and motor 4 rotates the endoscope once mounted. The 2nd digit is the direction a binary 0 for clockwise or 1 for counterclockwise. The 3rd digit is the limit switch variable, another binary 0 or 1 that informs the Arduino side whether to send responding signals from the limit switches while the motors are executing the commands. This is used to allow the motors to reverse their initial direction when hitting a limit switch, turning off the signal. This is done because when the signal for motor movement is sent, checks if the limit switch has been triggered between every step of stepper motor. Meaning that in an instance that the horizontal carriage holding the straightening system triggers the limit switch as it is going backwards, the program stops the carriage, checks the direction it was moving, then sends a command to reverse the direction a set distance. Before the signal to reverse is received, the limit switch is still triggered because of where the carriage is stopped. This means that before the system can begin reversing it will once again detect the switch and being the stop and reverse protocol. This locks the program in situation of the motor going back and forth, without moving while trying to reset. By disabling the limit switch for the reversing process motors can properly reset. The 4th – 7th digit is the speed which can uses values from 0 to 9999, the code will add extra 0's to the beginning of the number if a non-4-digit number is used for the speed, 123 becomes 0123 when sending data from the Python to the Arduino, for example. It is necessary to add the 0's creating a 4 digit value because of how the Arduino parses the received signal, as mention in the section prior. The 8th digit and beyond is the step count which specifies the number of steps that the stepper motors will execute. When the limit switches are triggered, they call the main motor control function, with the limit switch variable being 0 instead of 1.

Once the 8 minimum digits have been calculated by the motor control function, it is turned into a string and sent to the Arduino via the serial connection where it is parsed and put into the Arduino side motor control function. Considering the team's examples from earlier, a signal of 21130002 means that the 2nd motor (Lower rollers) is rotating counterclockwise, (Moving the roller up) while checking the limit switch, at a speed of 3000 (3000 micro steps between pulses), for 2 steps. Another example of a signal of 41199994294967295 means that the 4th motor (endoscope rotating motor), is rotating counterclockwise, while checking the limit switch, at a speed of 9999, for 4294967295 steps.

This chapter dives much deeper into the straightening device and detailed specifications of several key parts of the station. The next chapter outlines the electrical system configuration for both the measurement and straightening substations.

8 Electrical System Configuration

This chapter will give an overview of the electrical system as well as the rationale behind the choice of components for the microcontrollers, motor drivers, and power supplies. The electrical system was initially developed as two separate systems due to the separate and concurrent construction of the straightening and measurement substations, which were later combined into a single power system.

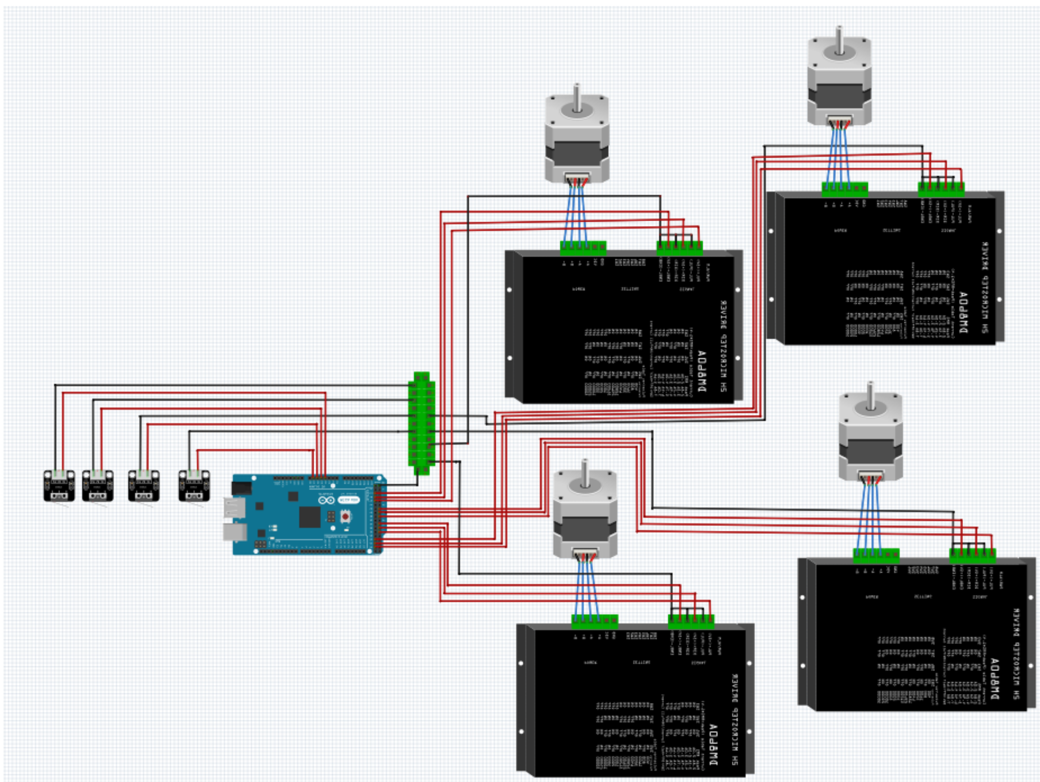

Figure 102: Overview of electrical system

8.1 Microcontroller Selection

The core aspect of the electrical system is the microcontroller; it is thought the microcontroller that the sensors will receive and respond to information, as well as motor control, will be carried out. The ME4320 B term runout measurement team used an Arduino Uno as their chosen microcontroller to during prototyping and suggested the use of the Raspberry Pi microprocessor when continuing the project. Based on the work and research, the MQP team explored 4 primary options for microcontrollers or processors. The microcontrollers researched were the Arduino Uno 4, ESP32, STM32 (L4+), and the Raspberry Pi 4, which is a microprocessor.

Table 22. Feature comparison between Microcontrollers and Microprocessors

Feature	Arduino (Uno R4)	ESP32	STM32 (L4+)	Raspberry Pi
Processor	Renesas RA4M1 (Arm® Cortex®-M4)	Xtensa dual-core (or single-core) 32-bit LX6 microprocessor	ARM 32-bit Cortex-M4 core	Broadcom BCM2711, Quad core Cortex-A72 (ARM v8) 64-bit SoC @ 1.8GHz
Software	Arduino IDE	Arduino IDE	Atollic® TrueSTUDIO® / Ardunio IDE	Visual Studio Code
Data storage	internal/EEPROM 256 kB Flash, 32 kB RAM	Internal/EEPROM 520 KiB RAM, 448 KiB ROM	Internal/EEPROM	External storage 2 - 8 GB RAM
Wi-Fi (integrated)	Yes	Yes	No	yes
Bluetooth (integrated)	No	Yes	No	yes
Ethernet	No	No	No	yes
Number of Pins	Variable	Variable	Variable	Variable
Serial communication	yes	Yes	Yes	Yes
Multithreading	No	Yes (multicore)	No	Yes (multicore)

Table 22 outlines what the team considered to be possible relevant features for selecting a microcontroller at the beginning of the MQP. One of the main points of research was how the system that calculates the runout would transmit and receive information from the system that will correct the runout. Based on the list of features and the overlap in functionality between many of the microcontrollers it was decided that either an Arduino based microcontroller, or the Raspberry Pi microprocessor would be used. If it was later determined that the system needed to use multithreading, (simultaneous execution of two or more programs) the ESP32 or Raspberry Pi would be used. Motor control testing began using the ME 4320 D terms Arduino Uno R3. Based on these initial tests, it was established that a serial connection between the Python program used for runout measurement and the chosen microcontroller would be suitable for the project. To this end, it was decided that an Arduino R4 with integrated Wi-Fi would not be required, and an Arduino Mega was selected instead, due to the increased number of digital pins compared to the Arduino Uno R3. Because the system relies on the serial connection between the Arduino Mega and the Python program, the Arduino Mega is easily powered by the device hosting the Python code, and no dedicated external power source is required.

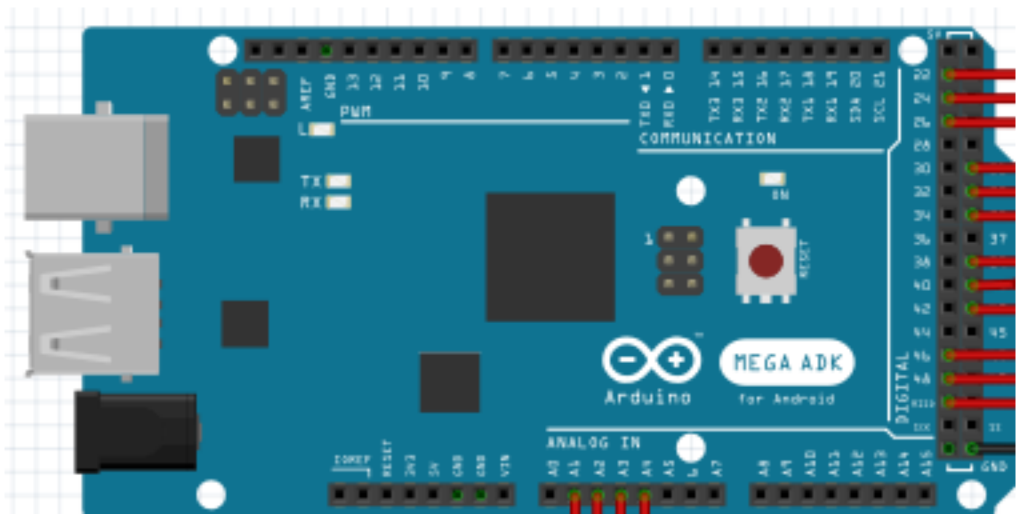

Figure 103: Zoom in of Arduino Mega

8.2 Measurement Substation Electrical System

The Measurement substation electrical system consists of the Balser Ace 2 Camera, NEMA 17 stepper motor, two 24V LED panels, and the Arduino Mega. Like the Arduino Mega, the Balser Ace 2 camera requires a connection to the Python program running the runout and correction code. Thus, it is powered via the USB port of the system laptop. The NEMA 17 stepper is used to rotate the endoscope within the measurement substation. To accomplish this, a KS42SH40-1204A motor, which is the same as the motors from the B term ME 4320 prototype, is used. This motor used the TB6600 motor driver and is connected to the same power supply, which is described in the following section. Prior to the subsystem being combined, this motor was powered by a 12V 10A switching power supply.

8.3 Straightening Substation Electrical System

Initially, the straightening subsystem's electrical design and components were based on the prototype created by the B term ME 4320 team. After expanding research on the material properties of the endoscopes as well as force requirements based on the MQP straightening system design new stepper motors were selected, as detailed in sections 7.5 Vertical Stepper Motor/Lead Screw and 7.8 Horizontal Stepper motor/lead screw. A new power supply was also selected due to the change in power requirements of the new motors, which will be discussed in the following section.

8.3.1 Motors

Initially the vertical lead screws used the KS42SH40-1204A NEMA 17 motors which require 1.2A per phase. Based on the research in section 7.5 the NEMA 17 model (Part No: 6627T64) was selected for the vertical lead screws. The NEMA 17 6627T64 requires .67A per phase. Because the current is lower than the previous motor used the same TB6600 motor driver was used. The current was limited to .7A average with a peak on 1.1A via the switches on the motor driver.

Based on feedback given to the ME4320 B term team, a single switching power supply was used rather than separate power supplies for the vertical and horizontal motors prototype. The motor used in the measurement subsystem will also be added to this power supply. From the team's research and the TB6000 motor drivers 20v minimum requirements an adjustable 24V 14.5A switching supply was selected.

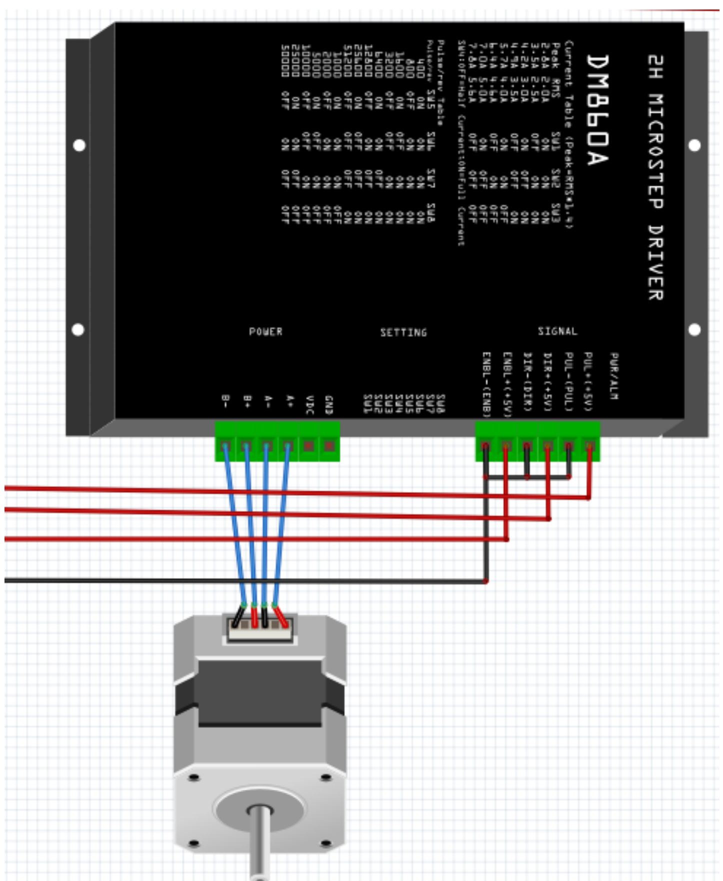

Figure 104: Single stepper motor connected to motor driver

Figure 102 shows the general wiring of a stepper motor used in the project. For 4 lead bi-poplar stepper motors the red and blue wire will be a pair for one coil while the green and black while will serve as the pair for the other coil. Along the signal ports of the driver ENA-. DIR- and PULSE- will be wired together and grounded via the ground pin of the Arduino Mega while ENA+, DIR+ and PULSE+ will be connected to specific pins on the Arduino Mega, with the specific pins depending on the motor. For the TB6600 and similar motor drivers ENA+ can be left grounded or low which activates the driver, in the case of this project it is connected to a digital pin in order for the Arduino to deactivate the driver by sending a high signal to the pin.

8.3.2 Limit Switches

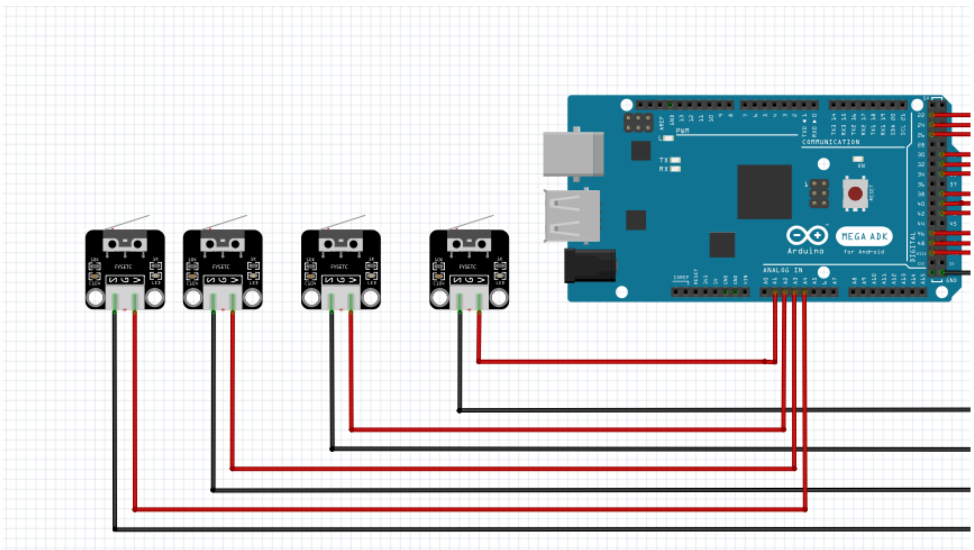

Figure 105: Limit Switches connected to Arduino MEGA

The limit switches used were KW12- 3AC 250V 5A in the normally open configuration. Four limit switches were used, each triggering in a specific position to stop a specific motor. Switch 1 connected to analog pin A1 triggers when the upper roller is at maximum height. Switch 2 connect to analog pin A2 triggers the lower roller is at minimum height. Switch 3 connected to analog pin A3 is located at the back of the rails for horizontal movement and triggers when the carriage moves backwards. Switch 3 is at the front of the rails for horizontal movement and triggers when the carriage moves forward. Normally open means that the line is open when the switch is not triggered and current does not flow through the system. When the switch is triggered, the system will close and the current will begin to flow, signaling the Arduino to stop the motors. The Arduino is constantly checking the analog pins that the limit switches are connected to, when the reading on these pins read a voltage above a certain value the motors will stop.

This chapter overviews the configuration of the electrical systems for the station, explains the team's microcontroller selection process, and provides additional details on motors and limit switches used. The next chapter thoroughly describes the team's testing processes and explains this project's results.

9 Testing and Results

This chapter provides a detailed overview of our findings across various aspects of the project, including the measurement station, measurement code, electrical systems, straightening code, straightening device, and the combined code system. We explore each component individually, discussing how they contribute to the project's objectives and highlighting the results achieved. The user manual, found in Appendix D, provides a guide through the process. This comprehensive review helps to understand how each part integrates with others and the overall impact on project performance. Our aim is to present a clear picture of our progress and offer insights into how each element has been developed and refined during the project.

9.1 Measurement Station

Testing and the subsequent results regarding the measurement station were focused on three characteristics of the station that would be unaffected by changes in the measurement code.

9.1.1 Lighting

The Final Lighting Design consisted of two LED panels equally Spaced away from the endoscope with their light Pointing Directly at the Endoscope. The Panels are [Dimensions] and use 24V LED strips to produce their lights. The Lighting is plugged into a separate source of power from the rest of the device for easy light changes to be implemented.

9.1.2 Background

The background is a sheet of 4.76 mm foam board cut to the size 150 x 762 mm . The team found after using it for a while that while it has the strength, texture, and color desired for optimum measurement, the board's ability to capture dust and acquire scratches and dents became a problem. The foam board would start creating visual errors in the measurement code by having dust particles, bends, or scratches reading as outliers in the code.

9.1.3 Camera Calibration

The finalized calibration process makes use of 2 Python programs developed by the team as well as the image capturing software developed by the Basler company. Figure 106: Endoscope overlay program, shown below displays the output of the first of these programs, the endoscope overlay program. This overlay program displays a green box with an adjustable width across the length of the camera's view. When the green box is parallel with straight rod the camera has been properly centered and can be safely calibrated. A bubble level is attached to the camera mount which was intended to serve as the primarily indicator of were the camera is properly positioned for calibration, but it was found during testing that there are instances where the camera is level, but the view is not properly parallel with the endoscope, resulting in a miscalibration and incorrect readings. This miscalibration was determined the system measured a runout on a metal rod that had been established as straight from manual measurements. The overlay program was created as another method of making sure the system is straight.

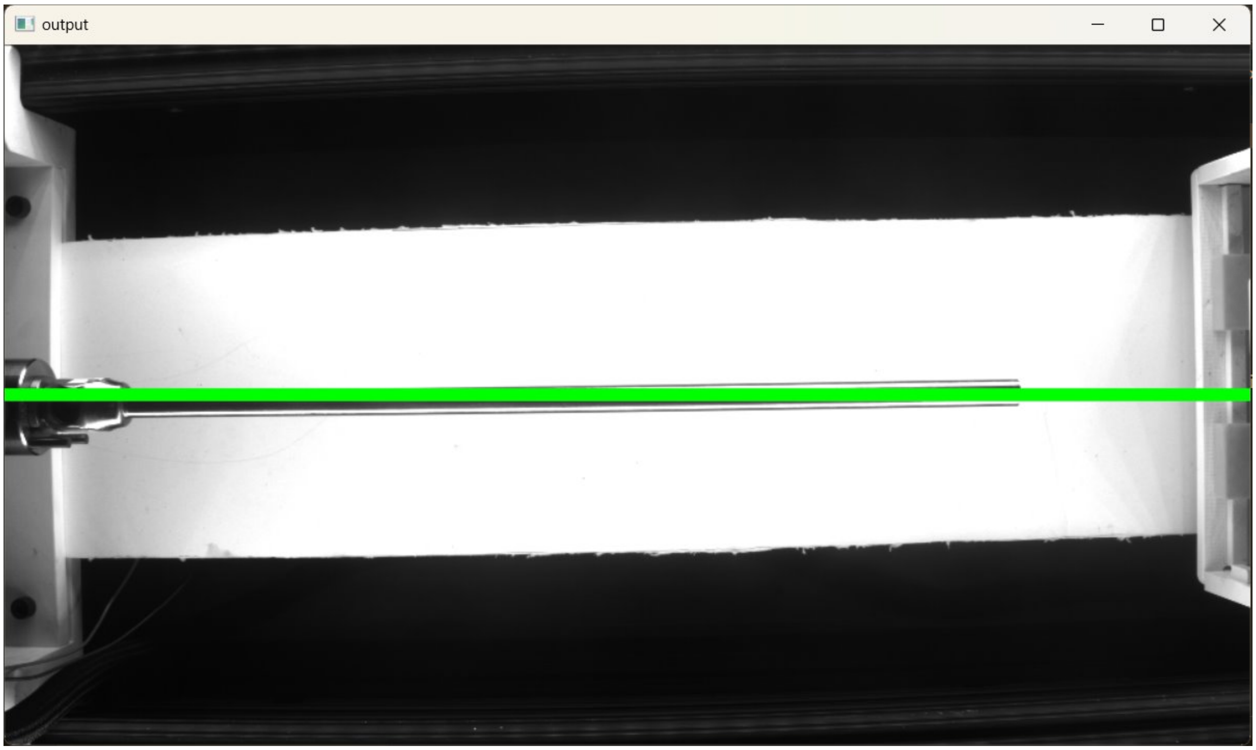

Figure 106: Endoscope overlay program

9.2 Measurement Code

The measurement code includes a few major functions with the methods tested mentioned in section four. The first function is capture and adjust ROI which it could capture one image and show a green ROI for user to adjust the left line and the rest of the lines are fixed. This step not only helps collect the ROI_X position which is needed for the straighten device to tell where to start but also helps the analysis more accurate due to a more focused region.

Once the ROI is selected by users, the second part of the code includes two functions: process frame and *start_video_processing_with_rotation*. The *start_video_processing_with_rotation* function allows the camera to show a live video while rotating the endoscope 360 degrees. At the same time the process frame could find the largest contour in the ROI and constantly pick the highest point by picking the largest y value on the contour while the endoscope is rotating.

Then using *calculate_highest_point* function with the time library, calculating the time where the highest point happens so that the endoscope could rotate the second time to where the camera could capture the highest point.

Next part of the code is analyzing the endoscope using *capture_and_undistort_image*, *detect_endoscope_nozzle*, *remove_outliers*, *FindRunout*. First, the code will recapture a new image and distort it based on the calibration file that was calculated previously. Then within the ROI, the largest contour would be considered as the endoscope nozzle. Then the function would draw lines that are 20 pixels apart from the top and bottom of the ROI to the nozzle contour and create intersection points. The first intersection point on the upper left is the starting point that is considered as (0,0) and draws a reference line from it. Comparing the rest of the y value of point on the upper contour and where y value has more than 2mm difference would be considered deviation points and marked as red points. The Lower intersection points and upper intersection points are in pairs in which the difference in y value would be the diameter. The code takes the average of the average of the difference values for the final diameter value. Length of the endoscope would be the x value difference between the rightest point and initial point.

Table 23. Endoscope Diameters

Endoscope	10	14	7	13	1
Manual	3.3 mm	5.50 mm	4.00 mm	4.00 mm	3.85 mm
Program	3.4 mm	5.70 mm	4.40 mm	4.30 mm	4.00 mm

Table 24. Deviation

Endoscope Number	10	14	7	13	1
Manual	3.15 mm	1.83 mm	2.00 mm	1.20 mm	2.20 mm
Program	3.30 mm	1.90 mm	2.03 mm	0.76 mm	2.05 mm

9.3 Electrical Systems

The eletrical system orginally made use of a 24V 14.5A switching power supply which was later changed during testing when it was determined that the input current while fine for the stepper motors was to large for the motor drivers, putting the system in a fault state. Based on further research of the data sheets of the motor contorls a 24V 10A switching power supply was purchased. Based on the information of the stepper motor controllers maximum input current and the confiuration of how the drivers connect to the swithcing power supply all motor drivers should have been in a normal funtioning state, but at times the driver for stepper controlling the lower roller would indiate it was at fault state, when not running. While the steppers where active this driver would indicate it was within normal conditons. There were no noticable errors in operation due to the motor driver briefly being in a fault state upon system startup.

9.4 Straightening Code

The straightening code consisted of 4 main functions. First is the Home function, using the limit switches as the bounds for homing the motors, ensuring a consistent zeroing of the motors each time. The Offset Formula function takes in the runout and the diameter measurements and calculates how much of an offset the rollers lower than true center to ensure the straightness of severe bends. The *Bendcorrection* function is what calls the motors to move such that the straightening occurs. This function closes the rollers around the endoscope and moves the entire device across the length of the endoscope until the desired sweep count is met, then resets the device.

9.5 Straightening Device

The testing of the straightening device consisted of 2 main phases. The first was to determine at the point the rollers were fully engaged with the endoscope, and the second was to determine the parameters of the straightening, which included testing the number of times the system rolled the rollers back and forth across the endoscope (sweeps) and how much the rollers would pull the endoscope down, counteracting the bend angle.

The first phase began by measuring the distance between the rollers and moving the upper and lower rollers to that distance to engage with the endoscope using individual motor control functions of the straightening code. From this, the team realized that the endoscope did not have an equal distance between the upper and lower rollers due to the placement of the limit switches in the straightening device. The distance was remeasured based on the center distance from the endoscope to the center distance of the roller. Within the code variables for the diameter of the endoscope, which was variable, the 5mm inner diameter of the roller was included so the roller would touch the edge of the endoscope. The upper roller was measured to be 37 mm, and the distance to the lower roller was measured to be 20.5 mm from the endoscope. When using these variables, the rollers visibly engaged with the endoscope, but when testing how well the sweeping motion was, the rollers did not spin. From this observation, it was determined that a greater area of contact was required. To this end, the distance that the upper roller is lowered to make contact with the endoscope was reduced by .25mm. After several repeat tests, lowering the upper roller by 39.25 mm resulted in the best engagement between the roller and endoscope. Once sufficient contact between the rollers and endoscope was established, the second phase of testing the straightening device began

Phase two of testing the straightening device focused on adjusting the number of sweeps used during bend correction and whether the rollers should engage the endoscope in the center of the system or push the endoscope below the centerline to counteract the upward bend.

Table 25. Table of measurements from straightening tests for endoscope 24

Endoscope 24	Initial Runout	Number of Sweeps	Offset from Center	Final Runout
5.5mm diameter	6.15 mm	10	0 mm	6.15 mm
425mm length	6.15 mm	20	0 mm	6.15 mm
	6.15 mm	10	2 mm	6.15 mm
	6.15 mm	10	8 mm	2.00 mm
	2.0 mm	10	8 mm	1.10 mm
	2.0 mm	10	8 mm	0.76 mm

The first endoscope test was endoscope 24, which was a 5.5 mm diameter endoscope with a length of 425 mm. Initially, the number of sweeps increased. Increasing the number of sweeps did not improve the runout of the endoscope, and at 20 sweeps, the straightening process alone would take over 5 minutes. After testing how the number of sweeps reduces the runout, the inclusion of an offset was tested. Within the measurement code, after finding the runout, the program rotates the endoscope 90 degrees counterclockwise so that the point of maximum runout is point straight up. Since the bend is consistently pointing up, the idea of the offset is for the rollers to pull the endoscope down, counteracting the bend, as opposed to simply meeting the endoscope where it has been mounted at the middle point. For example, in 3 trials, 10 sweeps, offset 2mm, the lower roller raises to 2mm below the point it would meet the edge of the endoscope, and the upper roller lowers 2mm below where it would usually engage, pushing the endoscope 2mm down and engaging it with the lower roller. The system then carries out the straightening process as normal. Because the first trial did not show much improvement, a larger offset was induced, pushing the endoscope 8mm down, which resulted in a large improvement in runout.

Subsequent testing focused on finding the optimal offset value based on feedback from the teams' sponsors. It was also the sponsor's suggestion that only 5 sweeps be used, as the change in sweeps was not shown to affect the reduction of runout as much as other variables.

Table 25: Endoscope 25 Straightening testing

Endoscope 25	Initial Runout	Number of Sweeps	Offset from Center	Final Runout
5.5 mm dia	2.6 mm	5	2 mm	2.4 mm
425mm len	2.4 mm	5	3mm	2.5mm
	2.5 mm	5	4mm	2.5mm
	2.5 mm	5	5mm	2.16mm
	2.16mm	5	6mm	0.89mm
	0.89mm	5	7mm	0.38mm

Table 26: Endoscope 27 Straightening testing

Endoscope 27	Initial Runout	Number of Sweeps	Offset from Center	Final Runout
2.7mm dia	7.9mm	5	2mm	7.9mm
290 mm len	7.9mm	5	3mm	7.3mm
	7.3mm	5	4mm	7mm
	7mm	5	5mm	6.6mm
	6.6mm	5	6mm	5.9mm
	5.9mm	5	7mm	4.8mm

Based on the data found in tables 25 and 26 it became clear that maximum, or close to the maximum offset reduced the runout of the endoscopes the most. This appeared to be the case for both the 5.5 and 2.7mm diameter endoscope, the tests that followed were designed to measure how much the runout can be reduced at max offset depending on the diameter of the endoscope.

9.6 Combined Code System

The combined code system calls functions from both the straightening code and measurement code to create one cohesive file to run for the entire system. The measure function starts by homing the straightening system to ensure it is out of the camera's sight lines. It then calls the *capture_and_adjust_roi* function from the measurement code to assign the ROI. Following the ROI assignment, the main straightening functions are called to complete the measurement process. At the end of this function, the straightness of the endoscope is used to determine the next steps. If the endoscope is not deemed straight and the desired max straightening count has not been reached, then the *straighten_end* function is then called, which in turn calls the *straighten_endoscope* function from the straightening code.

This chapter detailed the project's testing procedures and results in depth for several areas of the station. The next chapter describes the requirements achieved and outlines the broader impacts of this project.

10 Discussion

This chapter outlines the requirements for the semi-automated straightening machine, detailing what has been achieved and what aspects still need improvement as well as overviews the broader impacts of this project.

10.1 Requirements

Table 27. Requirements achievements

	Requirements	Achivied (Yes/No)	Our Results
Need	Measure the bends in endoscopes within 10-20 seconds	Yes	
	Measure the bends in endoscopes with an accuracy of 0.5 mm	Yes	
	Straighten endoscopes using rollers in under one minute	Yes	
	Straighten endoscopes using rollers with an accuracy up to 1.0 mm	No	up to 1.5 mm
	Straightening station location must be situated internally		
	Ensure compatibility with medical-grade rigid endoscopes ranging in diameter from 2.7 to 5.5 [mm]	Yes	
	Ensure compatibility with medical-grade rigid endoscopes ranging in length 6.9 to 45.7 [cm]	Yes	
	Light sources are required on both sides of endoscopes	Yes	
	Background against which measurements are taken should be white a matte finish	Yes	
	Cable management solutions to keep the setup organized	No	Significant improvements
	User-friendly interface or software	No	Mid range user friendly interface
	The design of the straighening device must not damage the endoscope	Yes	
	External parts have stable attachment with main station	Yes	
	Safety features	No	Limit Switches are integrated
Want	Ergonomic factors to provide comfort.	Yes	
	Mounting options available for accommodating different types of endoscopes	Yes	
	Modular design of station	Yes	
	All fixtures and included components can be easily cleaned and serviced	Yes	

The semi-automated straightening machine has successfully met a significant number of the critical requirements set for its performance and functionality, Table 27 Requirements achievements. It excels in quickly measuring and correcting bends in endoscopes, with the capability to complete these tasks within 10-20 seconds and under one minute, respectively, which is crucial for efficient clinical workflows. The machine is also well-suited to handle various sizes of medical-grade rigid endoscopes, thanks to its compatibility with devices ranging in diameter from 2.7 to 5.5 mm and in length from 6.9 to 45.7 cm. Additionally, the design ensures that the endoscopes are not damaged during the straightening process, a crucial factor for maintaining the integrity and lifespan of these delicate instruments.

Despite these achievements, there are areas where the device does not fully meet the set specifications. The accuracy of the straightening process, while satisfactory, does not reach the ideal threshold of 1.0 mm and currently stands at 1.5 mm. This discrepancy suggests that while the machine operates effectively, there is a slight compromise in precision that could potentially affect its application in more sensitive environments. Furthermore, the placement of the straightening station within the machine and the organization of cables have seen improvements but still fall short of fully realized goals. These aspects highlight ongoing challenges in optimizing the internal layout for ease of use and maintenance.

Moreover, the interface provided, though functional, is described as mid-range in terms of user-friendliness. This implies that while the interface is adequate, it may not provide the best user experience, especially for those who may not be technically inclined. Safety features have been addressed by the integration of limit switches, which add a protective measure, yet the full suite of anticipated safety protocols has not been implemented.

In conclusion, while the machine meets many of its intended specifications and demonstrates strong performance in key areas, the points where it falls short suggest avenues for further development. Enhancing precision in the straightening process, improving internal component layout, expanding safety features, and upgrading the user interface would make the device more robust and user-friendly, thereby extending its applicability and ensuring safer, more reliable operations.

10.2 Broader Impacts

The development of a machine for measuring and straightening medical-grade ridged endoscopes holds significant societal and global impacts, particularly in the realms of health, safety, and sustainability.

10.2.1 Engineering Ethics

The Mechanical Engineering Code of Ethics outlines principles that guide ethical behavior in the profession, emphasizing integrity and respect for welfare and the environment. These principles were integral to the development of the developed station. A key principle is to be honest and impartial, providing accurate and truthful representations in professional reports. In this project, the team was transparent about the capabilities and limitations of the developed station. This transparency is essential in ensuring that professionals can make informed decisions regarding the use of repaired endoscopes in medical procedures. The principle of environmental responsibility guided the team's efforts to promote sustainability in healthcare. By enabling the reuse of endoscopes through effective straightening, this project aimed to minimize the environmental impact associated with medical waste and the production of new equipment. This aligns with global efforts towards sustainable healthcare practices. While promoting sustainability and resource conservation, the automation of the repair process may lead to job displacement for individuals involved in traditional roles. Engineers must consider the socioeconomic impacts of this project and work towards mitigating any adverse effects through measures such as retention initiatives.

10.2.2 Societal and Global Impact

The team worked to automate the medical endoscope repair process to enhance accuracy and efficiency. The project directly affects the health and safety of patients undergoing endoscopic procedures. By automating the repair process and enhancing the accuracy of endoscope straightening, the likelihood of errors and complications during medical procedures is substantially reduced. The decrease in the acceptable margin of error from 4.5 mm to 2.0 mm enhances patient safety by ensuring that endoscopes meet stringent quality standards before being used in medical procedures. This translates to better patient outcomes and reduced risks of complications arising from faulty equipment. Streamlining the endoscope repair process through automation enables healthcare facilities to optimize their resource utilization. This can lead to more efficient allocation of healthcare resources, potentially resulting in cost savings for healthcare providers and improved access to medical services for patients. However, it's crucial to consider potential unintended consequences, such as the displacement of manual labor in endoscope repair and maintenance roles. While automation brings undeniable benefits in terms of efficiency and accuracy, it may lead to job displacement for individuals involved in traditional repair processes. Addressing this concern may require retraining and reskilling initiatives to ensure that affected workers can transition into new roles or industries, thereby mitigating any negative socioeconomic impacts.

10.2.3 Environmental Impact

The environmental impact of the project, focusing on the reuse of endoscopes through effective repair and straightening, is substantial and aligns closely with global sustainability objectives. By enabling the reuse of endoscopes through effective repair and straightening, the project contributes to reducing medical waste and conserving resources. This aligns with global efforts towards sustainable healthcare practices, as it minimizes the environmental impact associated with the disposal of endoscopes and the production of new ones. Consequently, the project supports the principles of environmental responsibility and resource efficiency in the medical field. The project directly addresses the issue of medical waste, a significant environmental concern. By enabling the reuse of endoscopes instead of disposing of them after a deemed bent, the project reduces the amount of medical waste generated by healthcare facilities. This minimizes the environmental footprint associated with the disposal of medical equipment. The project contributes to resource conservation by extending the lifespan of endoscopes. Rather than continually manufacturing new endoscopes to replace those discarded, the project promotes the efficient use of existing resources by repairing and straightening endoscopes for multiple uses. This conserves materials and energy that would otherwise be expended in the production, transportation, and disposal of new endoscopes, thereby reducing the overall environmental impact associated with their lifecycle.

10.2.4 Codes and Standards

To ensure operator safety during the operation, the incorporation of limit switches and an emergency stop button were used. Limit switches are fundamental safety components that detect the presence or absence of an object within a specified range of motion. In the team's design, limit switches were strategically placed to restrict the movement of critical components within safe operational limits, preventing collisions or damage to the machine. The emergency stop button served as a fail-safe mechanism, allowing operators to instantly halt machine operation in an emergency or unforeseen hazard. This immediate cessation of activity minimizes the risk of injury to operators and prevents potential damage to endoscopes or the machine itself. These safety features comply with regulatory requirements and prioritize operator safety.

10.2.5 Economic Factors

While the initial investment in technology may represent a significant financial commitment for healthcare facilities, the long-term benefits and cost savings associated with enhanced efficiency and equipment reuse must be considered. By streamlining the endoscope repair process and reducing the need for frequent replacements, the developed technology can lead to substantial cost savings for healthcare providers over time. Additionally, the improved accuracy and reliability of repaired endoscopes may result in fewer procedure-related complications, further reducing overall healthcare costs and enhancing patient outcomes. In terms of market competition, the introduction of this device may disrupt the manual repair processes. By offering a technologically advanced solution that prioritizes accuracy, efficiency, and safety, the team aimed to establish a competitive edge in endoscope repair automation.

This chapter presents the achieved requirements and broader impacts of this project. The next chapter describes the team's conclusions and recommendations.

11 Conclusions and Recommendations

In this chapter, the team summarizes the results of our work and present our recommendations. The team carefully review the outcomes of our analyses and outline suggested improvements or next steps based on these findings. This discussion is aimed at providing a clear understanding of our conclusions and guiding future actions or studies related to this project.

11.1 Measurement Station

The concept of the measurement station encompasses various elements including lighting, background settings, calibration programs, and measurement codes. In this chapter, we explore potential future improvements aimed at enhancing the station's functionality and robustness. These enhancements are crucial for optimizing the station's performance and ensuring more accurate and reliable measurements. We will consider various strategies to improve each component of the station, ensuring that it operates more efficiently and effectively in various conditions.

11.1.1 Lighting

The lighting environment created for the current system consisted of 2 24V LED panels located on both sides of the system. The lighting environment created within the system served its purpose of creating a district contort for the endoscope. The main future improvement would be to make use of an LED amplifier to integrate the lighting into the rest of the electrical system, opposed to having it powered by separate wall outlets.

11.1.2 Background

In terms of size and color the current background is suitable for the system. A major improvement on the background in the future would be to use a different material with a similar texture. The current background is easily dirtied and difficult to clean due to the material. Any damage due to bending, while easily fixed leaves lasting marks that may not be visible but will be detected by measurement programs contour detection which and result in inaccuracies in runout measurements.

11.1.3 Calibration Code

The current calibration process is rather involved and takes time to properly calibrate system because it uses 2 python codes and an outside program, as described in section 9.1.3. The team’s primary recommendation would be to combine all the functions of the current calibration process into a single file or program that the users can carry out. Because the user to needs to move the chessboard around the camera’s target area within the station a system, a combined program should show a live feed from the camera and prompt the user to take pictures when ready would be best. This program should also be able to create and save files and folders when taking pictures because the current calibration code uses the photo file names and location within the computer's directory.

11.1.4 Measurement Code

The Measurement Code is a crucial component designed to accurately assess various parameters of the endoscope using OpenCV. It calculates the endoscope's diameter, measures its total length, and identifies deviation points along the endoscope that indicate bending or misalignment. Key functions of the code include:

Nozzle Detection: The code locates the endoscope's nozzle, which serves as a critical reference point for further measurements.

Angle Determination: It calculates the angle at which maximum deviation occurs. This is essential for identifying the most pronounced bend in the endoscope.

Rotation Control: Based on the angle of maximum deviation, the code controls the mechanical system to rotate the endoscope to this specific angle. This positioning is vital for optimal interaction with the straightening device.

Measurement Analysis: After positioning, the code performs a detailed analysis to measure the endoscope's length, diameter and deviation points.

Improvement Needed: The current implementation requires manual intervention for selecting the Region of Interest (ROI), specifically the starting point of the left boundary. This step is crucial as it defines the area within which all measurements and analyses are conducted. Manual selection can introduce potential inaccuracies.

Enhancement: Developing a sophisticated algorithm for automatic ROI selection could significantly improve this process. The algorithm would analyze visual markers or predefined criteria to set the ROI boundaries dynamically, reducing manual input and increasing reproducibility and precision. This enhancement would streamline the setup process, making the system more user-friendly and robust in various operational environments.

11.2 Straightening Device

The straightening device achieved the team's goals from a mechanical standpoint, barring certain outliners. During testing, the system was able to reduce runout and correct bends to the point that the measurement program considered the endoscopes straight. Improving the degree of correction primarily relies on determining a more accurate formula for calculating the offset of the rollers based on the endoscope runout and diameter. To better use this offset, some recommendations are to reposition the limit switches so the upper and lower rollers have a larger range of motion, as well as increase the height of the straightening device, which will also increase the working area and range of motion of the rollers. The main limitation when calculating the offset formula was that the lower roller could only be offset by a maximum of ~8mm. Theoretically, the measurement program could be altered to rotate the endoscope in a manner that results in the bend pointing down, allowing for the offset to be larger as it is pushing the endoscope up. Doing this may solve one issue but introduce another, as it could cause issues should the runout exceed 8mm. As such, it would be best to increase the rollers' working area.

11.2.1 Straightening Code

The Straightening Code is a code that could successfully use Arduino and Python to actuate the motors of the straightening assembly, accomplishing the straightening of a bent endoscope. It uses the calculations of the endoscope's diameter, total length, and max deviation to create a unique straightening experience on the endoscope. Key functions of the code include:

1. **Motor Control:** The code sends information to the Arduino to control the movement of the horizontal motor, and both vertical motors. The horizontal motor is attached to the horizontal lead screw which moves the straightening device. The vertical motors are attached to their own vertical lead screws which control the separate halves of the roller system.
2. **Roller Engagement:** Using the diameter of the endoscope the upper and lower rollers move in opposite directions towards the center to engage with the endoscope at true center. The rollers pinch the endoscope between them slightly by closing slightly more than the true diameter of the endoscope.
3. **Safety:** The Home() function has both the vertical and horizontal motors rotate continuously in the negative direction until each respective limit switch is hit, once they are triggered the motors rotate forward slightly till they are no longer triggered. This ensures the straightening device and its motors are properly zeroed before use.
4. **Offset Analysis:** Using the specifics of the endoscope's diameter, total length, and max deviation the offset is calculated such that the endoscope is being pulled in the opposite direction of the max deviation to overcorrect the bend, allowing for greater straightening.

Improvement Needed: The current implementation has the endoscope's max deviation pointed up with the offset moving down, but looking at the physical build of the device, there is more space to move upward. The team suggests testing versions where the max bend is facing downward and the offset moves upward. Allowing for greater overcorrection process.

Enhancement: With the development of automatic ROI selection, the team could improve this process by allowing for adjusting the start position of the straightening device based on the true start of the endoscope. Each endoscope has different start positions and currently the team starts at the longest to allow for all endoscopes to be able to use it. If auto ROI was created, the team could use those numbers to adjust the start position of the straightening device accordingly.

11.3 Electrical Systems

The electrical system worked as required allowing for proper actuation of the components of the straightening devices and rotation of the endoscope. The primary improvement for the electrical system would be to switch to a 24V 7A switching power supply, assuming all steppers and drivers remain the same. The TB6600 motor driver enters a fault state when input current is above 5A. When using 3-port power supply two motor drivers connect to each port, resulting in parallel connection which divides the current while keeping the system voltage the same. By having a 7A output which is divided in half the motor drivers will receive well under 5A. Should other recommendations such as adding LED panels to the overall power system be used the necessary power supply of the system should be analyzed again. Another recommendation is to switch the configuration of limit switches from normally open to normally closed. The reason for this change is if the system is normally closed if one of the limit switches were to come unplugged that would also have the same result of the current dropping as the limit switch being triggered and the motor would be stopped.

11.4 Combined System

The combined system used the measurement and straightening codes to successfully become a system capable of accurately assessing various parameters of the endoscope using OpenCV, calculating the endoscope's diameter, measuring its total length, and identifying deviation points along the endoscope that indicate bending or misalignment. Then taking these important calculations and using Arduino and Python, actuating the motors of the straightening assembly, creating a unique straightening experience on each endoscope.

11.5 Future Work

11.5.1 Measurement Station

Future improvements to the measurement station could include optimizing the use of space within it. Based on the results of tests, establishing a fixed height for the station could eliminate the need for adjustable camera heights, thereby saving space. However, this would mean that the cameras would lose height adjustability. Additionally, the LED panels currently attached to the sides of the station should be mounted on a different material. After extended use, the heat dissipation causes the PVC panels to warp. Another area for improvement is the precision of the frame cuts. Currently, there are some gaps between parts of the station, which could potentially affect the lighting environment. By enhancing the accuracy of these cuts, we can ensure a more controlled and effective lighting setup.

11.5.2 Straightening Device

Significant progress has been made on the straightening device, but there are still areas that could benefit from further enhancements. First, the overall size of the straightening device could be reduced. By scaling down the dimensions, we can use less material for 3D printing the parts and decrease the amount of space the device occupies within the measuring station. Additionally, the horizontal lead screw/stepper motor coupler could be repositioned inside the station to better utilize space and enhance the rigidity of the setup.

Another improvement involves replacing the horizontal stepper motor with one that offers similar or higher speed with higher torque. This change would help prevent issues related to the stepper motor overheating during prolonged use. With a quicker speed and a higher torque, the overall speed for the straightening process would increase allowing for more passes over the endoscope in the same amount of time.

Furthermore, installing additional limit switches for the vertical stepper motor could be beneficial. These switches would define the maximum allowable deviation from the center, preventing the rollers from extending too far. This safety feature would help avoid situations where roller adapters mistakenly clamp onto the endoscope and damage each other due to programming errors. These updates would improve the efficiency, safety, and durability of the straightening device.

In addition to the we suggest running more tests of the straightening system overall, we did not have enough time to test as many varieties of endoscopes, as many times to ensure the accuracy and find the true extent to where the device starts and stops working. We also suggest testing different offset calculations as well as possibly swapping the direction of the offset as there is more playable space above rather than below the endoscope.

11.6 Reflections

11.6.1 Abigail Clemence

My involvement in this project significantly strengthened several of my soft skills including communication, collaboration, and presentation, as well as my academic and engineering knowledge and capabilities. Working on this team on our company-sponsored project provided a unique opportunity to gain real-world experience and learn from professionals in the field, which I am very thankful for. I gained more familiarity with designing parts and creating assemblies in SolidWorks and greatly increased my understanding and ability to comfortably use this CAD software. Performing finite element analysis, modeling the station in SolidWorks, and developing a prototype are just a few things I learned more about and gained more experience with over the course of the year. Thank you very much to Professor Pradeep as well as Austin Scott and George Ardamerinos for their support and guidance throughout this project.

11.6.2 Nikita Igoshin

I had practical experience by working with HSWoA on real-life project tasks alongside my colleagues in a cross-working environment throughout this project. I improved my Python programming skills by writing code to calibrate the camera and measure endoscope parameters. Additionally, I acquired skills in creating technical documentation alongside project progress and developing prototypes based on project requirements. My CAD skills developed significantly as I learned to turn models into actual manufactured parts using the GD&T concept. I appreciate Professor Pradeep and the sponsors' mentorship, who shared valuable insights into engineering teamwork. Their guidance and feedback were important in improving our outcomes.

11.6.3 Chenhao Li

Reflecting on this project, I've honed several essential skills that have significantly contributed to my professional development. I learned the importance of staying focused on core objectives to ensure project success and honed my ability to present complex information clearly and compellingly. On the technical front, I improved my proficiency with OpenCV for image and video processing and gained practical experience in motor control. These skills were crucial for meeting the project's technical requirements and have expanded my expertise in both software development and hardware integration.

11.6.4 Praniva Pradhan

Through working with HSWoA on this project, I have developed several hard and soft skills. On the soft skills side, I honed my communication abilities through regular team meetings and discussions, learning to effectively convey ideas and collaborate with colleagues. On the hard skills front, I enhanced my proficiency in CAD software, utilizing it to design and iterate upon the station. Furthermore, I gained hands-on experience in manufacturing techniques, from 3D printing to precision machining. The assembly processes improved my understanding of how to bring a concept to life in the physical realm. I extend my gratitude to Professor Pradeep, as well as Austin Scott and George Ardamerinos, for their invaluable support and guidance during this project.

11.6.5 Jessica M. Rhodes

Being a member of this team has honed several of my technical and soft skills and prepared me for a real-world project. As a member of this team, I spent countless hours working in Python, writing and debugging across all functions, working on CAD, using SolidWorks to bring to life my visions of parts and assemblies for this device, and developed a proper system design for this device. Aside from the technical work, I have acquired better group work skills, communication, and better understanding of how professionals handle criticism and differences in ideas. Overall, this has been a truly amazing and productive experience, and I would like to thank Professor Pradeep and the sponsors' liaisons for their guidance and feedback, as well as their continuous support. Without them, I would not have learned nearly as much.

11.6.6 George Shelton

As a member of this team the multi-disciplinary skills I have built up over my time at WPI were put to the test. I learned the importance of properly establishing project objectives and the requirements necessary to meet those objectives. My communication skills and presentation greatly improved over the course of the project due to the frequent meeting within our team and the to our advisor Professor Pradeep, and sponsors George Ardamerinos and Austin Scott. I unexpectedly gained great hands-on experience assisting with the assembly of the station as well as learning about the iterative process of machinal design and analysis through working alongside my teammates. This project has been a wonderful opportunity to broaden my theoretical knowledge in a practical setting taking designs from paper, to prototype, to product.

This chapter describes the team's conclusions and recommendations, explains future work to be done on the project, and includes individual reflections of the project. The next chapter lists the references used in this report and throughout the project.

12 References

[1] Henke Sass Wolf of America. (n.d.). Retrieved from https://www.henkesasswolf.de/en/company/global-presence/henke-sass-wolf-of-america/

[2] Boese, A., Wex, C., Croner, R., Liehr, U. B., Wendler, J. J., Weigt, J., Walles, T., Vorwerk, U., Lohmann, C. H., Friebe, M., & Illanes, A. (2022). Endoscopic imaging technology today. National Library of Medicine: National Center for Biotechnology Information. Available: https://www.ncbi.nlm.nih.gov/pmc/articles/PMC9140648/

[3] MedlinePlus. (2016). Endoscopy. Available: https://medlineplus.gov/endoscopy.html

[4] Argueta, V. (2022). Rigid endoscope design. OFH. Available: https://www.opticsforhire.com/blog/rigid-endoscope-optical-design/

[5] Ceraulo, L. (2022). Causes of damage to endoscopes. Cantel Medical. Available: https://www.cantelmedical.eu/in/causes-of-damage-to-endoscopes/

[6] GD&T Basics. (2014). Runout. Available: https://www.gdandtbasics.com/runout

[7] Kweon, H., et al. (2021). Determination of true stress-strain curve of type 304 and 316 stainless steels using a typical tensile test and finite element analysis. Nuclear Energy and Technology, 53(2). https://doi.org/10.1016/j.net.2020.07.014

[8] Gallagher Fluid Seals, Inc. (2016). PTFE rotary seals: Housing, pressure and shaft run-out. Available: https://www.gallagherseals.com/blog/ptfe-rotary-seals-housing-pressure-and-shaft-run-out

[9] Boisvert, M., Gupta, S., Jolin, G., Krimmel, S., Regan, L., & Weber, O. (2023). Improved endoscope straightening design. Worcester Polytechnic Institute. Unpublished.

[10] Barnes, I., Gibson, D., Gonzales, E., Milligan, D., Piccione, T., Steriti, S., & Sutherland, M. (2023). Runout measurement device for rigid endoscopes. Worcester Polytechnic Institute. Unpublished.

[11] Bradski, G., & Kaehler, A. (2008). Learning OpenCV: Computer vision with the OpenCV library. O'Reilly Media, Inc.

[12] Analytics Vidhya. (n.d.). Camera Calibration with OpenCV. Medium. Retrieved from https://medium.com/analytics-vidhya/camera-calibration-with-opencv-f324679c6eb7

[13] Zhang, Z. (2000). A flexible new technique for camera calibration. IEEE Transactions on Pattern Analysis and Machine Intelligence, 22(11), 1330-1334.

[14] OpenCV. (n.d.). Camera calibration with OpenCV. Retrieved from https://docs.opencv.org/2.4/doc/tutorials/calib3d/camera_calibration/camera_calibration.html

[15] Anirudh, N. (n.d.). Aruco_Tracker. Retrieved from https://github.com/njanirudh/Aruco_Tracker

[16] Zoner Learn. (n.d.). How to photograph shiny and glass products. Retrieved from https://learn.zoner.com/how-to-photograph-shiny-products-and-glass-products/

[17] Expert Photography. (n.d.). Tips for photographing reflective surfaces. Retrieved from https://expertphotography.com/reflective-surface-photography/

[18] "Hough Line Transform." OpenCV. Accessed 29 Apr. 2024. https://docs.opencv.org/3.4/d9/db0/tutorial_hough_lines.html

[19] "Basler Ace 2 Area Scan Camera." *The Basler Ace 2 Camera " Versatile Use | Basler AG*, www.baslerweb.com/en-us/cameras/ace2/#products. Accessed 30 Apr. 2024.

[20] Quinn, S., Dulieu-Barton, J., Eaton-Evans, J., & Tatum, P. (2007). Thermoelastic investigation of damage evolution in small stainless steel pipework. DOI: 10.1007/978-1-4020-6239-1_424

[21] Chiou, Y.-C. (2010). Experimental study of deformation behavior and fatigue life of AISI 304 stainless steel under an asymmetric cyclic loading. Journal of Marine Science and Technology, 18(1), Article 15. DOI: 10.51400/2709-6998.1873

[22] Kumar, R., Mikkelsen, L. P., Lilholt, H., & Madsen, B. (2020). Understanding the mechanical response of glass and carbon fibres: Stress-strain analysis and modulus determination. IOP Conference Series: Materials Science and Engineering, 942(1), Article 012033. https://doi.org/10.1088/1757-899X/942/1/012033

[23] CNC Router Source. (2024, March 6). Lead Screws. Retrieved from http://www.cncroutersource.com/lead-screws.html

[24] CNC Router Source. (n.d.). Lead screw forces. Retrieved from http://www.cncroutersource.com/lead-screw-forces.html

[25] McMaster-Carr. (2024, March 6). Retrieved from https://www.mcmaster.com/

13 Appendices

Appendix A

Table 1. Endoscope Inventory Log

Endoscope Name/Label	Diameter (mm)	Total Length (cm)	Stem Length (cm)	Number of bends (visually)	Location	Notes
Endoscope 1	2.375 mm	12.5 cm	7.3 cm	1 bend	HL HSWoA Teaching Lab (silver box on top of shelves)	
Endoscope 2	3.964 mm	19.5 cm	15.3 cm	1 bend	HL HSWoA Teaching Lab (silver box on top of shelves)	
Endoscope 3	5.420 mm	33 cm	30.2 cm	2 bends	HL HSWoA Teaching Lab (silver box on top of shelves)	
Endoscope 4	9.970 mm	37.3 cm	33.2 cm	0 bends	HL HSWoA Teaching Lab (silver box on top of shelves)	
Endoscope 5	5.439 mm	46 cm	42.5 cm	1 bend	HL HSWoA Teaching Lab (silver box on top of shelves)	Very dented
Endoscope 6	2.650 mm	None	None	None	HL HSWoA Teaching Lab (silver box on top of shelves)	BROKEN
Endoscope 7	3.950 mm	19.5 cm	15.7 cm	1 bend	HL HSWoA Teaching Lab (silver box on top of shelves)	
Endoscope 8	2.651 mm	10.7 cm	7.2 cm	3 bends	HL HSWoA Teaching Lab (silver box on top of shelves)	
Endoscope 9	2.456 mm	11 cm	7 cm	1 bend	HL HSWoA Teaching Lab (silver box on top of shelves)	Stem length is less clear
Endoscope 10	2.675mm	30.5 cm	27 cm	0 bends	HL HSWoA Teaching Lab (silver box on top of shelves)	
Endoscope 11	3.480 mm	24.3 cm	20.5 cm	3 bends	HL HSWoA Teaching Lab (silver box on top of shelves)	
Endoscope 12	3.950 mm	33.6 cm	29.5 cm	2 bends	HL HSWoA Teaching Lab (silver box on top of shelves)	
Endoscope 13	4.006 mm	18 cm	14 cm	1 bend	HL HSWoA Teaching Lab (silver box on top of shelves)	
Endoscope 14	5.457 mm	33 cm	30 cm	1 bend	HL HSWoA Teaching Lab (silver box on top of shelves)	
Endoscope 15	5.461 mm	32.6 cm	30 cm	5 bends	HL HSWoA Teaching Lab (silver box on top of shelves)	Very bent; could break at any minute
Endoscope 16	9.969 mm	38 cm	33.2 cm	0 bends	HL HSWoA Teaching Lab (silver box on top of shelves)	
Endoscope 17	10 mm	37.2 cm	33 cm	0 bends	HL HSWoA Teaching Lab (silver box on top of shelves)	

Appendix B

VerticalStepperMototrAnalysis Excel: VerticalStepperMotorAnalysis.xlsx

HorizontalStepperMotorAnalysis Excel: HorizontalStepperMotorAnalysis.xlsx

EndoscopesForceAnalysis Excel: EndoscopesForceAnalysis.xlsx

Appendix C

Appendix C.py

Appendix D

HSWoA User Manual.docx

Appendix E

Appendix E.py

Appendix F

Appendix F.py

Appendix G

Appendix G.py

Appendix H

Appendix H.py

Appendix I

Appendix I.py

Appendix J

Appendix J.py

Appendix K

Appendix K.py